LOCAL DELIVERY OF ANTIMICROBIAL PEPTIDES USING SELF-ORGANIZED TiO_2 NANOTUBES FOR IMPLANT-RELATED INFECTIONS

by

Menghan Ma

A THESIS SUBMITTED IN PARTIAL FULFILLMENT OF

THE REQUIREMENT FOR THE DEGREE OF

MASTER OF APPLIED SCIENCE

in

The Faculty of Graduate Studies

(Materials Engineering)

THE UNIVERSITY OF BRITISH COLUMBIA

(Vancouver)

December 2010

ABSTRACT

Among the various complications that lead to the failure of orthopaedic implants, prosthetic-related infections have been reported as one of the major causes. Local delivery of antimicrobial agents through the implants surface is an ideal solution to the peri-implant infection problem.

Due to the increasing resistance of pathogens to the current therapy utilizing antibiotics, developing novel antimicrobial agents has received much attention recently. Among the potential alternatives are the antimicrobial peptides (AMPs). Because of their broad-spectrum bactericidal ability, low toxicity and immunogenicity, as well as complex killing mechanisms, AMPs have much lower possibility of developing resistance than traditional antibiotics.

In the past decade, fabrication of TiO_2 nanotubular structures by anodization method has attracted great interests because of its controllable, reproducible results as well as the simple process. In light of their high surface-to-volume ratio, controllable dimensions, excellent biocompatibility, adjustable wettability and other promising properties, TiO_2 nanotubes are considered as an ideal carrier for drugs.

In the current study, self-organized, vertically-oriented TiO_2 nanotubes were successfully prepared by anodization method in both water based electrolytes (phosphoric acid based and ammonium sulphate based electrolytes) and organic based electrolytes (Glycerol based and Ethylene glycol based electrolytes). The nanotube coatings prepared in ethylene glycol based

electrolytes, with ~80nm diameter and ~7 μm thickness, were selected for the drug delivery purpose. HHC-36, one of the most potent broad-spectrum AMPs with the sequence of (KRWWKWWRR) was loaded onto the titanium dioxide nanotubes via a simple vacuum assisted physical adsorption method. Antimicrobial activity test against Gram-positive bacteria (*Staphylococcus aureus*) demonstrated that this novel AMP-loaded nanotube surface significantly inhibited bacteria proliferation and effectively reduced bacterial adhesion on the surface. It was also found that the antimicrobial activities of the samples were highly dependent on the drug loading conditions. By changing the loading conditions, the bacteria killing rate after 4 hour incubation increased dramatically from 90% to 99.9%. *In vitro* study showed that the AMP-loaded nanotube samples are not cytotoxic for MG-63 osteoblast-like cells.

TABLE OF CONTENTS

ABSTRACT ..... **ii**

TABLE OF CONTENTS ..... **iv**

LIST OF TABLES ..... **viii**

LIST OF FIGURES ..... **ix**

LIST OF ABBREVIATIONS ..... **xiv**

ACKNOWLEDGEMENTS ..... **xv**

Chapter 1 Introduction **1**

Chapter 2 Literature Review **3**

2.1 Orthopedic implants-related infections 3

2.1.1 Orthopedic implants 3

2.1.2 Implant-related infections 3

2.1.3 Pathogenesis of peri-implant infections 4

2.1.4 Treatment of implant-related infections 6

2.2 Antimicrobial peptides (AMPs) 7

2.3 TiO_2 nanotubes 9

2.3.1 TiO_2 properties and applications for orthopedic implants 9

2.3.2 Processing of TiO_2 nanotubes 9

2.3.3 The formation of TiO_2 nanotubes 13

2.3.4 Evolution of the TiO_2 nanotubes 15

2.3.5 Crystallographic structures of TiO_2 nanotubes 17

2.3.6 Functional properties of TiO_2 nanotubes 18

2.3.6.1 Biocompatibility 18

2.3.6.2 Adjustable wettability 19

2.3.6.3 Other properties 20

2.3.7 TiO_2 nanotubes for drug delivery 21

2.4 Local delivery of antibiotics through implant surface 22
2.4.1 Physical adsorption 24
2.4.2 Chemical immobilization 24
2.4.3 Surface coating 25
2.5 AMPs delivery 25
2.6 Summary 26
Chapter 3 Scope and Objectives 27
3.1 Scope 27
3.2 Objectives 28
Chapter 4 Materials and Methods 29
4.1 Preparation of TiO_2 nanotubes by anodization method 29
4.1.1 Anodizing setup 29
4.1.2 Processing of titanium dioxide nanotubes 30
4.1.2.1 Water based electrolytes 31
4.1.2.2 Organic based electrolytes 32
4.1.3 Post-anodizing annealing 33
4.1.4 Materials characterization 33
4.1.4.1 Scanning Electron Microscope (SEM) 33
4.1.4.2 Raman spectroscopy 34
4.2 Antimicrobial peptide loading onto TiO_2 nanotubes 34
4.3 Antimicrobial test against Staphylococcus aureus (S.aureus) 35
4.3.1 Antimicrobial Test 1 36
4.3.2 Antimicrobial Test 2 37
4.4 Bacteria adhesion on sample surfaces 38
4.5 *In vitro* Release of AMP 39
4.6 Cell adhesion and biocompatibility study 39

4.7 Cytotoxicity assay 40
4.7.1 MTT assay for HHC-36 40
4.7.2 MTT assay for AMP loaded samples 41
4.8 Statistical Analysis 42
Chapter 5 Results 43
5.1 Processing of TiO_2 nanotubes 43
5.1.1 Fluoride containing water based electrolytes 44
5.1.1.1 H_3PO_4 based electrolytes 44
5.1.1.2 $(NH_4)_2SO_4$ based electrolytes 47
5.1.2 Fluoride containing organic based electrolytes 49
5.1.2.1 Glycerol based electrolytes 49
5.1.2.2 Ethylene glycol based electrolyte 56
5.1.3 Summary 60
5.2 Effect of heat treatment on crystalinity of TiO_2 nanotubes 61
5.3 Antimicrobial activity test against S.aureus 62
5.3.1 Antimicrobial Test 1 63
5.3.2 Antimicrobial Test 2 65
5.3.3 Summary 67
5.4 Bacteria adhesion on sample surfaces 68
5.5 In vitro release of AMP from TiO2 nanotubes 70
5.6 Cell culture: adhesion of osteoblast-like cells on sample surfaces 71
5.7 Cytotoxicity assay 73
5.7.1 MTT assay of AMPs 73
5.7.2 MTT assay for TiO_2 nanotubes 74
Chapter 6 Discussion 75
6.1 Selection of cationic antimicrobial peptides 75
6.2 HHC-36 loading onto TiO_2 nanotubes via physical adsorption method 76

6.3 Selection of nanotubes for AMPs delivery 77

6.4 Effect of AMP loading conditions on drug loading efficiency 78

6.5 Effect of crystallinity on the AMP delivery 79

6.6 Amorphous vs. Anatase TiO_2 nanotubes 81

Chapter 7 Conclusions 82

Chapter 8 Recommendations for future work 84

REFERENCES 86

APPENDICES 95

Appendix A: ANOVA for antimicrobial test 2 95

Appendix B: MTT assay for AMPs 95

LIST OF TABLES

Table 2. 1 Advantages of local drug delivery over systemic drug therapy (Reprinted from [25] with permission from Elsevier)..... 6

Table 4. 1 Summary of the anodizing parameters 33

Table 4. 2 Design of experimental groups for antimicrobial test 1 37

Table 4. 3 Design of experimental groups for antimicrobial test 2 38

Table 4. 4 Design of experimental groups for MTT assay 41

Table 5. 1 Effect of water content on nanotube diameter and length 54

Table 5. 2 Antimicrobial activity test 1 against *S.aureus* 64

Table 5. 3 Antimicrobial activity test 2 against *S.aureus* 66

Table 5. 4 P value of Holm t-test between every two groups for antimicrobial test 2 after 60 minutes incubation 66

Table 5. 5 P value of Holm t-test between every two groups for antimicrobial test 2 after 240 minutes incubation 66

Table 1 ANOVA tables for antimicrobial test 2 after 60 minutes incubation 94

Table 2 ANOVA tables for antimicrobial test 2 after 240 minutes incubation 94

Table 3 P value of Holm t-test on the results of MTT assay for HHC-36 94

LIST OF FIGURES

Figure 2. 1 a) Major pathogenic species for implant-related infections; b) Proportion of antibiotic resistant of infection-related bacteria to antibiotics (Reprinted from [14] with permission from Elsevier) 5

Figure 2. 2 Typical Antimicrobial peptides structures (A) Mixed structure of human β-defensin-2; (B) looped thanatin; (C) β-sheeted polyphemusin; (D) rabbit kidney defensin-1; (E) α-helical magainin-2; (F) extended indolicidin (Reprinted from [26] with permission from American Society for Microbiology)..... 8

Figure 2. 3 Schematic of two typical morphologies (nanoporous and nanotubes) of oxide layers formed by the anodization method [7,38]..... 10

Figure 2. 4 Depending on the anodization conditions, the oxide layer can be either compact, or nanoporous (Reprinted from [6] with permission from Elsevier) 11

Figure 2. 5 Coloring of the clinical titanium implants prepared by galvanostatic oxidation; the native oxide film (far left), the interference colors consecutively anodized at 20, 40, 80, 100, 180 and 200 V to the right, in 0.5 M tartaric acid [39]. 12

Figure 2. 6 Schematic diagram of the TiO_2 oxide layer formation mechanism: a). Compact oxide layer; b). Nanoporous oxide layer (Reprinted from [6] with permission from Elsevier); c). Evolution of a nanotube during anodization process: (Stage 1) thin compact oxide layer formation, (Stage 2) pit formation on the oxide layer, (Stage 3 & 4) growth of the pit into tubular structure (Reprinted from [41] with permission from Elsevier); d). Typical current density vs. time response observed for a titanium anodization behavior (400nm Ti foil anodized at 10V in HF-based electrolyte) (Reprinted from [35] with permission from Elsevier) 14

Figure 2. 7 SEM images of TiO_2 nanotubes grown by different anodization processes: (A) Typical morphology obtained in HF-based electrolytes; (B) glycerol/fluoride electrolytes; (C) ethylene glycol/fluoride electrolytes; (D) tubes grown by a different approach: rapid breakdown anodization (RBA); these tubes grow in disordered bundles within seconds at comparably high anodic potentials (Reprinted from [6] with permission from Elsevier) 16

Figure 2. 8 The crystal structure of TiO_2 nanotubes annealed at different temperatures: a) XRD pattern (Reprinted from [6] with permission from Elsevier); b) Raman spectroscopy pattern (Reprinted from [52] with permission from John Wiley and Sons) 18

Figure 2. 9 Four different drug loading methods using horseradish peroxide (HRP) as a hydrophilic model drug: (I) immersion without any TiO_2 surface modification, (II) immersion after OPDA modification in the upper nanotube layer (hydrophobic cap), (III) covalently attached HRP over the entire nanotube layers, (IV) OPDA cap in the upper nanotube layer and covalently attached HRP in the lower nanotube layer (Reprinted from [58] with permission from American Chemical Society) 22

Figure 2. 10 Schematic diagram of the drug delivery methods: Physical adsorption, Chemical immobilization and release from a surface coating (Reprinted from [64] with permission from Elsevier) 23

Figure 4. 1 Schematic diagram of the anodizing setup 29

Figure 4. 2 Experimental setup for titanium foil anodization 30

Figure 5. 1 Color changes of titanium foil during anodizing process 43

Figure 5. 2 SEM images of samples anodized in electrolyte: 0.3M H_3PO_4 + NH_4F: a) 0.07M, b) 0.1M, c)0.14M, d)0.2M, e) 0.27M at 30V for 2h and f) EDS result of the nanotube coating indicated that the coating contains titanium and oxide 45

Figure 5. 3 Nanotube diameter vs. NH_4F concentration. Error bars indicate standard deviation (n=10)..... 46

Figure 5. 4 SEM images of TiO_2 nanotubes in cross-sectional view of samples anodized in electrolyte: 0.3M H_3PO_4 + NH_4F 0.1M (left) and 0.27M (right) at 30V for 2h, both of them shows the thickness within 400-500nm..... 47

Figure 5. 5 SEM images of samples anodized in electrolyte: 1M $(NH_4)_2SO_4$ + NH_4F: 0.1M, 0.14M and 0.2M at 20V for 2h, top view (left) and cross-sectional view (right)..... 48

Figure 5. 6 SEM images of TiO_2 nanotubes in a top (a), bottom (b), and cross-sectional (c, d) view. Anodized in glycerol/water electrolyte (25:75 vol.%) containing 0.27 M NH_4F at 20V for 6h..... 51

Figure 5. 7 SEM images of TiO_2 nanotubes in a top (a), bottom (b), and cross-sectional (c, d) view. Anodized in glycerol/water electrolyte (50:50 vol.%) containing 0.27 M NH_4F at 20V for 6h..... 52

Figure 5. 8 SEM images of TiO2 nanotubes in a top (a), bottom (b), and cross-sectional (c, d) view. Anodized in glycerol/water electrolyte (75:25 vol.%) containing 0.27 M NH_4F at 20V for 6h..... 53

Figure 5. 9 SEM images of TiO_2 nanotubes in a top (a), bottom (b), and cross-sectional (c, d) view. Anodized in glycerol/water electrolyte (98:2 vol.%) containing 0.27 M NH_4F at 20V for 6h..... 53

Figure 5. 10 SEM images of TiO_2 nanotubes in a top (a), bottom (b), and cross-sectional (c, d) view. Anodized in glycerol/water electrolyte (75:25 vol.%) containing 0.27 M NH_4F at 30V for 6h..... 55

Figure 5. 11 SEM images of TiO_2 nanotubes in a top (a), bottom (b), and cross-sectional (c, d) view. Anodized in glycerol/water electrolyte (98:2 vol.%) containing 0.27 M NH_4F at 30V for 6h..... 55

Figure 5. 12 The Ti surface after removal of nanotube layer (left) and the EDS analysis of the nanoporous surface (right) 56

Figure 5. 13 SEM images of TiO_2 nanotubes in a top (a), bottom (b), and cross-sectional (c, d) view. Anodized in 98% ethylene glycol solution containing 0.27M NH_4F at 30V for 6h. 57

Figure 5. 14 SEM images of TiO_2 nanotube samples anodized in 98% ethylene glycol solution + 0.27 M NH_4F at 30V for 6h, then ultrasonic washed for (a) 0, (b) 5, (c) 10 and (d) 20 mins respectively. 58

Figure 5. 15 Thickness of nanotube layer vs. anodizing duration curve 59

Figure 5. 16 SEM images of nanotubes anodized in 98% ethylene glycol solution + 0.27 M NH_4F for 6h at 30, 40, 45V respectively. 60

Figure 5. 17 Raman spectroscopy of TiO_2 nanotubes: As-prepared, 200°C annealed, and 400°C annealed 62

Figure 5. 18 Antimicrobial activity test 1 against S.aureus. Error bars indicate standard deviation (n=3)..... 64

Figure 5. 19 Antimicrobial activity test 2 against S.aureus. Error bars indicate standard deviation (n=3)..... 67

Figure 5. 20 SEM images of S.aureus colonies after 4 hour culture on: ApNT, ApNT-AMP, AnNT and AnNT-AMP respectively 69

Figure 5. 21 The amount of peptide released from TiO_2 nanotubes in 1 hour. Error bars indicate standard deviation (n=3). The as-prepared nanotube and 400 °C annealed nanotube groups showed an average AMP release amount of 9.52 and 12.99 µg/cm2, respectively..... 70

Figure 5. 22 SEM images of MG-36 cells after 30 hour culture on: ApNT, ApNT-AMP, AnNT and AnNT-AMP respectively 72

Figure 5. 23 MTT assay was performed to evaluate the cytotoxicity of HHC-36 with MG-63 osteoblast-like cell in the solution. Error bars indicate standard deviation (n=3). No statistical difference in cell activity between the control and HHC-36 solutions when the concentration is lower than 200µg/ml 73

Figure 5. 24 MTT assay was performed to evaluate the cytotoxicity of TiO_2 nanotube samples with/without AMP. Error bars indicate standard deviation (n=3). High standard deviations were found for the nanotube samples 74

Figure 6. 1 Comparison of antimicrobial activities of samples loaded with different protocols..79

LIST OF ABBREVIATIONS

AMP	Antimicrobial peptide
ANOVA	One-way analysis of variance
Arg (R)	Arginine
CaP	Calcium phosphate
CFU	Colony forming unit
CJRR	Canadian Joint Replacement Registry
DMSO	Dimethyl sulfoxide
EDS	Energy dispersive spectroscopy
EDTA	Ethylenediaminetetraacetic acid
Lys (K)	Lysine
M	mol/L
MHB	Mueller Hinton Broth
MRSA	Methicillin-resistant *Staphylococcus aureus*
MTT	(3-(4, 5-dimetyl-2-tiazolyl)-2, 5-diphenyl-2H-tetrazolium bromide
PAA	Porous anodic alumina
pI	Isoelectric point
QSAR	Quantitative structure activity relationship
RBA	Rapid breakdown anodization
S. aureus	*Staphylococcus aureus*
SEM	Scanning electron microscopy
S. epidermidis	*Staphylococcus epidermidis*
TiO_2	Titanium dioxide or Titania
Try (W)	Tryptophan
XRD	X-ray Diffraction

ACKNOWLEDGEMENTS

I would like to thank my supervisor Dr. Rizhi Wang for giving me such a great chance to work on this exciting project and for all the guidance, support and inspirations during the past two years.

I want to thank Dr. Chuan-fan Ding and Dr. Joy Hui for performing mass spectrometry on my samples; Dr. R.E.W.Hancock and Dr. Jayachandran N Kizhakkedathu for all the suggestions and technical supports for my project; and all my lab-mates: Vincent Ebacher, Mehdi Kazemzadeh Narbat, Shanshan Lu, Millie Kwan, Jianpeng Zou, Chia-Jade Lee, Timothy Chan and Tengteng Tang for the great time we had together. I want to express my special thanks to Dr. Mehdi Kazemzadeh Narbat for his extensive assistance in the antimicrobial tests, cell culture and MTT assay.

Finally, I want to express my deep appreciation to my family and all my friends for everything you have done for me, without your consistent love and support, I can never achieve my current stage.

Chapter 1 Introduction

Among the various complications that lead to the failure of orthopaedic implants, prosthetic-related infections have been reported as one of the major causes. Local delivery of antimicrobial agents through the implants surface is an ideal solution to the peri-implant infection problem, and has received much attention recently. There are two key challenges: the proper selection of the antibiotics and the development of the drug delivery system.

The rising problem of infections caused by multi-antibiotic resistant bacteria, or so-called superbugs, makes traditional antibiotics less effective for peri-implant infections. The family of antimicrobial peptides (AMP) is one of the promising alternatives to traditional antibiotics. In the past three decades, such AMPs have drawn significant attention because of their rapid reaction on broad-spectrum bactericidal strains (including Gram-positive and Gram-negative bacteria, viruses, fungi, and some parasites [1-3]), low toxicity and immunogenicity [3], as well as complex killing mechanisms. AMPs thus have much lower possibility of developing resistance than traditional antibiotics. Most recently, significant progresses have been made in new AMPs identification and synthesis by combining QSAR modeling and rapid screening approaches in Dr. Hancock's Microbiology Lab at UBC, and a group of highly active small broad spectrum AMPs were achieved [4].

Titanium and titanium oxide are among the most commonly used materials for orthopaedic implants because of their unique functional properties, such as excellent mechanical properties, chemical inertness and biocompatibility. In 1999, Zwilling first reported on the

fabrication of TiO_2 nanoporous structure by anodization method [5]. In the follow decade, this process was optimized, and vertically oriented, well-organized TiO_2 nanotube arrays were achieved. In light of their high surface-to-volume ratio, controllable dimensions, excellent biocompatibility [6,7], adjustable wettability [6,8] and other promising properties, TiO_2 nanotubes are considered as an ideal carrier for drugs.

Despite active studies on using TiO_2 nanotubes to control the release of small molecules [9] and proteins [10], there have been very limited reports on antibiotics delivery using nanotubes, especially with AMPs. In the current study, we examined the possibility of using TiO_2 nanotubes prepared by anodization method as a carrier for AMP delivery. AMPs were loaded onto the nanotubes and the antimicrobial activities of the AMP-loaded TiO_2 nanotubes surfaces were investigated, as well as the biocompatibility and cytotoxicity of the samples. The goal of this research is to develop an anti-infectious surface that could be potentially applied to antimicrobial implants.

Chapter 2 Literature Review

2.1 Orthopedic implants-related infections

2.1.1 Orthopedic implants

The widespread use and dramatic success of orthopedic implants, including artificial joints and fracture fixation devices, has greatly improved the life of many patients suffering from joint diseases [11]. According to Canadian Joint Replacement Registry (CJRR) 2008-2009 annual report [12], the number of hospitalizations for hip and knee replacement has been increasing steadily in the past 10 years. In 2006, over 70,000 hip and knee replacements were performed in Canada. In US, it is estimated that the number of annual primary total knee replacements will increase from 450,400 in 2005 to 3.48 million by 2030, compared with a growth of annual primary total hip replacements from 208,600 in 2005 to 572,100 by 2030 (From American Academy of Orthopaedic Surgeons).

After the primary surgery, various complications may lead to the revision of the orthopedic implants such as dislocation, loosening, prosthetic-related infections, and etc.

2.1.2 Implant-related infections

Implant-related infections after joint replacement usually lead to increased antibiotic use, prolonged hospital stay, substantial costs, morbidity and mortality. When peri-implant infections happen, the bone marrow swells, which leads to the reduced blood supply to the bone because of the compression of blood vessels in the bone marrow [7,13]. As a result of inadequate blood

supply, the functions of bone cells (including osteoblasts, osteoclasts, and osteocytes) are drastically compromised, and some parts of the bone may die.

The risk for such implant-related infection after surgeries is reported to be in the range of 0.5-5% [14], while about 14% of the total hip and knee revisions are due to infections [15]. However, after revision surgery, the infection rate can significantly increase by up to 10% [14]. The cost for treating such infections is estimated to be at least $50,000 per patient and $250 million per year in US [16]. Considering the huge population of patients with orthopedic implants and the serious consequences, this problem should never be underestimated.

2.1.3 Pathogenesis of peri-implant infections

After the implantation surgery, the immune system defenses at the region around the implant are mostly depleted, which created favorable conditions for microbial colonization [14]. Despite the sterile techniques used, bacteria may attach to the implant surface at the time of surgery or at a later stage (via a haematogenous route). The bacteria adhesion onto implant surface can be described as a two-phase process: the initial, instant and reversible physical phase and the subsequent time-dependent, irreversible molecular and cellular phase [13,17]. After the initial physical adhesion phase, some of the bacteria may subsequently grow into a biofilm on the implant surface. This is the essential factor in the evolution of infections and is 10-1000 times less susceptible to the host immune system and antibiotics mainly because of the poor antibiotic penetration into the biofilm and the stationary phase of growth of the bacteria underlying the surface layer [14,18-20].

Most of the implant-related infections are caused by staphylococci, and two specific staphylococcal species, *Staphylococcus aureus* (*S.aureus*) and *Staphylococcus epidermidis* (*S.epidermidis*), which contribute to roughly 70% of all the infection cases (showed in Figure 2.1a) [14]. In order to prevent or treat implant-related infections, antibiotics are used. However, both *Staphylococcus aureus* and *Staphylococcus epidermidis* have long been noticed to have high potential of developing antibiotic resistance to traditional antibiotics, such as penicillin and methicillin/oxacillin (showed in Figure 2.1b), especially after the formation of biofilms on the implant surface [14]. One standard treatment procedure is to use high doses of antibiotics over a long period of time, which may exacerbate antibiotic resistance of the bacteria [21]. The development of antibiotic resistance can lead to devastating effects in the absence of any valid medical treatment to control the infection. One solution is by using non-traditional antimicrobial agents that have a low possibility of developing resistant phenotypes.

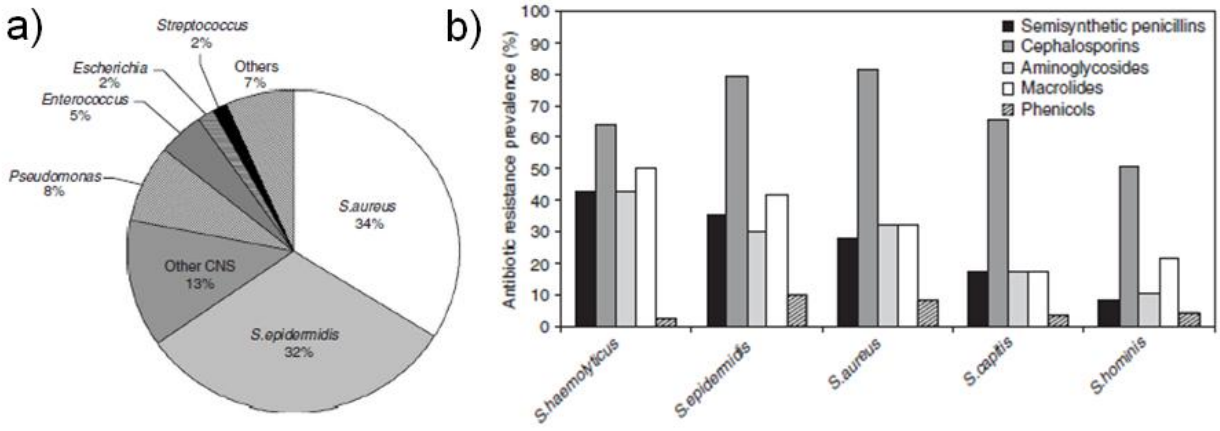

Figure 2. 1 a) Major pathogenic species for implant-related infections; b) Proportion of antibiotic resistant of infection-related bacteria to antibiotics (Reprinted from [14] with permission from Elsevier)

2.1.4 Treatment of implant-related infections

The common treatments of implant-related infections include: removal of the implant and associated cement, debridement of all devitalised tissue, and long-term antimicrobial treatment [22]. Despite the aggravated health condition, prolonged hospitalization, as well as the high cost, such treatments are not always effective. In order to prevent implant-related infections or lower the risk, various methods have been developed. Local delivery of antimicrobial agents through the implants surface is an ideal solution to the peri-implant infection problem, and has received much attention recently [13,23,24]. Although drugs are clinically administered in diverse ways, the delivery strategies can be generally divided into systemic drug delivery (intravenous, intramuscular and oral) and local drug delivery. Comparing with systemic drug delivery methods, locally delivering antibiotics through implant surface demonstrates numerous advantages, listed in Table 2.1.

Table 2. 1 Advantages of local drug delivery over systemic drug therapy (Reprinted from [25] with permission from Elsevier)

1. Low doses required
2. Greater control over toxicity and bioavailability of dose
3. Less susceptibility to promoting antibiotic resistance
4. Extended duration of release
5. Possibilities to combine local and systemic drugs with different kinetics
6. Controlled release from surfaces of combination devices directly to site
7. Avoidance of systemic drug exposure
8. Direct mitigation of device-centered infection using combination device release

To reach a good therapeutic effect, a careful assessment of the antibiotic agent, including effective dosage, release kinetics, as well as the side-effects to the patient is essential. Taking

implant-related infection as an example, the pathogens of the infection (microbial colonization and biofilm formation), antibiotic resistant, and the toxicity of the antibiotics, have to be considered when we are selecting antibiotics and drug delivery strategies. An ideal local antibiotic release profiles for implant-related infection should exhibit burst release (high release rate) in the initial stage to kill all the bacteria attached on the implant during the surgery, followed by a long term drug release with the therapeutically effective dosing zone to continually prevent infection [25].

2.2 Antimicrobial peptides (AMPs)

Due to the increasing resistance of implant-related infection pathogens to the traditional antibiotics, a family of non-traditional antimicrobial agents – antimicrobial peptides (AMPs) – are considered as potential alternatives to traditional antibiotics. Antimicrobial peptides have been found widely distributed in organisms, and function as part of their first line of defence [26]. These peptides can be directly antimicrobial or can play an important role in the functioning and orchestration of innate immune and inflammatory responses of mammals, amphibians, and insects [3,27]. In general, AMPs are amphipathic (having hydrophobic and charged, hydrophilic patches on their surfaces), small (12-50 amino acids) and cationic (have at least two positive charges because of arginine or lysine residues) [1,26]. There are four major structural categories of AMPs (shown in Figure 2.2), including α-helices, β-sheets, loop structures and extended structures [3].

In the past three decades, such AMPs have drawn significant attention because of their rapid reaction on broad-spectrum bactericidal strains (including Gram-positive and Gram-negative bacteria, viruses, fungi, and some parasites [1-3]), low toxicity and immunogenicity [3], and as well as complex killing mechanisms, which make them less possible to develop resistance than traditional antibiotics. Recently, significant progresses were made in new AMPs identification and synthesis by combining quantitative structure activity relationship (QSAR) modeling and rapid screening approaches in Dr. Hancock's Microbiology Lab at UBC, and a group of highly active small broad spectrum AMPs were achieved [4].

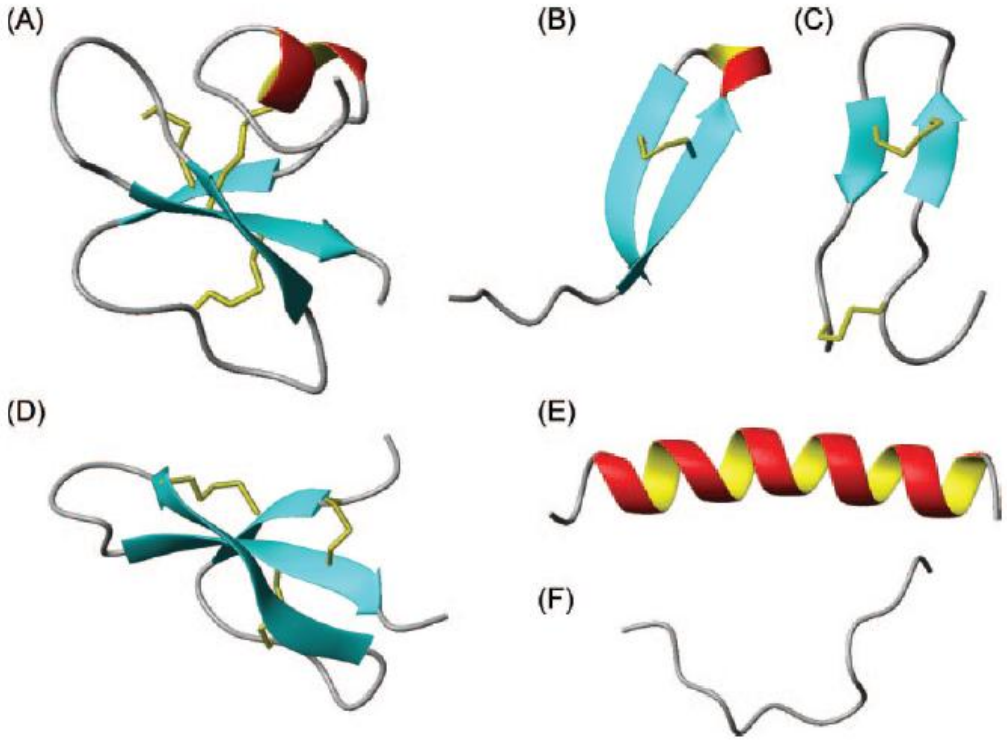

Figure 2. 2 Typical Antimicrobial peptides structures (A) Mixed structure of human β-defensin-2; (B) looped thanatin; (C) β-sheeted polyphemusin; (D) rabbit kidney defensin-1; (E) α-helical magainin-2; (F) extended indolicidin (Reprinted from [26] with permission from American Society for Microbiology)

2.3 TiO_2 nanotubes

2.3.1 TiO_2 properties and applications for orthopedic implants

Titanium dioxide (TiO_2), or titania, the most common compound of titanium, has been used in a wide variety of applications, including paints, anticorrosion, self-cleaning coatings, solar cells, photocatalysis, and biomedical applications because of its highly functional properties, such as wide band gap semiconductivity, excellent mechanical properties, chemical inertness and biocompatibility. There are three major types of TiO_2 crystal structures: rutile, anatase and brookite; rutile is the most common and stable form in nature [28].

Titanium and its alloys, particularly Ti-6Al-4V and Ti-6Al-7Nb, are among the most widely used materials for orthopedic and dental implants since 1970, because of their excellent biocompatibility [7,29]. It has been reported that the natural oxide layer formed on the surface plays a critical role in the biocompatibility [30-31]. Pure titanium metal lacks bioactive properties, such as osteoconductivity. Thin TiO_2 layer on Ti surface would enable titanium implants to bind with natural bone [32-34].

2.3.2 Processing of TiO_2 nanotubes

Several methods have been developed for the titania nanotubes fabrication, such as deposition into nanoporous template, sol-gel, seeded growth, hydrothemal processes and anodization method [35]. Among these technologies, anodization of titanium in fluoride-based electrolyte has received great interest because of its controllable, reproducible results as well as the simple process [36].

In 1999, Zwilling first reported on the fabrication of self-ordered TiO_2 nanotubular structure by anodizing Ti in electrolytes containing fluoride ions [5]. In the following years, this process was optimized, and well organized, vertically oriented nanotube arrays with variable diameter (10-300nm) and thickness (0.5-360μm) [7,37] were achieved. Meanwhile, this method was extended to diverse transition metals (such as Hf, Ta, W, Nb, and Zr) as well as their alloys (such as TiNb, TiZr, TiAl, Ti6Al7Nb and Ti6Al4V) [38].

Depending on the materials to be anodized, as well as other anodizing parameters (such as electrolyte, temperature, voltage etc.), two morphologies are typically achieved: nanoporous and nanotubular structure (showed in Figure 2.3) [7]. The reason for these two different morphologies is not very clear yet. One possible explanation is because of the electric field and local heating-enhanced dehydration [7].

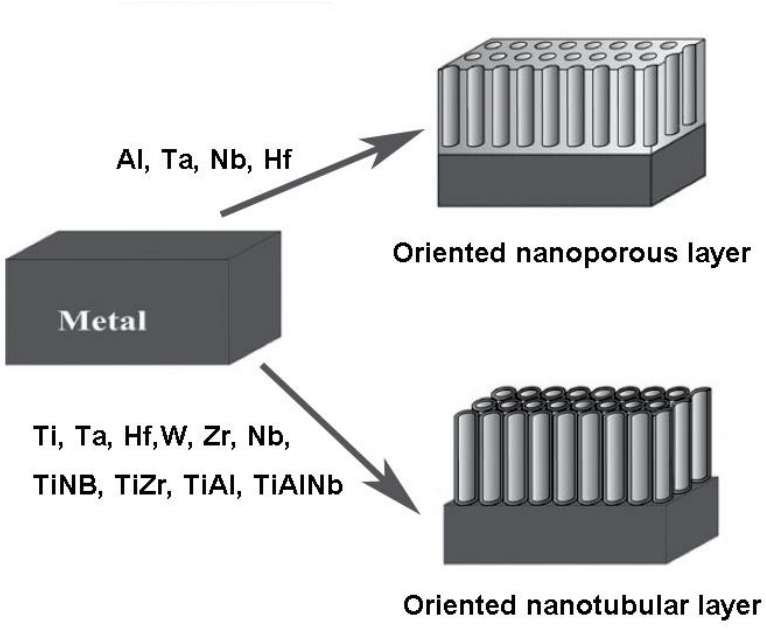

Figure 2. 3 Schematic of two typical morphologies (nanoporous and nanotubes) of oxide layers formed by the anodization method [7,38]

Formation of oxide layer on transition metals (such as Ti) surface using anodizing method has been carried out for almost one century [38]. Depending on the anodization conditions, the oxide layer formed on the titanium surface can be either compact (for most electrolytes) or nanoporous (in electrolytes containing F^- ions, showed in Figure 2.4) [6].

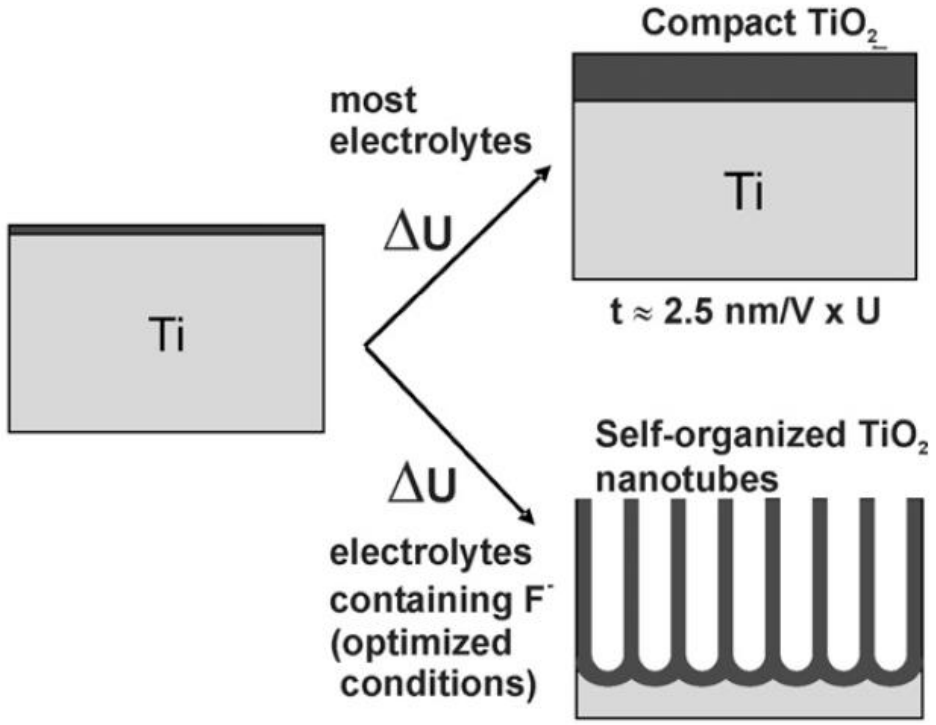

Figure 2. 4 Depending on the anodization conditions, the oxide layer can be either compact, or nanoporous (Reprinted from [6] with permission from Elsevier)

As we know, there is a very thin natural oxide layer (few nanometers thickness) on the titanium surface that protects the metal from corrosion. In order to improve the corrosion resistant property, efforts have been made on making thicker and uniform oxide layers on Ti surface using anodization method, also known as coloring process [32]. Figure 2.5 shows an example of the oxide layer on titanium implants prepared under different anodizing voltages. By

increasing the anodizing voltage, the thickness of the oxide layer increases, which leads to the coloring of the screws because of the optical effect [32,39].

Figure 2. 5 Coloring of the clinical titanium implants prepared by galvanostatic oxidation; the native oxide film (far left), the interference colors consecutively anodized at 20, 40, 80, 100, 180 and 200 V to the right, in 0.5 M tartaric acid (Reprinted from [39] with permission from Elsevier)

The formation process of the compact oxide layer on titanium surface is generally explained using a so-called high field mechanism [38], illustrated in Figure 2.6a. The key process is the diffusion of ions through the oxide layer (Ti^{4+} ions migrate towards oxide-electrolyte interface from the metal-oxide interface, while the O^{2-} ions migrate towards metal-oxide interface from the electrolyte-oxide interface) under the applied field. With the increasing of the oxide layer thickness, the process will gradually slow down and finally become self-limited [38]. Increasing the anodizing voltage will improve the diffusion of the ions, which will lead to a thicker oxide layer.

2.3.3 The formation of TiO_2 nanotubes

It was not until 1999, when Zwilling reported on fabrication of self-ordered TiO_2 nanotubular structure by anodizing Ti in electrolytes containing fluoride ions [5], that scientists first realized that TiO_2 nanotubes can be fabricated by anodization method. In the past few years, some studies were done on the nanotube growth mechanism. It is generally accepted that the forming mechanism of TiO_2 nanotubes is similar with that of nanoporous alumina (PAA), shown in Figure 2.6b [6,35,40]. There are three key processes involved:

I. Water in the electrolyte interacts with Ti anode, and a thin compact oxide layer is formed on Ti surface;

$$\begin{aligned} &Anode: Ti + 2H_2O \rightarrow TiO_2 + 4H^+ + 4e \\ &Cathode: 2e + 2H_2O \rightarrow H_2 \uparrow + 2OH^- \end{aligned} \qquad (1)$$

II. Field-assisted dissolution of the oxide at the oxide/electrolyte interface [35]. Under the application of the electric field, Ti^{4+} ions migrate from the metal/oxide interface towards the oxide/electrolyte interface and dissolved into the electrolyte, while the free O^{2-} anions migrate towards the metal/oxide interface to interact with the metal;

$$Ti^{4+} + 6F^- \rightarrow [TiF_6]^{2-} \qquad (2)$$

III. Chemical dissolution of titania as soluble fluoride complexes at the oxide/electrolyte interface;

$$TiO_2 + 6F^- + 4H^+ \rightarrow [TiF_6]^{2-} + 2H_2O \qquad (3)$$

Figure 2.6c is the schematic diagram of the TiO_2 nanotubes formation process. In the first stage, a compact titania layer is formed on the Ti foil surface. After that, small pits formed

randomly on the surface (stage 2), due to the localized dissolution of the oxide, mainly process II (the distribution of the field-assisted dissolution is strongly influenced by the Ti surface morphology [35,40]). These pits will function as pore forming centers and convert into bigger pores and increase density. Meanwhile, the tube growth occurs due to the inward movement of the oxide layer at the bottom of the pore (stage 3) [40-42]. Finally, when a balance between reactions 1-3 is established (the oxide formation rate is equal to the dissolution rate), the thickness of the nanotube layer stops increasing (stage 4).

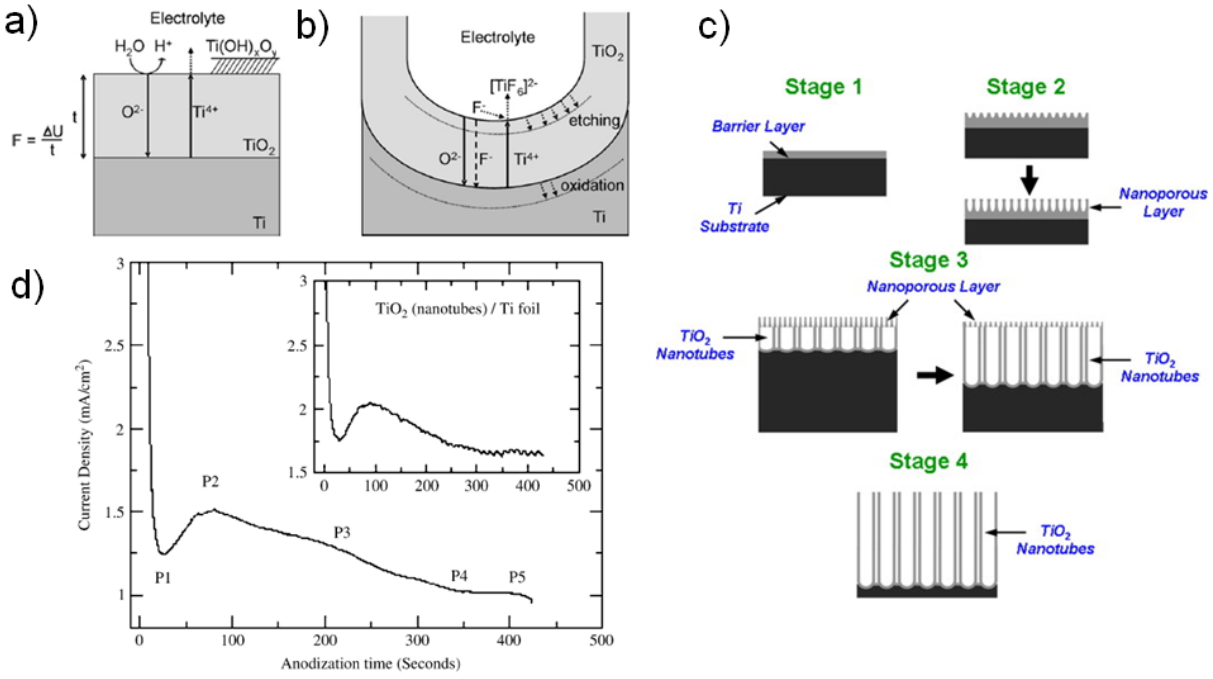

Figure 2. 6 Schematic diagram of the TiO_2 oxide layer formation mechanism: a). Compact oxide layer; b). Nanoporous oxide layer (Reprinted from [6] with permission from Elsevier); c). Evolution of a nanotube during anodization process: (Stage 1) thin compact oxide layer formation, (Stage 2) pit formation on the oxide layer, (Stage 3 & 4) growth of the pit into tubular structure (Reprinted from [41] with permission from Elsevier); d). Typical current density vs. time response observed for a titanium anodization behavior (400nm Ti foil anodized at 10V in HF-based electrolyte) (Reprinted from [35] with permission from Elsevier)

Figure 2.6d shows a typical current density vs. time curve acquired during titania nanotube growth. In the first stage, a compact oxide layer formed on Ti foil, which functions as the barrier layer that leads to the rapid drop of the current density (P1). In stage 2, small pits start to form, which make the ion transport possible again. As a result, the current density increases slightly (P2). Finally, a balance between oxide formation and dissolution is established, so the current density becomes stable gradually (P3, P4 & P5) [35,40].

2.3.4 Evolution of the TiO_2 nanotubes

In the past decade, three generations of fluoride-based electrolytes have been developed for anodic TiO_2 nanotube array preparation [6,43,44]. The first generation of TiO_2 nanotubes was grown in dilute hydrofluoride acid (HF) aqueous electrolytes. But the limited thickness of the oxide layer (only up to a few hundreds of nanometers) has restricted its applications [6,43-44]. The reason for that is assumed to be the fast dissolution of TiO_2 in HF-containing electrolytes because of the high acidity [45]. Therefore, in order to have better control of the pH value, buffered neutral electrolytes (NaF or NH_4F), instead of HF, were used, and the second generation of TiO_2 nanotube arrays with a few micrometers thick were successfully fabricated in 2005 [44-46]. Later, by using nonaqueous electrolytes (such as glycerol or ethylene glycol), ultrahigh aspect ratio (length/diameter) nanotubes were achieved [6,43,44]. For example, Haripriya and coworkers [37] reported successful fabrication of nanotubular membrane with a thickness of 360um using ethylene glycol based electrolyte in 2007. Meanwhile, it has been found that by using water-free electrolytes, nanotubes with very smooth wall can be obtained. Some examples of TiO_2 nanotubes prepared under different conditions are showed in Figure 2.7.

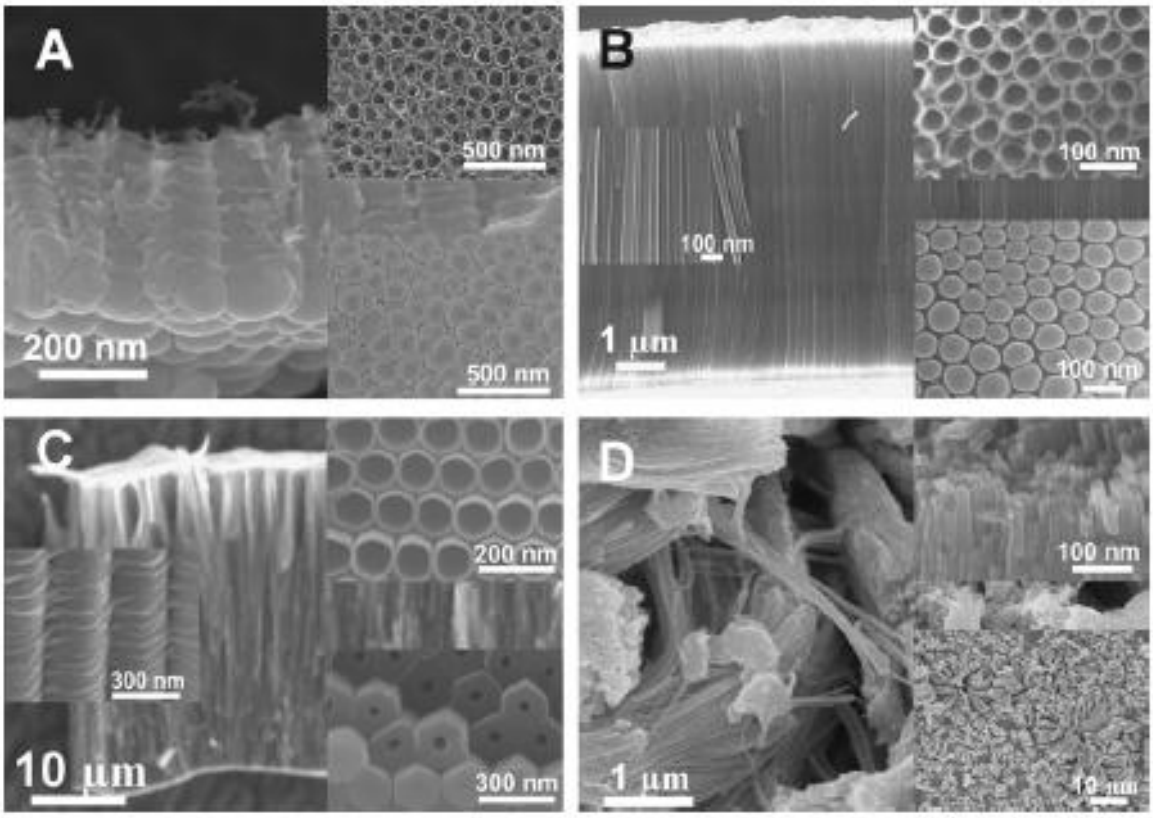

Figure 2. 7 SEM images of TiO_2 nanotubes grown by different anodization processes: (A) Typical morphology obtained in HF-based electrolytes; (B) glycerol/fluoride electrolytes; (C) ethylene glycol/fluoride electrolytes; (D) tubes grown by a different approach: rapid breakdown anodization (RBA); these tubes grow in disordered bundles within seconds at comparably high anodic potentials (Reprinted from [6] with permission from Elsevier)

Moreover, several new morphologies have also been reported. By selective chemical etching of the nanotubes on the bottom side, two-ends open nanotubes were made [47]. When an alloy with multi-phase structures was anodized, oxide nanotubes with two discrete size scales can be achieved [48]. Under some specific conditions, double-walled TiO_2 nanotubes can also been formed [49].

Most recently, active studies have been done on two-step anodization method. For example, Li and coworkers [40] found that when the voltage in the second-step was lower than the first-step, a lotus root-shaped TiO_2 nanostructure was achieved. There are some advantages with the two-step anodization method. First, by applying different anodizing conditions (voltage, electrolytes, temperatures etc.) in two steps, multilayer nanotubes with different morphologies at different layers can be achieved [37,50]. Second, if the nanotube layer formed in the first step were removed, the bottom imprints left on Ti foil can function as the "pre-ordering" guides for the second nanotube layer, thus improving the ordering of the nanotube arrays [40,51].

2.3.5 Crystallographic structures of TiO_2 nanotubes

It has been reported that as-prepared TiO_2 nanotubes are amorphous. In order to produce crystalline phases, post heat-treatment is necessary [6,35,38,52]. After annealing at temperature higher than 300°C in air, the amorphous nanotubes can be transformed into anatase phase; while rutile phase would appear when the temperature is higher than 450°C (shown in Figure 2.8) [6,38]. However, up to now, a complete transformation to rutile phase without morphology deterioration is still not successful. In order to completely transform anatase phase TiO_2 nanotubes into rutile phase, high temperature (higher than 650°C) is necessary, when sintering and collapse of the tubes happen [6,38].

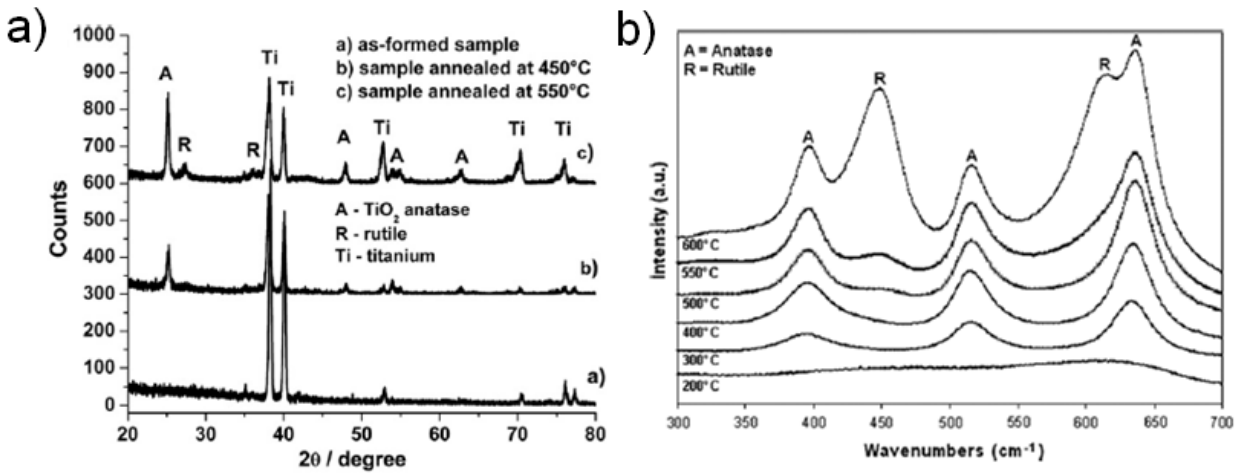

Figure 2. 8 The crystal structure of TiO_2 nanotubes annealed at different temperatures: a) XRD pattern (Reprinted from [6] with permission from Elsevier); b) Raman spectroscopy pattern (Reprinted from [52] with permission from John Wiley and Sons)

2.3.6 Functional properties of TiO_2 nanotubes

2.3.6.1 Biocompatibility

Titanium and titania has been extensively used for biomedical applications, such as implants, tissue engineering, and drug delivery systems, because of their excellent biocompatibility. It is well known that the cellular response is strongly affected by the surface morphology. Studies have demonstrated positive cell response to nanotopography, both *in vitro* and *in vivo* [33]. Therefore, when the well-organized, vertical-oriented TiO_2 nanotube arrays were successfully fabricated, it attracted wide interests from biomaterials researchers.

Studies by Oh et al. have showed that the presence of the TiO_2 nanotube layer significantly accelerated osteoblasts' growth and adhesion [34]. A much stronger bone bonding

compared to micro-porous sandblasted Ti surfaces was found after four weeks of implantation in rabbit tibia [53]. Further study showed that the osteoblast behavior changed with the nanotube diameters: small diameter (~30 nm) promoted the highest degree of osteoblast adhesion, while larger diameter (70–100 nm) nanotubes elicited a lower population of cells with extremely elongated cellular morphology and much higher alkaline phosphatase (ALP) levels [33]. Similar phenomenon was observed in human mesenchymal stem cells (hMSC): small (~30nm) nanotubes promoted adhesion without noticeable differentiation, whereas larger (70-100nm) nanotubes elicited a dramatic stem cell elongation, which induced cytoskeletal stress and selective differentiation into osteoblast-like cells [54]. *In vitro* studies by other groups also demonstrated the excellent biocompatibility of the TiO_2 nanotubes. For example, primary bovine aorta endothelial cells (BAECs) showed enhanced mobility, vasodilating bioactivity and endothelialization on nanostructured TiO_2 surface compared with flat Ti surface [55]. The increased adhesion of chondrocyte (cartilage synthesizing cells) on nanotube arrays provided opportunities for cartilage applications [56]. *In vivo* studies of TiO_2 nanotubes (diameter 30nm) in the front scull of pigs also confirmed the enhanced osteoblast functions and bone formation [57].

2.3.6.2 Adjustable wettability

The wettability of implant surface plays a very important role in biomolecule adsorption and cell adhesion [8]. It is a great advantage if the wettability of implant surface can be adjusted according to its applications. Up to now, the reported approaches to control the wettability of TiO_2 nanotubes include the use of organic monolayers and UV illumination [6,8].

It has been reported in the literature [6,8,58-61] that the water contact angle for as-prepared TiO_2 nanotubes without any modification is very close to 0°, showing super-hydrophilic behavior. However, by attaching organic molecules onto the surface, the wettability can be modified dramatically, from super-hydrophilic (contact angle lower than 5°) to super-hydrophobic (contact angle higher than 150°). For example, Balaur et al [8] reported that by covering the nanotubes with octadecylsilane or octadecylphosphonic acid molecules, the contact angle increased up to 165±2° for the silane-SAMs, and 167±2° for phosphonic acid-SAMs. Moreover, such kind of modification is reversible. By adjusting UV illumination duration, the contact angle can be altered according to the application requirement [8,58,61].

2.3.6.3 Other properties

In addition to the biocompatibility and adjustable wettability mentioned above, TiO_2 nanotubes showed other promising properties for biomedical applications. One example is the excellent photocatalysis. It has been reported that TiO_2 could be used as a photocatalyst to decompose unwanted and harmful organic compounds in contaminated air and water (self-cleaning properties) [51,62]. Recently, promising result has also been reported to apply the photocatalysis for photo-induced cancer cells killing [62]. Another example is that, TiO_2 nanotubes layer can be used as the template for calcium phosphate deposition. Jin et al. illustrated that accelerated HAp formation by the presence of NaOH treated TiO_2 nanotubes [63].

2.3.7 TiO_2 nanotubes for drug delivery

In light of the diverse functional properties of TiO_2 nanotubes, including the high surface-to-volume ratio, controllable diameter and length, excellent biocompatibility, adjustable wettability, and self-cleaning property, TiO_2 nanotubes prepared by anodization method are considered as an ideal drug delivery carrier, and some previous studies have shown promising results. For example Popat et al. demonstrated the controllable release of proteins (bovine serum albumin and lysozyme) [10] and antibiotics (gentamicin) [13], loaded onto TiO_2 nanotubes (80nm diameter and 400nm long), in the order of hours. Both studies also showed that there was a slower and sustained release from the nanotubes loaded with a higher amount of protein/drug than those loaded with lower amounts. Recently, Peng and coworkers [9] reported the influence of TiO_2 nanotube size (diameter/length) on the drug loading amount and release profile, and it illustrated the possibility of controlling long term elution of small molecule and protein (small molecules delivery in the order of weeks, while larger molecules in the order of months). Furthermore, four different drug loading methods were investigated (showed in Figure 2.9) [58], and it demonstrated the feasibility of loading drug onto TiO_2 nanotubes by either physical adsorption or chemical immobilization method.

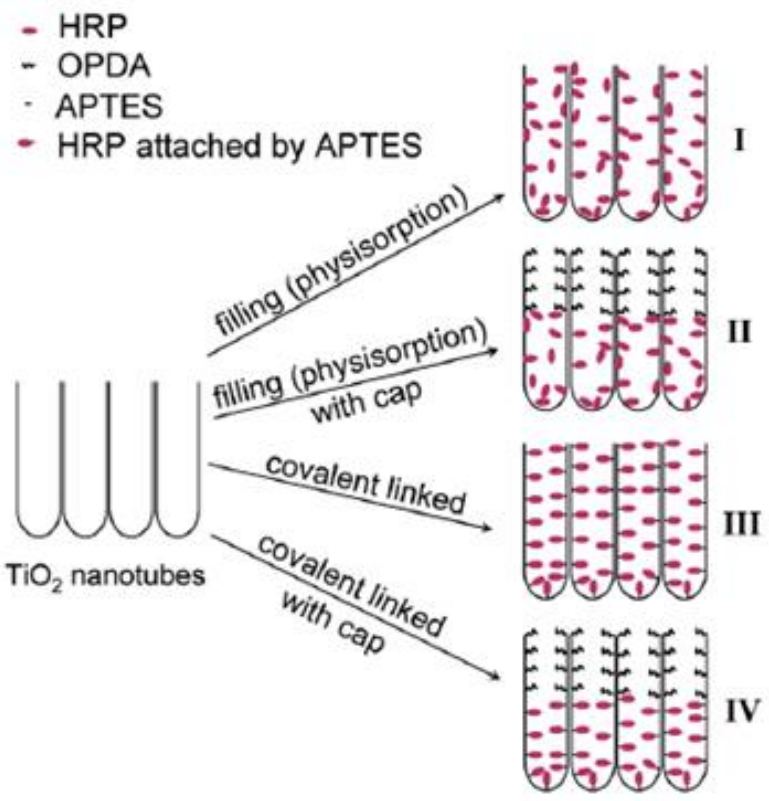

Figure 2. 9 Four different drug loading methods using horseradish peroxide (HRP) as a hydrophilic model drug: (I) immersion without any TiO_2 surface modification, (II) immersion after OPDA modification in the upper nanotube layer (hydrophobic cap), (III) covalently attached HRP over the entire nanotube layers, (IV) OPDA cap in the upper nanotube layer and covalently attached HRP in the lower nanotube layer (Reprinted from [58] with permission from American Chemical Society)

2.4 Local delivery of antibiotics through implant surface

As discussed above, one ideal solution for implant-related infections is to develop an antimicrobial implant surface that can locally deliver antibiotics. To fulfill this purpose, there are two key challenges. The first one is the proper selection of the antibiotics that can avoid

antibiotic resistance, such as AMPs. The second one is to develop a suitable drug delivery system that can effectively release the antibiotics according to the ideal local antibiotic release profiles mentioned in Section 2.1.4.

The diverse drug delivery techniques developed so far can be generally divided into physical adsorption, chemical immobilization, and surface coating method (shown in Figure 2.10).

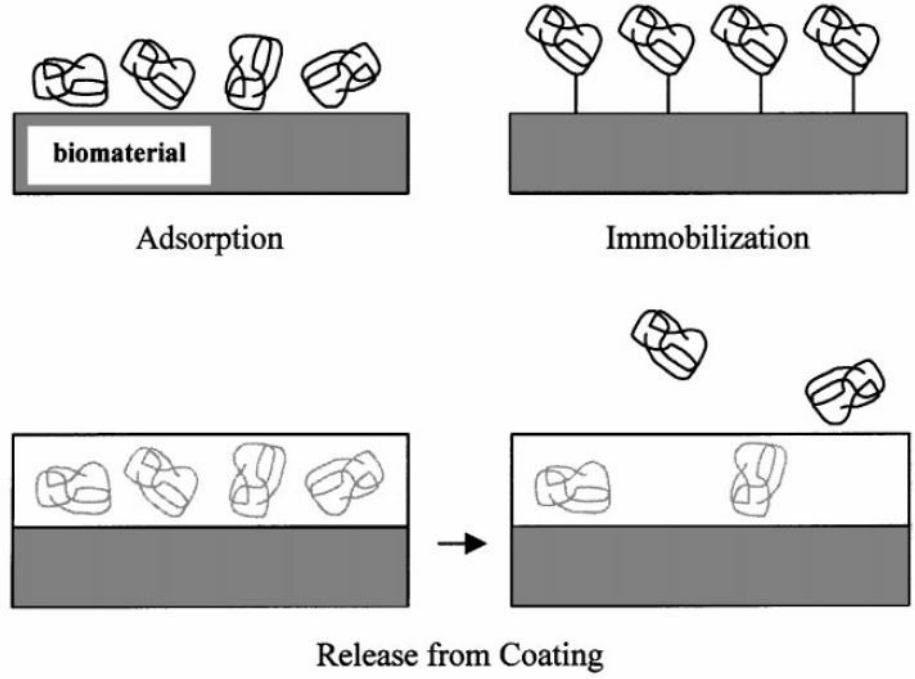

Figure 2. 10 Schematic diagram of the drug delivery methods: Physical adsorption, Chemical immobilization and release from a surface coating (Reprinted from [64] with permission from Elsevier)

2.4.1 Physical adsorption

The simplest way to load antibiotics onto implant surface is by soaking it directly into a solution with antibiotics. Through the van der Waals, hydration force (due to the nature of hydrophilic/hydrophobic), and electrostatic force, drug molecules will be able to attach to the implant surface. Martin and coworkers [64-66] showed that by loading growth factor (rhTGF-β) onto tricalciumphosphate (TCP) coated implant surface (Ti-6Al-4V) using simple physical adsorption method; the peri-implant bone formation process was accelerated. However, there is less control over the drug release profiles which makes it unsuitable for long term applications.

2.4.2 Chemical immobilization

Grafting biomolecules onto implant surface is an alternate drug loading method. Since there are chemical bonds (commonly covalent bonds) between drug molecules and implant surface, the biomolecules are expected to able to retain on the surface for a relatively longer period than physical adsorption method. For the metals used in orthopedic applications, due to the very thin natural oxide layer, there would be some hydroxyl groups on the surface, which provide locations for the bonding using silane chemistry [64]. Up to now, biomolecules, such as proteins, peptide and enzymes, have been successfully immobilized onto Ti [67], Ti alloys [68] and other biomaterials. Besides the control over the drug release profiles, chemical immobilization method also provides possibility of particular orientation of drug molecules on implant surface.

2.4.3 Surface coating

Incorporating biomolecules with surface coating is another drug delivery method. Compared with physical adsorption, this method has better control of the biomolecule release profile. Up to now, various coating materials, such as calcium phosphate (CaP), silica gel, collage, poly(lactide-coglycolide) (PLGA) and etc [64,69], have been explored for the drug delivery purpose. Because of its chemical similarity with the mineral component of natural bone, CaP coatings are commonly used for orthopedic applications (such as implant for bone reconstruction) [69,70]. It has been reported in literature that organic components (such as collagen and growth factors) can be incorporated with the porous CaP coatings to achieve different purposes. The TiO_2 nanotube coating, discussed above, is another potential inorganic surface coating for bone implants.

2.5 AMPs delivery

Despite active researches on the immobilization of peptides onto implant surfaces to enhance cell adhesion and bone growth, reports regarding the delivery of antimicrobial peptides on a solid surface have been very limited [20]. Our previous study suggested that AMPs can be effectively attached onto titanium surface through physical adsorption, chemical immobilization (covalent bond) and CaP coatings, and all of them showed positive bacteria inhibitory activity. However, under physiological conditions, a burst release of the majority of the peptides attached onto titanium surface via physical adsorption method is expected during the first few hours, therefore, the long term effect could not be guaranteed. On the other hand, immobilization of peptides onto Ti surfaces through short linker may limit the peptide mobility, which may

compromise the antimicrobial activities of the peptide [70]. The best results came from the CaP coatings. However, the weak interface of the coating makes it unsuitable for long term applications. In light of their nanosize morphology, unique functional properties, as well as the strong interface, TiO_2 nanotube coating is a potential carrier for delivering AMPs.

2.6 Summary

An ideal treatment for peri-implant infections is to locally deliver antimicrobial agents through the implant surface. Traditional antibiotics are facing the challenge of increasing resistance of pathogens. Due to their board-spectrum activity and complex killing mechanism, antimicrobial peptides have attracted great interests and are considered as potential alternatives to traditional antibiotics to kill implant infection-related bacteria. Studies on TiO_2 nanotubes prepared by anodization method have illustrated their excellent biocompatibility, adjustable wettability and some other functional properties for biomedical applications. Therefore, it is considered as an ideal candidate for the antimicrobial drug delivery. There have been very limited studies on locally delivering antibiotics, especially with AMPs, using TiO_2 nanotubes. The goal of this study is to develop a novel antimicrobial implant surface by loading AMPs onto TiO_2 nanotubes.

Chapter 3 Scope and Objectives

3.1 Scope

This study is a part of the collaborating project named "Novel Antimicrobial Surfaces for Orthopaedic Applications" funded by CHRP. The goal of this thesis is to develop an antimicrobial implant surface that can locally deliver antibiotics for peri-implant infection problems.

In past years, progresses in designing, screening and processing antimicrobial peptides using the peptide spot synthesis method have been made in Dr. Hancock's Microbiology Lab at UBC, and several short, cationic, and potent AMPs have been successfully developed. In this study, one of the most potent broad-spectrum AMP, HHC-36 (KRWWKWWRR), was selected as the test AMP for local delivery and antimicrobial activity study.

TiO_2 nanotubular structures fabricated by anodization method have attracted great interest in the past decade because of its simple process, controllable and reproducible results [36]. In light of their high surface-to-volume ratio, controllable dimension, excellent biocompatibility [6,7], adjustable wettability [6,8] and other promising properties, the TiO_2 nanotubes are considered as an ideal carrier for drugs.

There have been no reports in literature on AMP delivery using TiO_2 nanotubes prepared by anodization method. Since the goal is to develop an anti-infectious implant surface, the antimicrobial activities, biocompatibility and cytotoxicity of the AMP-loaded TiO_2 nanotubes samples will need to be investigated.

3.2 Objectives

The specific objectives of this study are:

1. Optimizing the anodizing process and investigating the influences of anodizing conditions on nanotube morphology, including the electrolyte composition, pH value, voltage, anodizing time.

2. Testing the effect of AMP loading conditions, such as time and concentration, on the drug loading efficiency.

3. Evaluating the antimicrobial activities of the AMP-loaded samples by *in vitro* bacteria culturing.

4. Detecting AMP *in vitro* release profile.

5. Examining the biocompatibility and cytotoxicity of the AMP-loaded TiO_2 nanotube samples, *in vitro.*

Chapter 4 Materials and Methods

4.1 Preparation of TiO_2 nanotubes by anodization method

4.1.1 Anodizing setup

In the current study, titanium dioxide nanostructures were prepared by anodization method using the experiment setup showed in Figure 4.1. A typical 2-electrode system was used, including a computer controlled DC power supply (Matsusada R4K-80 Series) and an electrochemical cell.

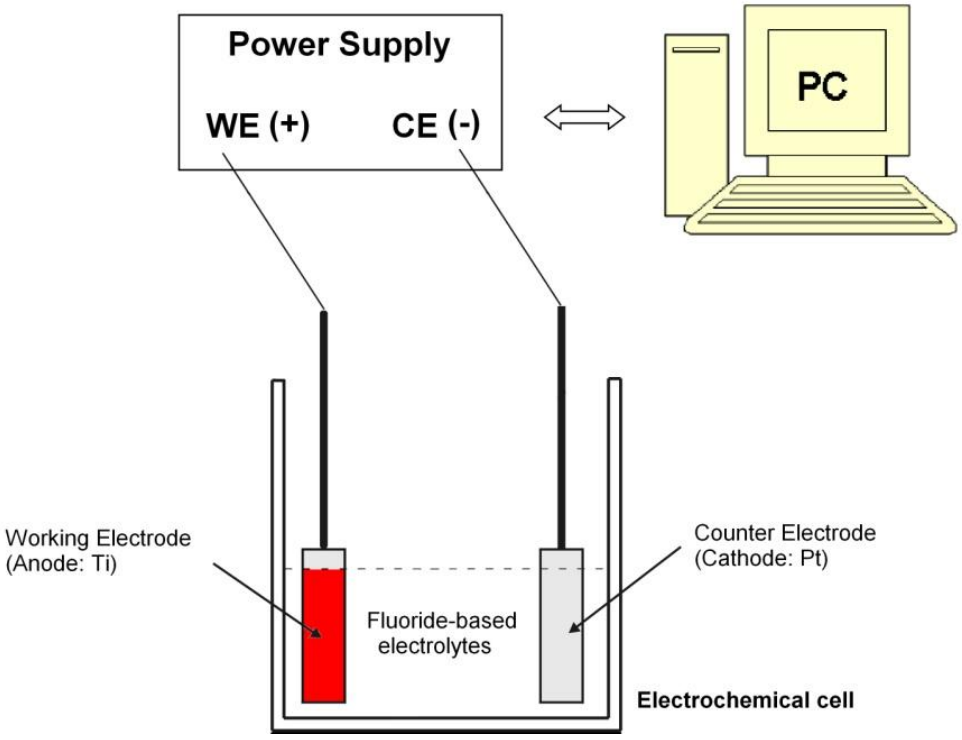

Figure 4. 1 Schematic diagram of the anodizing setup

Commercially pure titanium foils (0.1mm, 99.6% purity, Goodfellow) were used as the working electrode (anode), while a piece of platinum foil was functioned as the counter electrode

(Cathode). As showed in Figure 4.2, the system includes a beaker, an electrode fixture, 2 electrodes (Ti foil and Pt foil) and a magnetic stirrer (HAAKE MRS). The magnetic stirrer was used to reduce the thickness of the double layer at the Anode/electrolyte interface, and ensure uniform local current density and temperature over the Ti electrode surface [42].

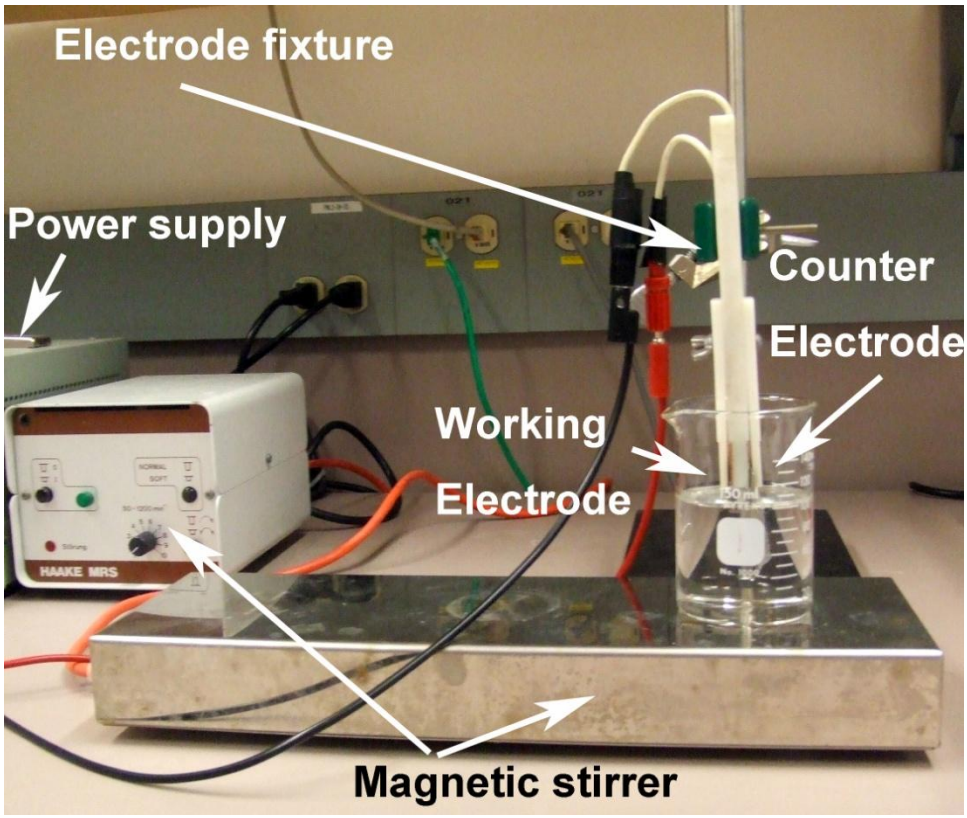

Figure 4. 2 Experimental setup for titanium foil anodization

4.1.2 Processing of titanium dioxide nanotubes

Before anodizing, commercially pure Ti foils were cleaned ultrasonically in acetone, absolute ethanol, distilled water for 15 minutes respectively, and dried in the air stream. Then, both titanium and platinum foil were mounted on the fixture and partially immersed in the

electrolyte. During the anodizing process, a constant voltage was applied by the power supply for a given time. After the experiments, the samples were rinsed with large amount of distilled water and dried in the air. In this study, all the processes were performed at room temperature.

To optimize the anodizing process, the effects of various anodizing conditions were studied, including electrolyte composition, pH value, voltage, anodizing duration. Table 4.1 provides a summary of these conditions. Several electrolyte systems were used in the current study, including water based electrolytes (phosphoric acid based and ammonium sulphate based electrolytes) and organic based electrolytes (glycerol based and ethylene glycol based electrolytes).

4.1.2.1 Water based electrolytes

In our first set of experiments, TiO_2 nanotube fabrication were conducted in 0.3M phosphoric acid (H_3PO_4) solution containing a small amount of ammonium fluoride (NH_4F) within the range 0.07-0.27M. Later, in order to have a better control of the pH value, buffered neutral electrolytes, ammonium sulphate $(NH_4)_2SO_4$ was used, instead of H_3PO_4. Previous studies suggested that anodization voltage is the key factor controlling the nanotube diameter [6,71]. Therefore, in order to prepare nanotubes with different diameters, different voltages ranging from 20 to 40V were applied. To evaluate the change of nanotube film thickness with processing time, anodizing duration was varied from 1h to 6 h.

4.1.2.2 Organic based electrolytes

Organic based electrolytes, specifically glycerol based and ethylene glycol based electrolytes were used in our study in order to generate thicker TiO_2 nanotube coatings. It has been demonstrated in literature [72] that highly viscous organic electrolytes can effectively suppress local concentration fluctuations and pH bursts during anodizing process which result in smoother walls and higher aspect ratios and as a result a thicker coating can be achieved.

4.1.2.2.1 Glycerol based electrolytes

A set of experiments were carried out in solutions containing 0.27M NH_4F consisting of glycerol/water mixture with different volumetric ratios (98:2%, 75:25%, 50:50%, 25:75%). The aim of this study is to investigate the influence of electrolyte viscosity on the anodizing process and to generate better nanotube coatings. Estimation of the viscosity of glycerol-water mixture is still incomplete in the literature yet. Some formulas have been reported, however, most of them are only applicable to limited conditions [73]. But it is clear that increasing water content lead to a lower viscosity. The applied anodizing voltage varied from 20V to 40V, and anodizing duration was varied from 1h to 6 h.

4.1.2.2.2 Ethylene glycol (EG) based electrolytes

Additional experiments were performed in 98% ethylene glycol solution containing 0.27M NH_4F. The aim is to produce thicker nanotube coatings, because it was difficult to obtain nanotube coatings with a thickness over 5μm in other electrolyte systems. The applied anodizing voltage varied from 20V to 40V, and anodizing duration was varied from 1h to 22 h.

Table 4. 1 Summary of the anodizing parameters

	Supporting electrolyte	NH_4F (M)	Voltage (V)	Duration (h)
Water based electrolytes	0.3M H_3PO_4/ 1M $(NH_4)_2SO_4$	0.07-0.27	20-40	1-6
Glycerol based electrolytes	Water	0.27	20-40	1-6
EG based electrolytes	2% Water	0.27	20-40	1-22

4.1.3 Post-anodizing annealing

To investigate the effect of annealing on the morphology and crystal structure of the TiO_2 nanotube coatings, as well as the influence of crystallinity on the antimicrobial drug loading and eluting efficacy, the processed nanotubes were annealed at different temperatures.

The annealing was carried out in a chamber furnace (CARBOLITE Type 3216). Specimens were heated from room temperature (about 20°C) to the final setting temperatures (200/400°C) in air at a heating rate of 5°C/min, held for 3 hours, and cooled down in the furnace.

4.1.4 Materials characterization

4.1.4.1 Scanning Electron Microscope (SEM)

Scanning electron microscope (SEM Hitachi S3000N) was used for morphological observation of the titanium oxide coatings. Samples were sputter-coated with Au-Pd (60:40) alloy using Denton Vacuum Desk II sputtering coater (Moorestown, NJ, USA) before the

characterization. The thickness of the nanotube layer was measured directly from the SEM cross-sectional images of mechanically bent samples. The chemical composition of the nanotube coatings was analyzed using the Energy Dispersive Spectrometer (EDS) equipped in the SEM.

4.1.4.2 Raman spectroscopy

The crystalline phases of the coating were examined using a Renishaw Laser Raman Spectroscopy (inVia). The analysis was performed within the range 200-700cm^{-1}, which is an optimal region for discriminating between different crystal phases of TiO_2 [52].

It has been reported in literature that X-ray diffraction (XRD) can also be used for phase analysis of the nanotube coatings. However, in the current study, we found that the signals of the TiO_2 nanotubes were too weak, compared to the Ti substrate. However, due to its metallic nature, Ti has free electrons preventing the lattice vibrations [32] and as a result, Ti substrate does not have any peaks in the Raman spectrum.

4.2 Antimicrobial peptide loading onto TiO_2 nanotubes

One of the most potent broad-spectrum AMPs identified in Dr. Hancock's Microbiology Lab at UBC [21], HHC-36 (KRWWKWWRR), was selected for the current drug delivery study.

Our previous study [70] suggested that chemical immobilization of peptides onto Ti surfaces may limit the peptide mobility, which may compromise the antimicrobial activities of

the peptide. Therefore, in this study, a simple vacuum assisted physical adsorption method was used.

To load HHC-36 onto the nanotube samples, a 1mg/ml peptide solution was prepared by dissolving HHC-36 powders into a buffer solution (50 mM Na_2HPO_4 (CALBIOCHEM, Canada), and the pH value was adjusted by N/10 NaOH to 7.40). Then, samples (1×1cm) were immersed into 1ml of this peptide solution in vials, and the vials were placed in a vacuum system for 10 minute and kept for 1 hour at room temperature while being shaken gently. After that, the samples were rinsed with the buffer solution for 3 times, 30 seconds each time, to remove the excess peptide on the surface.

In order to investigate the effect of AMP loading conditions on drug loading efficiency, we later changed our AMP loading protocol by increasing the concentration of peptide solution from 1mg/ml to 2 mg/ml, and placed the samples (with peptide solution) into the vacuum system for 30 minutes and followed by gentle shaking for 20 hours at room temperature.

4.3 Antimicrobial test against *Staphylococcus aureus* (*S.aureus*)

As discussed in Chapter 2.1.3, about 70% of implant-related infections are caused by *Staphylococcus aureus* (*S.aureus*) and *Staphylococcus epidermidis* (*S.epidermidis*) [14]. In the current study, the antimicrobial activities of all specimens were tested against Gram-positive bacteria, *S.aureus*.

For each antibacterial experiment, *S. aureus* strains (in freeze-dried form) were cultured in rich media overnight prior to the experiment. After that, 100µl of the original bacteria solution was transferred into a sterile tube containing 5ml Mueller Hinton Broth (MHB) and incubated for 1h at 37^{o}C to obtain bacteria in the mid logarithmic phase of growth. The *S. aureus* bacterial suspension was then re-suspended in MHB to dilute the solution and provided a final density of ~10^{6} cells/ml.

To test the antimicrobial property of the AMP-loaded samples, a survival assay was performed. First, samples (1*1cm) were each placed in a well in a 12-well culture dish, and 1ml bacteria solution (~10^{6} cells/ml) was dripped into each well. After specific intervals of incubation (37^{o}C, humidified, 5% CO_2 and 20% O_2, keep shaking), the residual bacteria in the solutions were tested by incubating the bacteria solutions on nutrient agar plates overnight at 37°C and the number of survival bacteria was assessed by counting colony forming units (CFU).

4.3.1 Antimicrobial Test 1

Four groups of samples were tested against *S.aureus*, including: one negative control (bacteria solution only), one positive control (as-prepared TiO_2 nanotubes) and two AMP-loaded sample groups (as-prepared nanotubes and 400 °C annealed nanotubes). The purpose of including the annealed TiO_2 nanotube group was to investigate the effect of crystallinity on the antimicrobial efficacy. Three samples were tested from each group. The testing intervals were set to: 0, 30, 60,120 and 240 minutes. The antimicrobial activities of the groups were compared among the groups by ANOVA test and t-tests between every two groups. Table 4.2 is a summary

of the four groups used for antimicrobial test 1. Three samples were tested from each group. The testing intervals were set to: 0, 30, 60,120 and 240 minutes. The antimicrobial activities of the groups were compared among the groups by ANOVA test and t-tests between every two groups.

Table 4. 2 Design of experimental groups for antimicrobial test 1

Experiment Groups	**Design**
Control	Bacteria solution only
ApNT	As-prepared TiO_2 nanotubes
ApNT-AMP	As-prepared TiO_2 nanotubes loaded with AMP
AnNT-AMP	400 °C Annealed TiO_2 nanotubes loaded with AMP

4.3.2 Antimicrobial Test 2

To test the effect of loading conditions on the AMP loading efficiency, we changed our AMP loading protocol and a second antimicrobial test (Test 2) was performed.

Five groups of samples were tested, including: one negative control (bacteria solution only), two positive control groups (as-prepared nanotubes and annealed nanotubes) and two AMP-loaded sample groups (as-prepared nanotubes and annealed nanotubes). Table 4.3 is a summary of the groups for antimicrobial test 2. Three samples were tested from each group. The testing intervals were set to: 0, 60 and 240 minutes. The antimicrobial activities of the groups were compared among the groups by ANOVA test and t-tests between every two groups.

Table 4. 3 Design of experimental groups for antimicrobial test 2

Experiment Groups	Design
Control	Bacteria solution only
ApNT	As-prepared TiO_2 nanotubes
ApNT-AMP	As-prepared TiO_2 nanotubes loaded with AMP
AnNT	400 °C Annealed TiO_2 nanotubes
AnNT-AMP	400 °C Annealed TiO_2 nanotubes loaded with AMP

4.4 Bacteria adhesion on sample surfaces

The bacteria adhesion and the morphologies of bacteria (*S. aureus*) colony formed on different sample surfaces were studied. The samples for antimicrobial test 2, after 4 hour of bacteria growth, were examined using SEM. Before imaging, the bacteria fixation onto the sample surface, a critical part of the analysis, was performed using the following protocol:

1. Samples were washed with 0.1 M PBS three times, 1 min each time.
2. Samples were fixed with 2.5% glutaraldehyde in 0.1 M PBS for 2 hour at room temperature.
3. Samples were washed with 0.1 M PBS three times, 1 min each time.
4. Samples were dehydrated in graded ethanol (50, 70, 80, 90, 95 and 100%), 15 min each time.
5. Samples were dried in a critical point dryer.

After bacteria fixation, the samples were gold sputtered, and imagined using SEM.

4.5 *In vitro* Release of AMP

The *in vitro* drug release profile of the AMP-loaded nanotubes samples (both as-prepared nanotubes and 400°C annealed nanotubes) were studied using liquid chromatography-mass spectrometry (LC-MS, Varian). Each sample was placed in a capped vial containing 1ml buffer solution (the same buffer solution used for AMP loading) and was kept shaking at 37 ºC.

A 200µl solution was collected at regular intervals for up to 7 days (i.e. 1, 4, 24, 72, 168h). At each time point the vial was replenished with 200 µl flesh buffer solution to keep the volume constant. After 7 days, samples were dried and kept for further analysis. All solution samples were stored in capped microtubes before testing.

A series of standard solutions with known concentration of HHC-36 (0, 0.1, 0.5, 1, 5, 10 and 50µg/ml) were tested together with the release samples to provide a calibration curve by which the AMP concentration in buffer solutions can be calculated (External Standard Method).

4.6 Cell adhesion and biocompatibility study

MG-63 osteoblast-like cells from human osteosarcoma (ATCC® CRL-1427TM, USA) were cultured at 37°C in an incubator in standard culture medium Dulbecco's Modified Eagle Medium (DMEM, GIBCO, Canada), consisting of a minimal essential medium, supplemented with 10% fetal bovine serum, and 1% non-essential amino acids (GIBCO, Canada). The medium was replaced every 2 to 3 days. The detachment of the confluent osteoblast cultures (passage nine) from the culture flask was achieved by adding 0.1% trypsin and 0.1%

ethylenediaminetetraacetic acid (EDTA) into the flask for 5 min. After that, the MG-63 solution was centrifuged at 400g for 10 minutes, and re-suspended in the medium.

To study the cell adhesion and biocompatibility of the samples, the MG-36 responses on four different surfaces were investigated, including ApNT, ApNT-AMP, AnNT, and AnNT-AMP. **S**amples (1*1cm) were first placed each in a well in the 12-well culture dish. Before seeding, all the samples were washed with 70% ethanol for 3 times, for the purpose of sterilization. Samples were then washed with warm PBS for 3 times and cells were plated at a density of ~10,000/well. After 30 hour culture in an incubator (37°C, humidified, 5% CO_2 and 20% O_2), the media were removed and the cells were fixed onto the sample surface for SEM imaging. Same protocol used for the bacteria fixation was used for cell fixation.

4.7 Cytotoxicity assay

Same as cell culture, prior to cytotoxicity assay test, MG-63 osteoblast-like cells (ATCC-® CRL-1427TM, USA) were cultured in standard culture medium. The growth and viability of cells colonizing on different samples were evaluated by measuring the mitochondrial dehydrogenase activity using a modified MTT (3-(4, 5-dimetyl-2-tiazolyl)-2, 5-diphenyl-2H-tetrazolium bromide) (Biotium Inc., USA) reduction assay.

4.7.1 MTT assay for HHC-36

To evaluate the cytotoxicity of HHC-36, the MTT assay was performed by culturing MG-36 cells, at a density of ~10,000 cells, in HHC-36 solutions with different concentrations: 0

(control), 25, 50, 75, 100, 125, 150, 175, 200, 300 and 500μg/ml. After 16 hours incubation (37°C, humidified, 5% CO_2 and 20% O_2), MTT solution in 1ml serum free medium was added and the plate was incubated for 4 hours. The solution was then removed, dimethyl sulfoxide (DMSO) was added, and the plate was shaken for 15 min before measuring absorbance at wavelength of 570 nm (the reference value was 690 nm) on an ELISA microplate reader (Bio-Tek Instruments).

4.7.2 MTT assay for AMP loaded samples

To study the cytotoxicity of AMP loaded TiO_2 nanotube samples, the MTT assay was performed by culturing MG-36 cells on different sample surfaces. Samples were first placed each in a well in a 12-well culture dish. Before seeding, all the samples were washed with 70% ethanol and warm PBS for 3 times, for the purpose of cleaning. MG-36 cells, at a density of ~10,000/well, were then seeded onto each sample. Same method was used as for HHC-36 mentioned before, the MTT assay for these samples was performed after 1, 2 and 5 days. Table 4.4 is a summary of the groups of samples for MTT assay.

Table 4. 4 Design of experimental groups for MTT assay

Experiment Groups	Design
Ti	Cleaned Ti foil
ApNT	As-prepared TiO_2 nanotubes
ApNT-AMP	As-prepared TiO_2 nanotubes loaded with AMP
AnNT	400 °C Annealed TiO_2 nanotubes
AnNT-AMP	400 °C Annealed TiO_2 nanotubes loaded with AMP

4.8 Statistical Analysis

In general, the data of experimental groups was analyzed with one-way analysis of variance (ANOVA) test and Holm t test. Since most of our experiment designs involves multiple groups (at least 3 groups), an ANOVA test was first performed to check whether or not there is any difference in all the groups. Then, Holm t tests were used for multiple comparisons to check if there is any difference between any two groups. The confidence level was set at 0.05 (α=0.05). A P value lower than 0.05 ($p < 0.05$) indicates a statistical difference between testing groups; otherwise, there is no significant difference between testing groups ($p > 0.05$).

Chapter 5 Results

5.1 Processing of TiO_2 nanotubes

The first part of the study was dedicated to develop a reproducible process for TiO_2 nanotube arrays. The effects of various anodizing conditions on nanotube morphology (such as thickness of the nanotube coating and diameter of the nanotubes) were studied. Various test parameters were used, including: different electrolyte composition, pH value, voltage, and anodizing duration. It has been reported in literature that the electrolyte composition and its pH value affect both the nanotube formation rate and the dissolution rate of titanium oxide. Therefore, to fabricate nanotube layers with controllable thickness, several electrolyte systems were investigated in this study: fluoride containing water based electrolytes (H_3PO_4 based and Na_2SO_4 based electrolytes) and organic based electrolytes (glycerol based and ethylene glycol based electrolytes).

Generally, during anodizing process, the surface color of the titanium foil surface changes from gold, purple, blue, to light green, and finally brown (showed in Figure 5.1). The mechanism is the same as the coloring process discussed in Chapter 2.3.2. The current decreases rapidly in the first 5 minutes, and becomes stable gradually, following a similar trend to the curve shown in Figure 2.6.

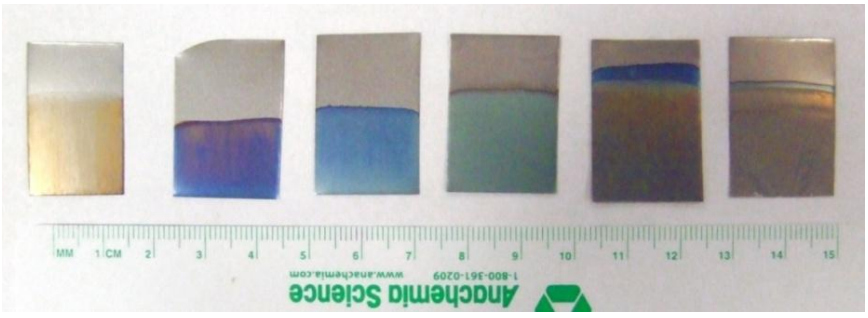

Figure 5. 1 Color changes of titanium foil surface during anodizing process

5.1.1 Fluoride containing water based electrolytes

5.1.1.1 H_3PO_4 based electrolytes

The first electrolyte used in this study was 0.3M phosphoric acid (H_3PO_4) solution containing a small amount of ammonium fluoride (NH_4F). As discussed in Chapter 2.3.2, the existence of fluoride ions plays a key role in the formation of TiO_2 nanotubes. To identify the minimum addition required for nanotube growth, the fluoride concentration was varied systematically, within the range of 0.07-0.27M. SEM images below (Figure 5.2b-e) show nanotube coatings over a wide range of F^- concentration (0.1M-0.27M), and EDS results illustrate that the coatings contain titanium and oxygen (Figure 5.2f). However, when the F^- concentration was lower than 0.1M, a compact oxide layer, instead of nanoporous oxide layer, was formed (Figure 5.2a). Although it has been reported in the literature that the nanotubes can be formed at 20V in HF based electrolytes [71,74-76], it was hard to obtain nanoporous oxide layer when the voltage is lower than 30V in our experiments. The formation of TiO_2 nanotube includes three key processes: compact oxide layer formation, field-assisted dissolution and chemical dissolution of titania (detail information can be found in Chapter 2.3.3). When the F^- concentration was too lower, both field-assisted dissolution and chemical dissolution were not strong enough to form the pores on the compact oxide layer. Similarly, when the voltage was not higher enough, the field-assisted dissolution was not strong enough to break the compact oxide layer. Thus, thin compact oxide layers were formed instead of nanoporous structure.

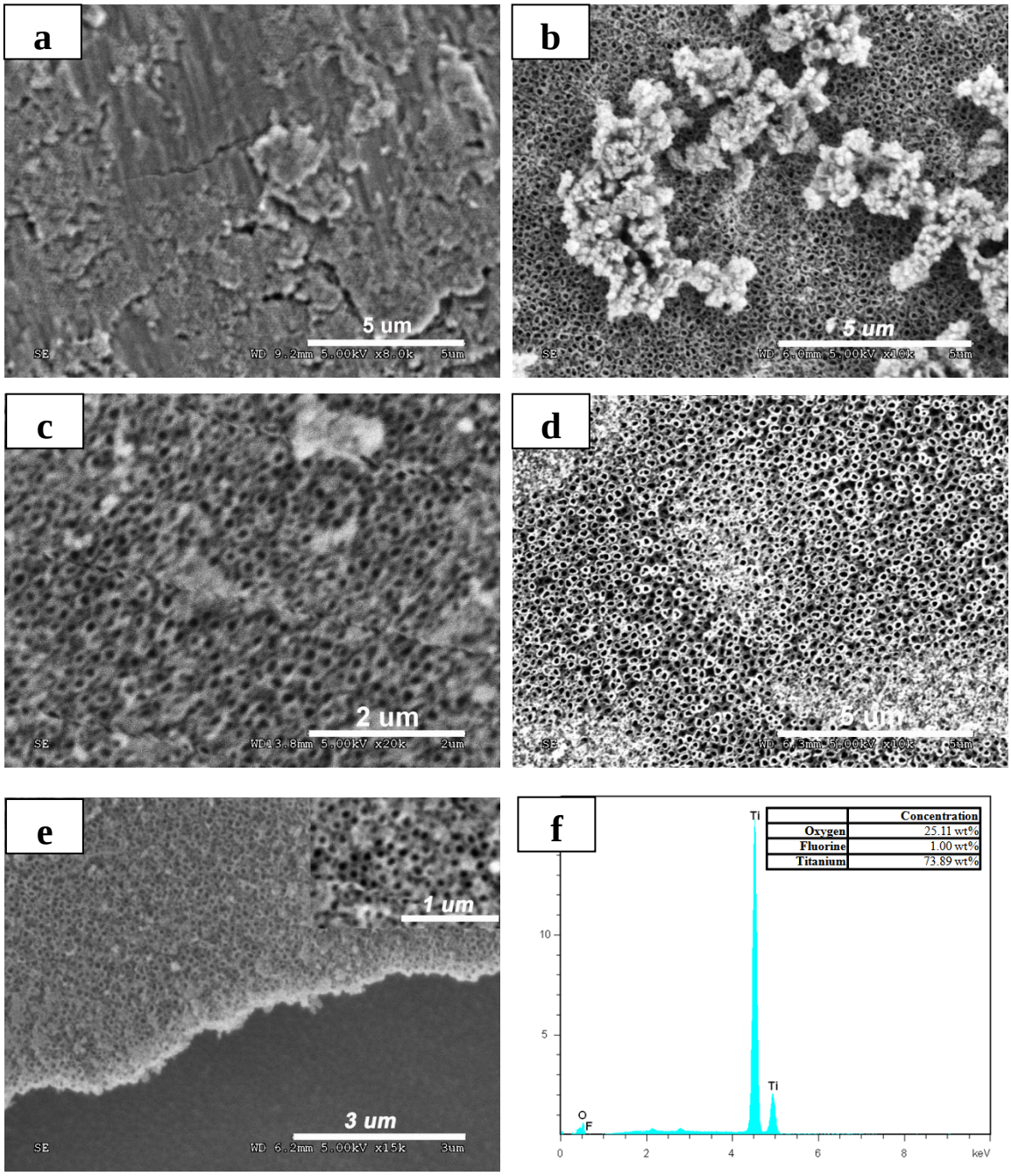

Figure 5. 2 SEM images of samples anodized in electrolyte: 0.3M H_3PO_4 + NH_4F: a) 0.07M, b) 0.1M, c)0.14M, d)0.2M, e) 0.27M at 30V for 2h and f) EDS result of the nanotube coating indicates that the coating contains titanium and oxide

The effect of F^- concentration on the nanotube morphology was evaluated by measuring the thickness and the diameter of the nanotubes prepared in the electrolytes with different F^- concentration from SEM images. It was found by increasing F^- concentration, smaller nanotube diameters were obtained (Figure 5.3), while the thickness of the coating did not change much (within 400-500nm, shown in Figure 5.4). The decreasing nanotube diameter, and thus, more nanotubes per unit area, may be explained with the nanotube formation mechanism: by increasing F^- concentration, the dissolution rate of titania accelerates, leading to more small pits at stage 2 (Section 2.3.3) that would develop into nanotubes in the later stages.

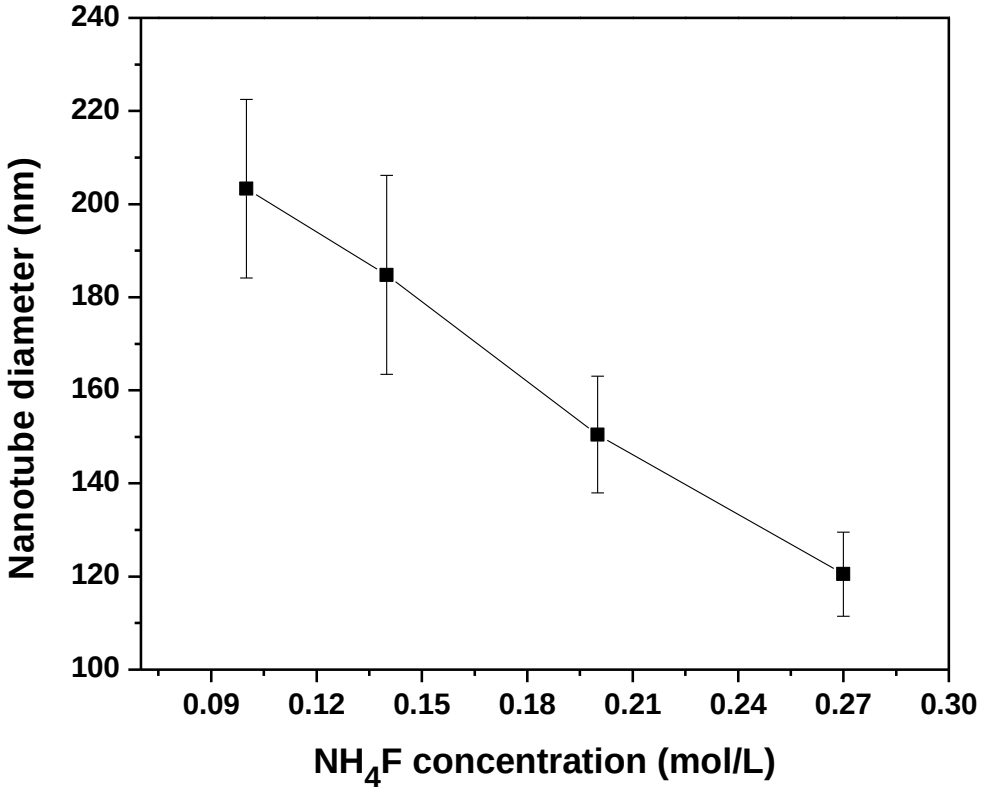

Figure 5. 3 Nanotube diameter vs. NH_4F concentration. Error bars indicate standard deviation (n=10)

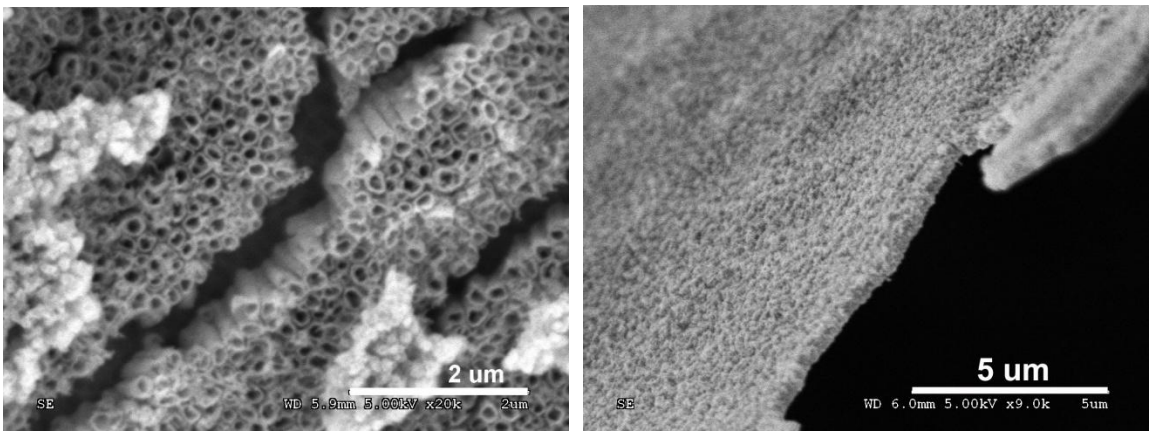

Figure 5. 4 SEM images of TiO_2 nanotubes in cross-sectional view of samples anodized in electrolyte: 0.3M H_3PO_4 + NH_4F 0.1M (left) and 0.27M (right) at 30V for 2h, both of them shows the thickness within 400-500nm

In order to prepare thicker nanotube coatings, extended anodizing time (up to 6h) was applied. However, it did not show significant increase in nanotube thickness, which was still within 400-500nm. Constant thickness with extended anodizing time is an indication of the balance between reactions 1-3 (Chapter 2.3.3). Therefore, after 2 hour of anodizing process, the optimal thickness of the TiO_2 coating was reached.

5.1.1.2 $(NH_4)_2SO_4$ based electrolytes

The thickness of the nanotube layer is essentially the result of the equilibrium between electrochemical formation of TiO_2 at the bottom of pores and the dissolution of TiO_2 in an F^- containing solution [46]. One of the key conditions that restricted the thickness of the TiO_2 nanotube layer in H_3PO_4 based electrolytes was the low pH value, which resulted in the high dissolution rate. To obtain a thicker nanotube layer, instead of 0.3M H_3PO_4, 1M $(NH_4)_2SO_4$ was used as the supporting electrolyte in our experiment. The SEM images (Figure 5. 5) showed that

the thickness of the oxide layer increased to ~1.5μm. The diameter of the nanotubes was within 80-110nm, which was much smaller than the ones prepared in H_3PO_4 based electrolytes.

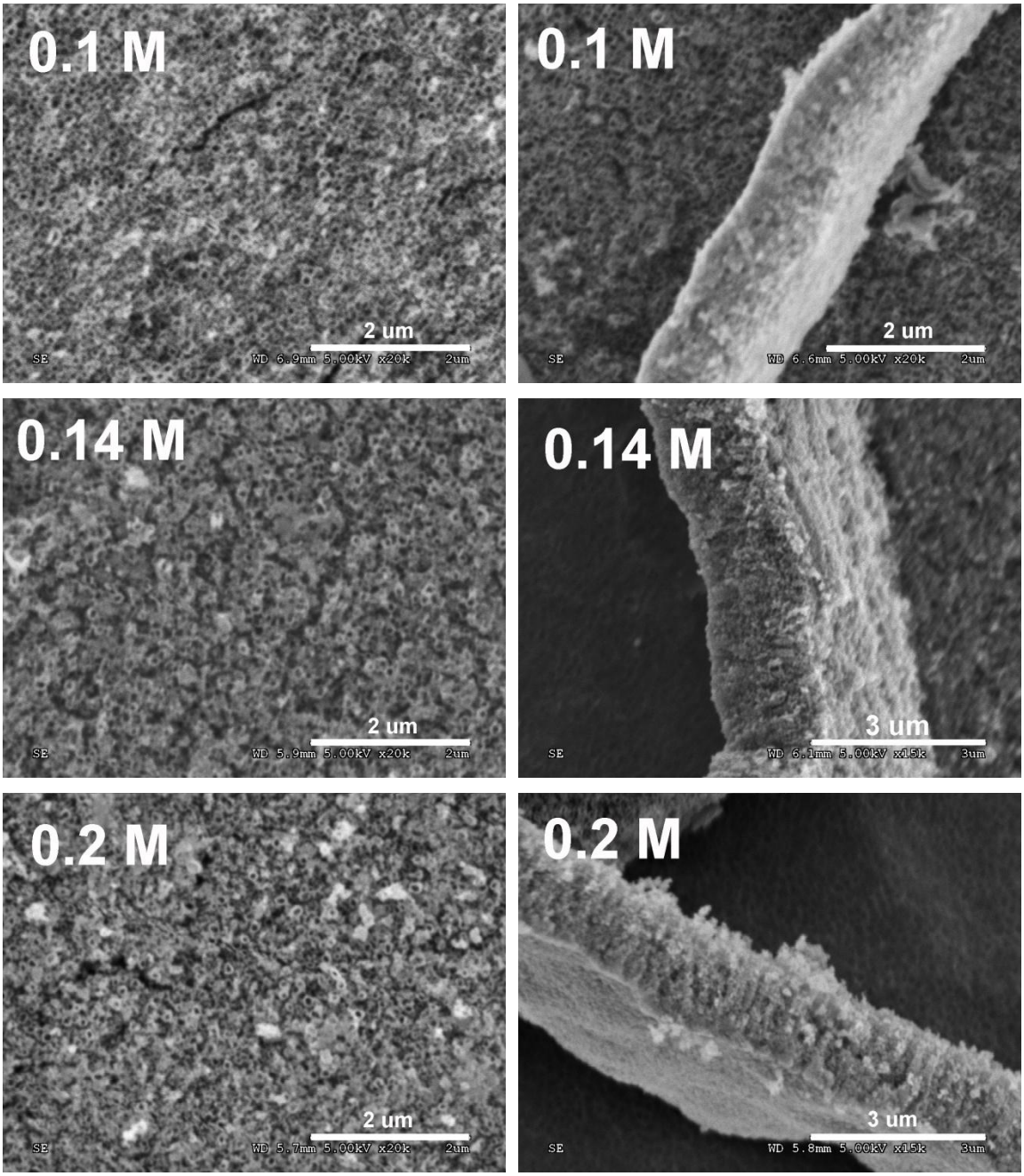

Figure 5. 5 SEM images of samples anodized in electrolyte: 1M $(NH_4)_2SO_4$ + NH_4F: 0.1M, 0.14M and 0.2M at 20V for 2h, top view (left) and cross-sectional view (right)

Moreover, as mentioned previously, it was difficult to obtain nanoporous oxide layer when the voltage is lower than 30V in H_3PO_4 based electrolytes. However, for $(NH_4)_2SO_4$ based electrolytes, the anodizing process can be performed under relatively lower voltage (20V). This may be due to the higher concentration and ionic strength of the supporting electrolyte (1M $(NH_4)_2SO_4$), which enhanced the conductivity of the solution. When higher voltages (30V or higher) were applied, sponge-like nanoporous coatings were formed instead of well organized nanotube layer, which may be ascribed to the high dissolution rate.

Extended anodizing time (up to 6h) was used, and it did not show significant increase of the coating thickness, which indicates the achievement of the equilibrium.

5.1.2 Fluoride containing organic based electrolytes

5.1.2.1 Glycerol based electrolytes

In this study, the maximum thickness of the nanotube coating prepared in water based electrolytes was ~1.5μm, due to the high dissolution rate. However, by using highly viscous organic based electrolytes (such as glycerol), it is possible to obtain thicker nanotube coatings. To achieve that, it is important to evaluate the effect of electrolyte viscosity on nanotube processing. Estimation of the viscosity of glycerol-water mixture is still incomplete in the literature yet. Some formulas have been reported, however, most of them are only applicable to limited conditions [73]. But it is clear that increasing water content leads to a lower viscosity. Therefore, in the current study, a set of experiments were carried out in solutions containing

0.27M NH_4F consisting of glycerol/water mixture with different volumetric ratios (98:2%, 75:25%, 50:50%, 25:75%).

The SEM images (Figure 5.6-Figure 5.11) showed that TiO_2 nanotubes were successfully fabricated in all these electrolytes, however, the morphology of the oxide layer varied dramatically with the water content of the electrolytes. When the water content was greater than 50 vol.%, randomly assembled nanotubes were obtained (Figure 5.6a and Figure 5.7a), while self-organized nanotube arrays (Figure 5.8a and Figure 5.9a) were achieved when the water content was less than 25vol.%. As discussed in Section 2.3.3, the compact oxide layer is dissolved with a rather random spatial distribution at the stage 2, which leads to the irregular morphology when the dissolution rate is too high. Decreasing water content or increasing the viscosity of the electrolyte prolongs the ion diffusion process, which leads to a lower dissolution rate. Therefore, well-organized nanotubes can be formed when the water content is low enough.

The water content of the electrolyte also influenced the morphology of the tube walls. By decreasing the water content in the electrolyte, nanotubes with very smooth walls (with fewer ripples, shown in Figure 5.9d) were achieved. It has been reported in the literature [40,43] that the nanotubes formed in most electrolytes have obvious thickness variation, also known as ripples. So far, the ripples are attributed to the periodic oscillations of the current during anodization [40,51]. By using highly viscous electrolytes, instead of aqueous electrolytes, the ion diffusion process can be significantly slow down, which results in a steadier nanotube growth and smooth wall tubes.

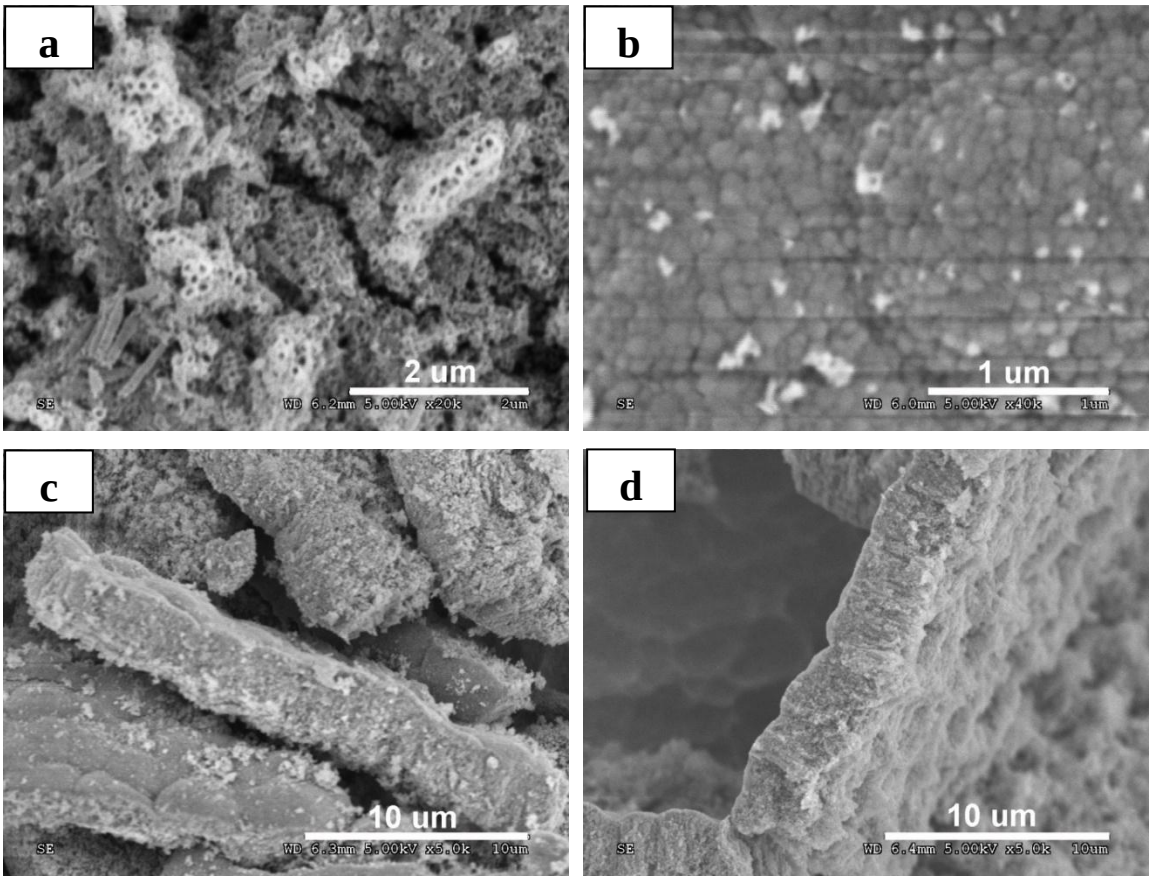

Figure 5. 6 SEM images of TiO_2 nanotubes in a top (a), bottom (b), and cross-sectional (c, d) view. Anodized in glycerol/water electrolyte (25:75 vol.%) containing 0.27 M NH_4F at 20V for 6h.

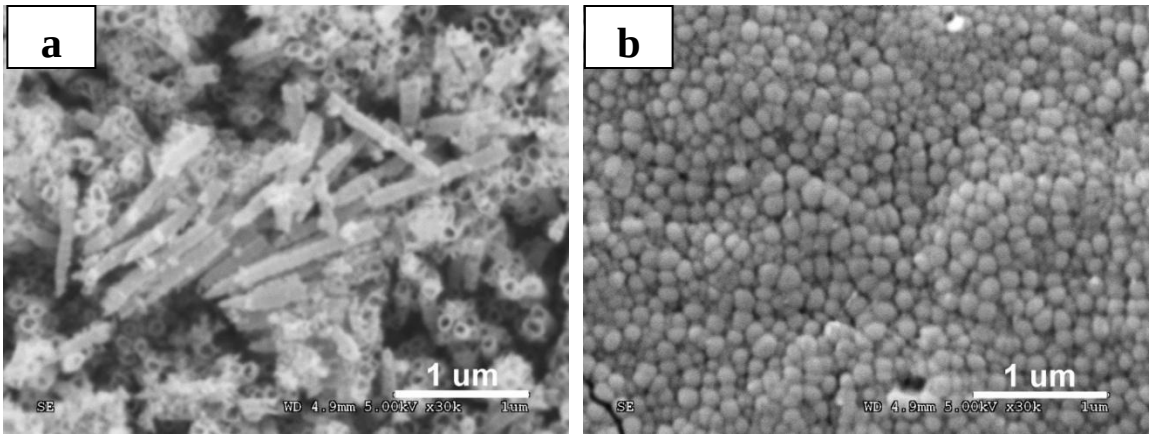

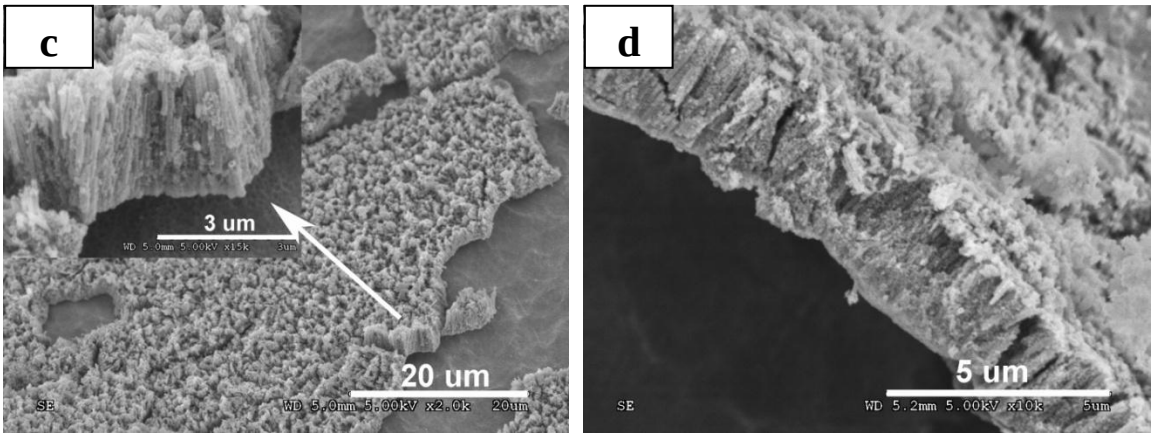

Figure 5. 7 SEM images of TiO_2 nanotubes in a top (a), bottom (b), and cross-sectional (c, d) view. Anodized in glycerol/water electrolyte (50:50 vol.%) containing 0.27 M NH_4F at 20V for 6h.

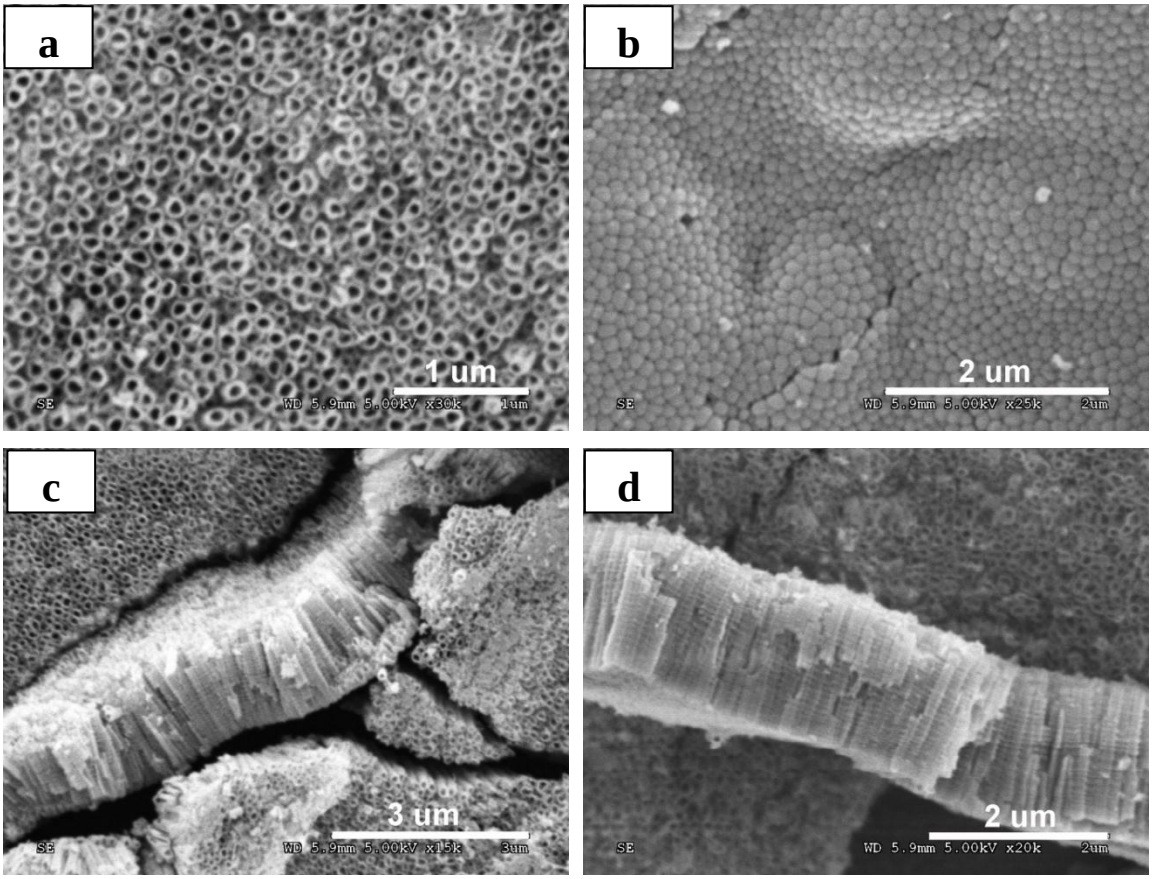

Figure 5. 8 SEM images of TiO_2 nanotubes in a top (a), bottom (b), and cross-sectional (c, d) view. Anodized in glycerol/water electrolyte (75:25 vol.%) containing 0.27 M NH_4F at 20V for 6h.

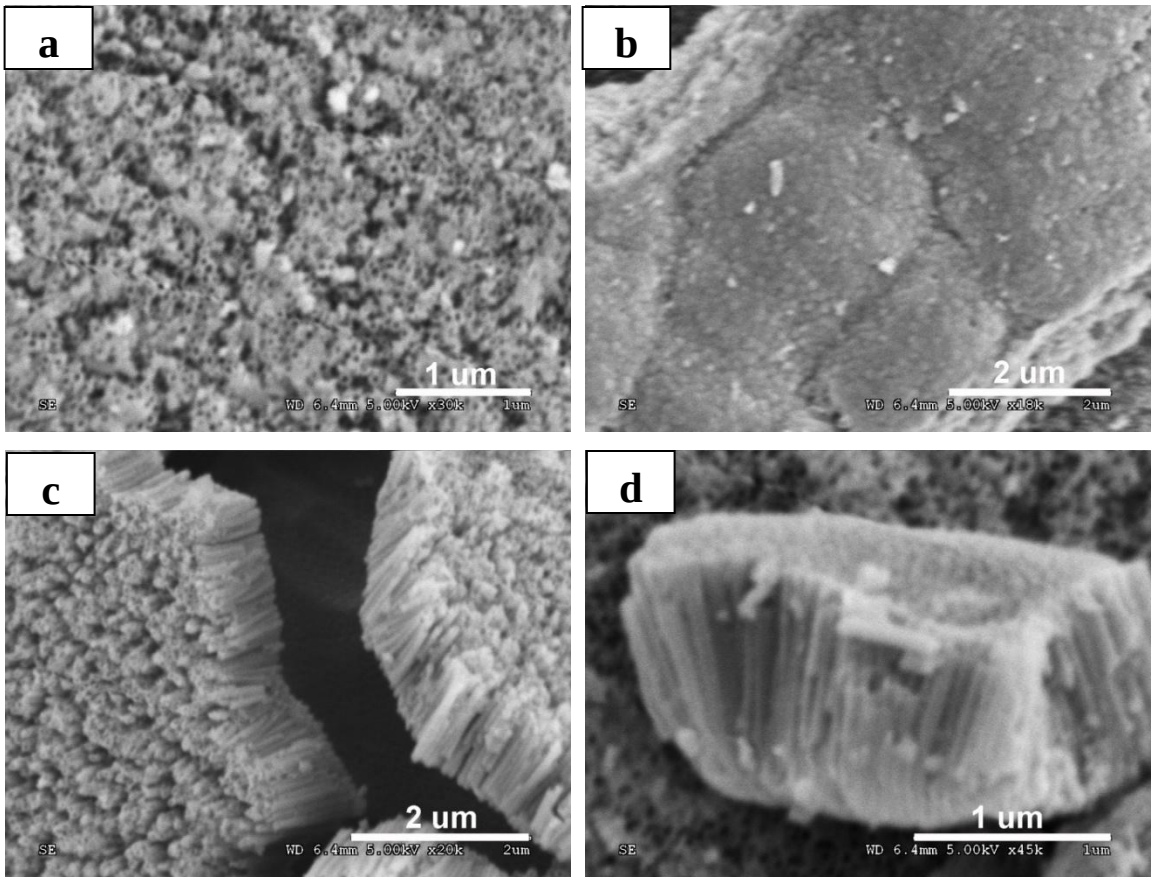

Figure 5. 9 SEM images of TiO_2 nanotubes in a top (a), bottom (b), and cross-sectional (c, d) view. Anodized in glycerol/water electrolyte (98:2 vol.%) containing 0.27 M NH_4F at 20V for 6h.

Table 5.1 shows the tube diameters and lengths measured from the SEM. It was found that with decreasing of the water content, the nanotube diameter decreased, as well as the coating thickness, which may also be ascribed to the slower ion diffusion process.

Table 5. 1 Effect of water content on nanotube diameter and length

Glycerol : Water (vol.%)	Diameter (nm)	Length (μm)
25:75	110.2±12.7	3.07±0.17
50:50	103.8±16.4	2.44±0.20
75:25	100.6±8.8	1.59±0.055
98:2	59.3±7.1	1.08±0.096

For low water content glycerol based electrolytes (lower than 25vol.%), higher voltage (30V) was applied, and the SEM images of the samples are showed in Figure 5. 10 and Figure 5.11. The tube diameters and lengths are following: 159.7±24.6nm and 1.84±0.14μm (25vol.% H_2O), 90.2±6.3nm and 1.54±0.11μm (2vol.% H_2O). It suggests that higher voltage leads to larger and longer nanotubes.

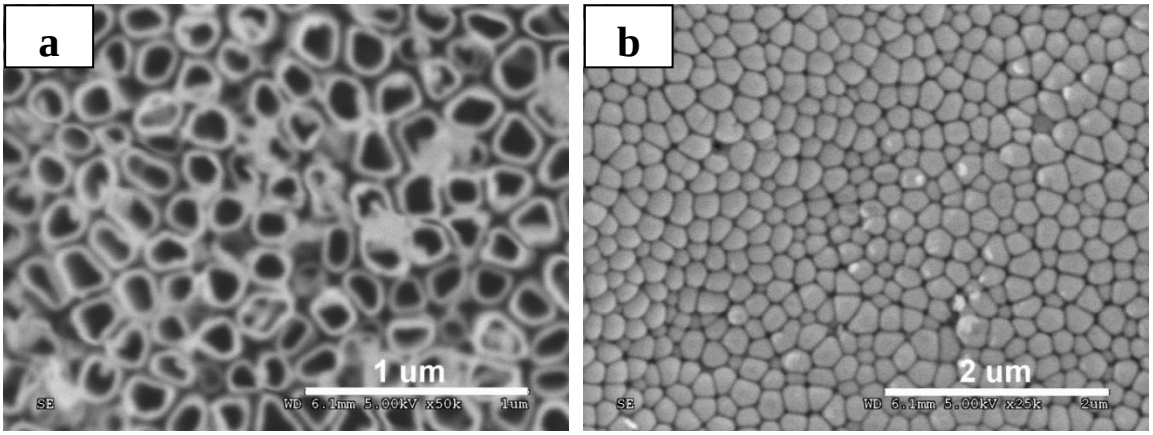

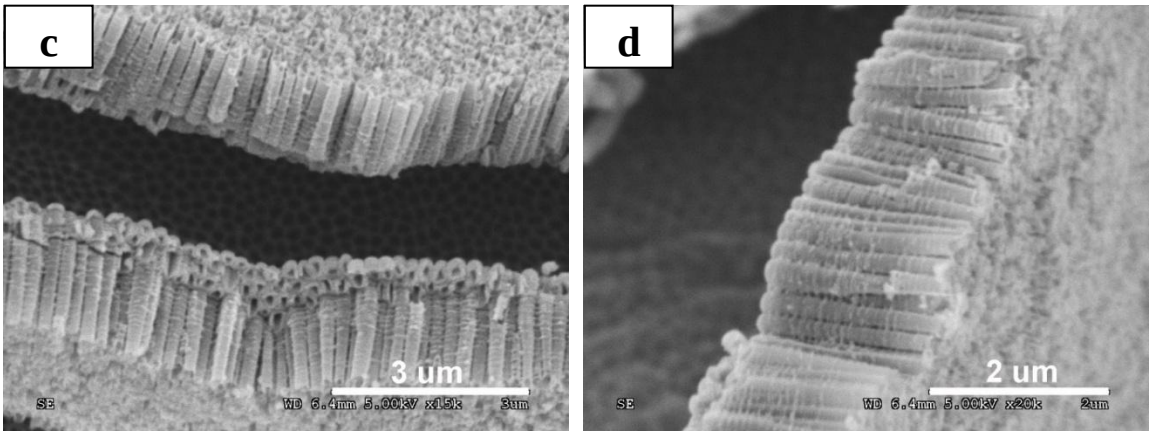

Figure 5. 10 SEM images of TiO_2 nanotubes in a top (a), bottom (b), and cross-sectional (c, d) view. Anodized in glycerol/water electrolyte (75:25 vol.%) containing 0.27 M NH_4F at 30V for 6h.

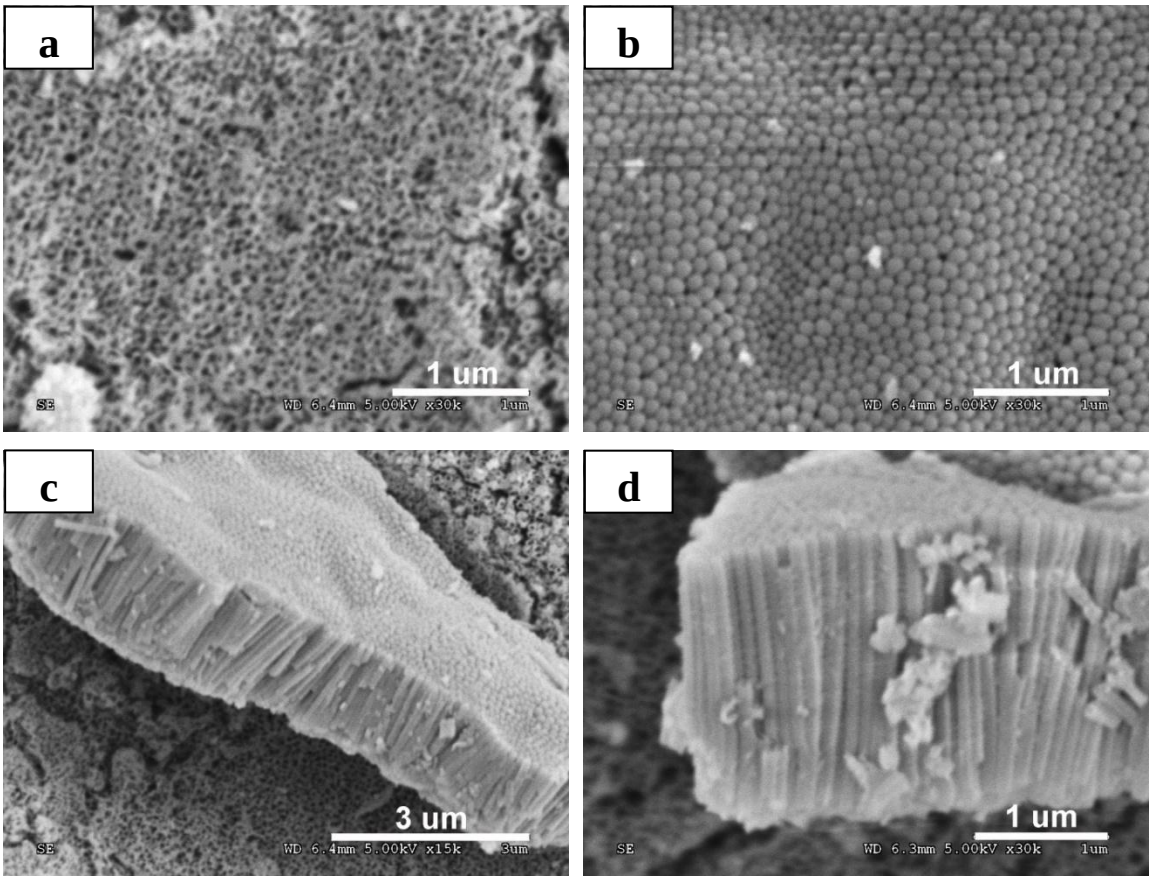

Figure 5. 11 SEM images of TiO_2 nanotubes in a top (a), bottom (b), and cross-sectional (c, d) view. Anodized in glycerol/water electrolyte (98:2 vol.%) containing 0.27 M NH_4F at 30V for 6h.

Nanoporous Ti surface was observed when the nanotubes were peeled off, shown in Figure 5.12. EDS analysis found that the sample had mostly Ti, with little O. Such porous Ti surface may also have some other potential applications.

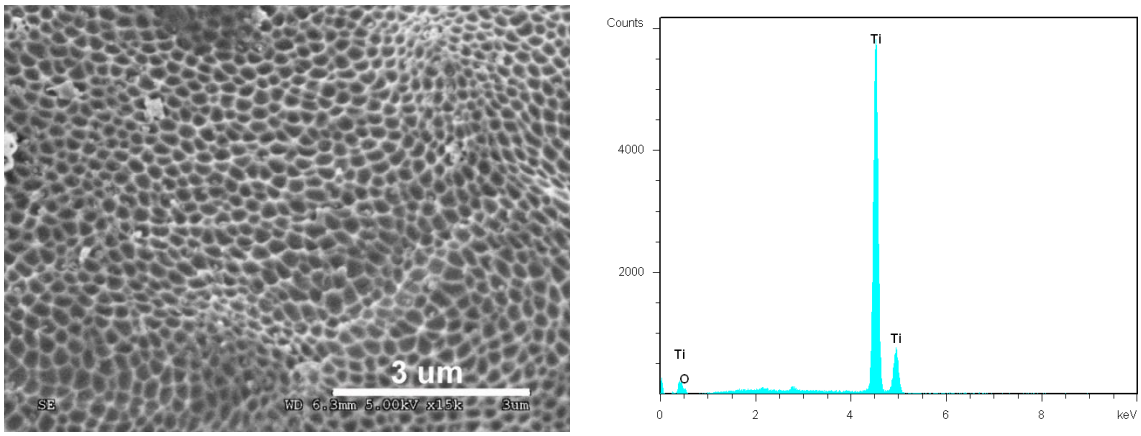

Figure 5. 12 The Ti surface after removal of nanotube layer (left) and the EDS analysis of the nanoporous surface (right)

5.1.2.2 Ethylene glycol based electrolyte

Although thicker nanotube coatings were prepared in glycerol based electrolytes (~2μm), it is still not thick enough for the drug delivery purpose. Therefore, ethylene glycol based electrolytes were used in our experiment. Figure 5.13 shows the SEM images of the TiO_2 nanotubular structure prepared in 98% ethylene glycol solution containing 0.27M NH_4F. Compared with the samples anodized in water-based and glycerol based electrolytes, some obvious differences were observed in nanotube morphology:

1. There was a barrier layer (or nanowire layer) covering the top of the nanotubes;
2. The nanotubes were closely packed with each other, there was no obvious gaps between the tubes;

3. The nanotube walls were extremely smooth;
4. The coating was much thicker (~7μm after 6 hour anodizing process).
5. The diameter of the tubes was small (~80nm for 30V)

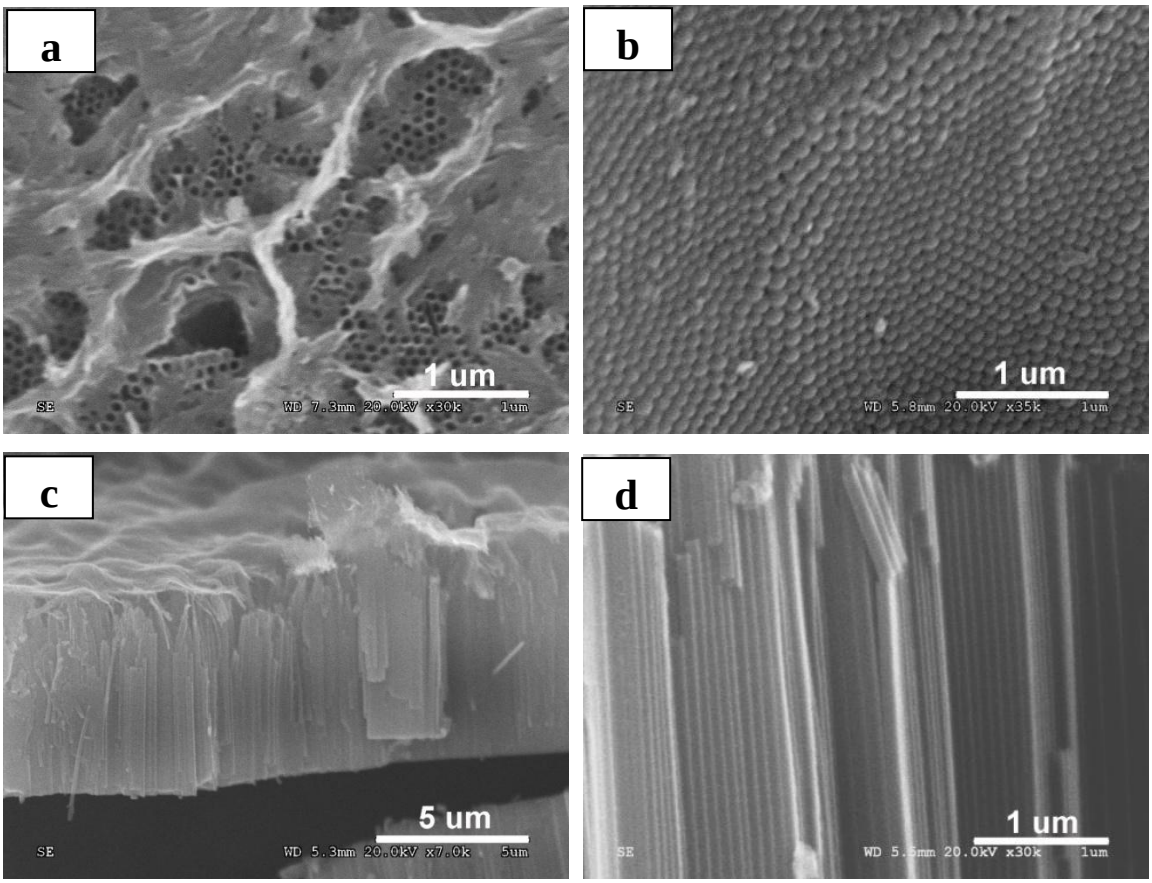

Figure 5. 13 SEM images of TiO_2 nanotubes in a top (a), bottom (b), and cross-sectional (c, d) view. Anodized in 98% ethylene glycol solution containing 0.27M NH_4F at 30V for 6h.

The forming mechanism of the barrier layer is not very clear yet. It may be ascribed to the etching of the top layer by the residual electrolyte on the surface or in the nanotubes at the end of processing. It has been reported in the literature that the barrier layer can be removed by either washing the specimen in a dilute solution of hydrofluoric acid (1vol.%) or ultrasonic cleaning in isopropyl alcohol [32,37]. In this study, the barrier layer was removed by washing ultrasonically in absolute ethanol. However, there is one drawback for this ultrasonic washing

method: it may damage the interface between the oxide layer and the titanium substrate underneath. To remove the barrier layer without damage the interface, it is essential to minimize the ultrasonic duration. To determine the minimal time required, a set of samples were prepared under the same conditions, and then ultrasonically cleaned in absolute ethanol for different times (0, 5, 10 and 20mins). The SEM images (Figure 5.14) showed that, after 5mins of ultrasonic cleaning, most of the barrier layers were removed, and uniformly distributed, self-organized, vertically-oriented TiO_2 nanotubes were observed. However, with extended ultrasonic washing time (over 10mins), cracks and debonding of the coating were observed.

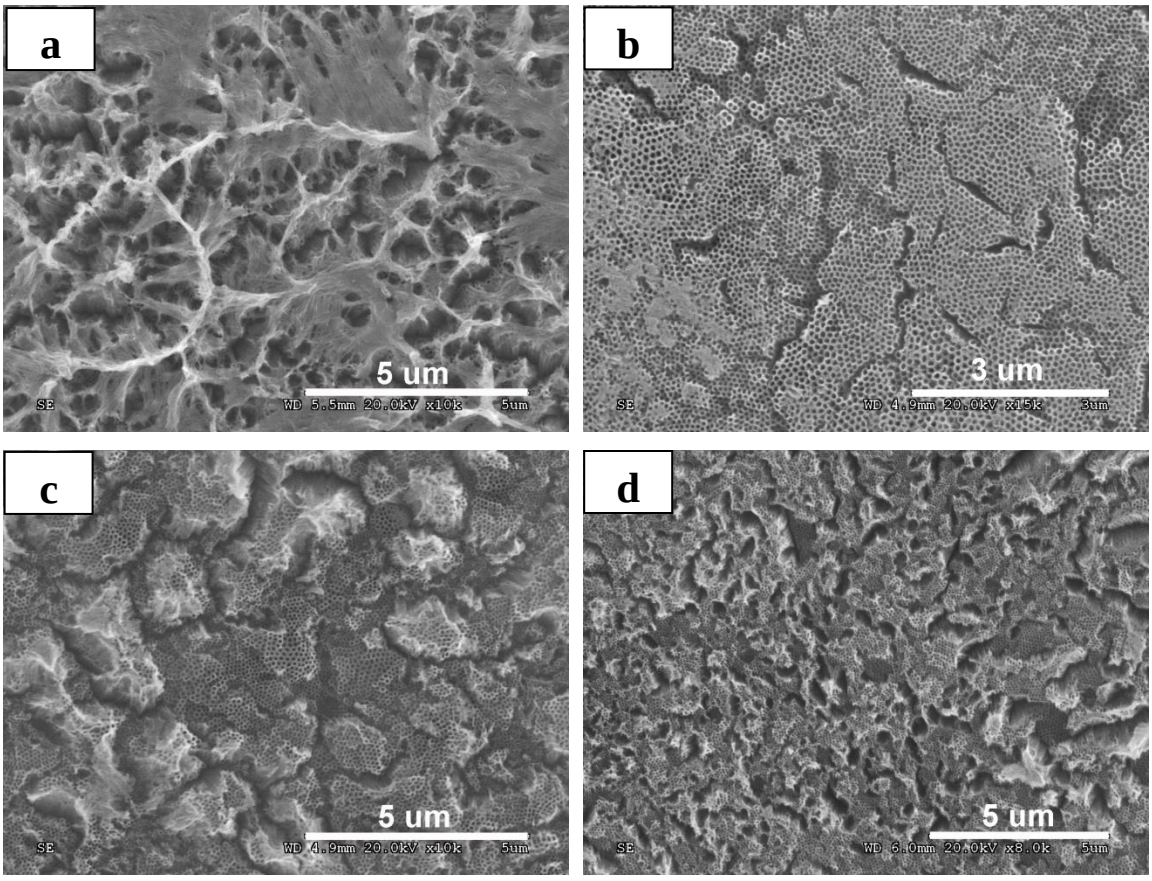

Figure 5. 14 SEM images of TiO_2 nanotube samples anodized in 98% ethylene glycol solution + 0.27 M NH_4F at 30V for 6h, then ultrasonic washed for (a) 0, (b) 5, (c) 10 and (d) 20 mins respectively.

One of the main advantages of using ethylene glycol based electrolytes was that a much thicker nanotube coating can be formed on titanium surface. By changing the experiment conditions, such as anodizing time, the thickness can change from several microns to several hundreds of micron. To investigate the influence of the anodizing duration on the nanotube thickness, a set of samples were anodized in 98% ethylene glycol solution containing 0.27 M NH_4F at 30V for different durations, within the range 1-22h. The thicknesses of the oxide layers were measured directly from the SEM cross-sectional images, and a thickness vs. duration curve was plotted in Figure 5.15. Mathematical simulation indicated a linear relationship between the thickness of the nanotube coating and the anodizing duration, within the range 1-22 hour. According to the nanotube growth kinetics discussed in chapter 2.3.3, the nanotube growth rate should slow down when it approaches the equilibrium. The linear curve indicated that 22 hours is not long enough to achieve the equilibrium, in other words, it is still possible to obtain a thicker coating by prolonging the duration.

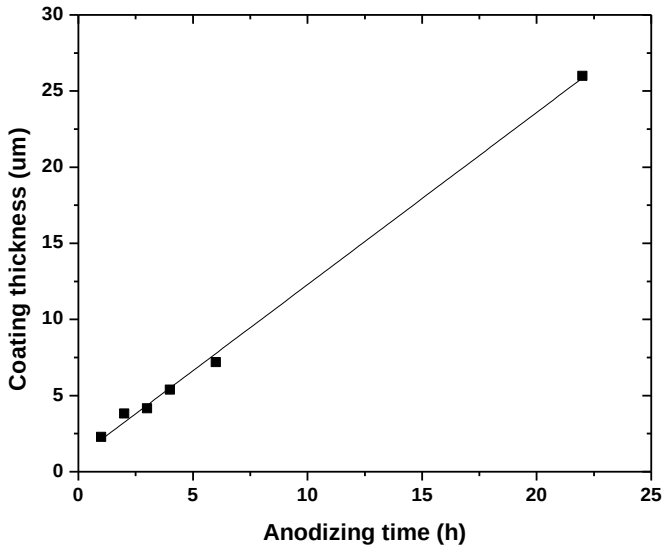

Figure 5. 15 Thickness of nanotube layer vs. anodizing duration curve

Different voltages (20-40V) were applied, and the SEM images of the samples are showed in Figure 5.16. The tube diameters and lengths are the following: 66.7±5.8nm and 3.08±0.07μm (20V), 84.2±5.1nm and 6.99±0.35μm (30V), 104.6±9.1nm and 12.9±0.4μm (40V). Similar to the glycerol based electrolytes, higher voltage leads to larger and longer nanotubes.

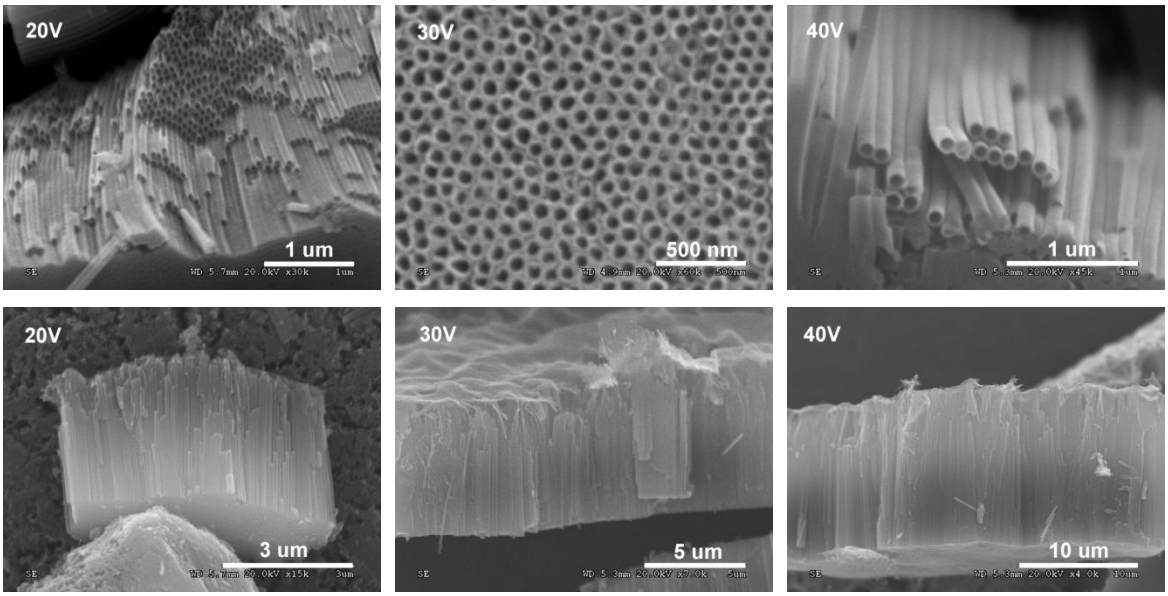

Figure 5. 16 SEM images of nanotubes anodized in 98% ethylene glycol solution + 0.27 M NH_4F for 6h at 20, 30, 40V respectively.

5.1.3 Summary

TiO_2 nanotubes were successfully prepared in both water based electrolytes (phosphoric acid based and ammonium sulphate based electrolytes) and organic based electrolytes (Glycerol based and Ethylene glycol based electrolytes). For phosphoric acid based electrolytes, the TiO_2 layer can only grow up to 400-500nm, which restricted its applications. It was found that by using ammonium sulphate, instead of phosphoric acid, thicker coatings can be achieved. However, the maximum value was ~1.5μm in the current study. In spite of their limited

thickness, the nanotubes prepared in water based electrolytes are rough, i.e. there are ripples on the tube walls. Therefore, organic based electrolytes were used. Well-organized TiO_2 nanotube array were obtained in glycerol based electrolytes when the water content was lower than 25vol.%, and the thickness of the coatings increased up to 2μm. With the decreasing of the water content, the nanotube walls became smoother. The best results came from the ethylene glycol based electrolytes. Nanotubes with extremely smooth walls and ultrahigh aspect ratio (length/diameter) were prepared, and the thickness can be controlled by adjusting anodizing time, from several microns to tens of micron.

5.2 Effect of heat treatment on crystalinity of TiO_2 nanotubes

Post heat treatment (200 and 400°C) was done to the samples anodized in 98% ethylene glycol solution containing 0.27 M NH_4F at 30V for 6h. Figure 5.17 is the Raman Spectroscopy result. It showed that both as-prepared and 200°C annealed nanotube samples do not have any obvious peaks within the range 200-700cm^{-1} (an optimal region for discriminating between different crystal phases of TiO_2), indicating their amorphous nature. It is possible that there are some small crystalline areas in the nanotubes, but they are too small to be detected in amorphous matrix by Raman spectroscopy.

On the other hand, 400°C annealed sample showed typical anatase phase peaks at ~400 cm^1 (B_{1g} vibration mode), ~520cm^{-1} (A_{1g} mode) and ~640cm^{-1} (E_g mode) [52], which suggested that the phase change of TiO_2 nanotubes. Due to the nanosize scale of the tubes, interfacial

vibrations broaden the peaks and slightly shifted them towards lower wavelengths, when compared to the vibration mode for bulk TiO_2 [32].

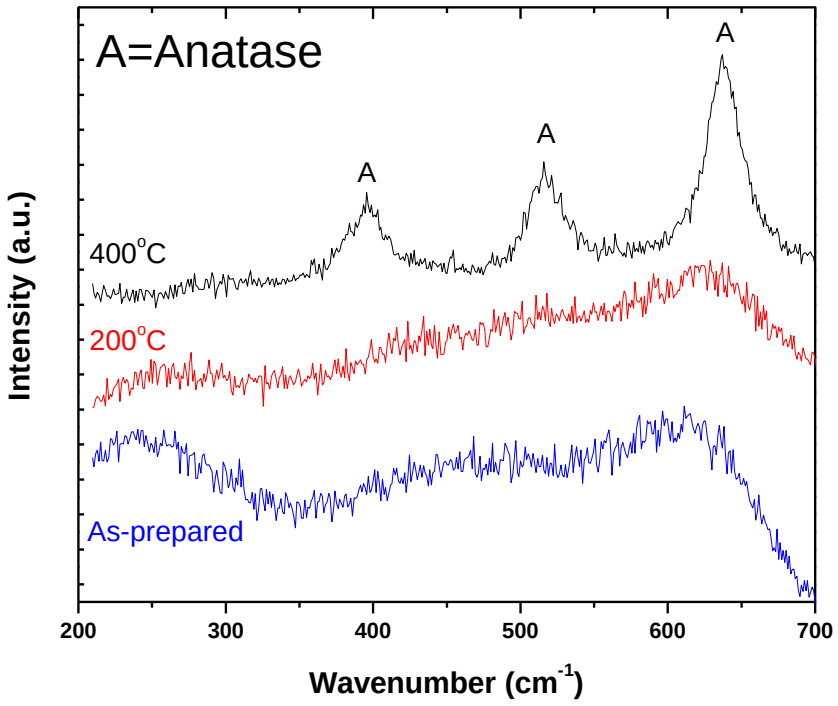

Figure 5. 17 Raman spectroscopy of TiO_2 nanotubes: As-prepared, 200°C annealed, and 400°C annealed

5.3 Antimicrobial activity test against *S.aureus*

Two separate antibacterial tests were performed with different batches of samples (listed in Table 4.5-4.6). The purpose of Test 1 was to evaluate the possibility of killing bacteria using the peptide-loaded TiO_2 nanotube samples. To improve the antimicrobial activities of the AMP-loaded samples in Test 2, the drug loading protocol was modified. The results are discussed below.

5.3.1 Antimicrobial Test 1

The first antimicrobial test was designed to test the bacteria killing abilities of AMP-loaded TiO_2 nanotube samples, as well as to evaluate the efficiency of our AMP loading method.

Table 5.2 and Figure 5.18 show the results of the antimicrobial test 1. The four curves in Figure 5. 18 correspond to one negative control group (bacteria solution only), one positive control group (ApNT: as-prepared TiO_2 nanotubes without AMP) and two sample groups (ApNT-AMP: as-prepared TiO_2 nanotubes loaded with AMP; AnNT-AMP: 400°C annealed TiO_2 nanotubes loaded with AMP). No significant differences were observed between the control group and ApNT group, in terms of bacteria growth, which indicates that the amorphous TiO_2 nanotubes without AMP does not have any antimicrobial activities.

There was 100 times difference of bacteria colony number observed between the as-prepared TiO_2 nanotubes with and without AMP (ApNT-AMP and ApNT) after 4 hours incubation; this result indirectly indicated the successful loading of the peptide onto the nanotubes via the simple vacuum assisted physical adsorption method we used.

Both as-prepared (amorphous) and annealed (crystalline) TiO_2 nanotubes loaded with AMP showed positive bacterial inhibition after incubation with *Staphylococcus aureus* for 60, 120 and 240 minutes. However, better bacteria inhibition was observed in annealed Ti nanotube samples. After 240 min incubation, the annealed samples (AnNT-AMP) showed approximately 90% decrease in bacteria colony forming unit (CFU), and was 100 times less than that of the as-prepared samples (ApNT-AMP).

Table 5. 2 Antimicrobial activity test 1 against *S.aureus*

Mean±SD	***CFU/ml (× 10 E06)***			
Time (min)	**Control**	**ApNT**	**ApNT-AMP**	**AnNT-AMP**
0	1.25±0.553	1.25±0.553	1.25±0.553	1.25±0.553
30	2.0±0.283	4.0±0.5	2.0±2.00	1.43±0.575
60	8.25±2.63	4.23±0.252	1.05±0.606	0.86±0.361
120	55±21.2	33.3±25.2	2.1±1.205	0.478±0.507
240	1000±0	1000±0	10.7±9.86	0.112±0.135

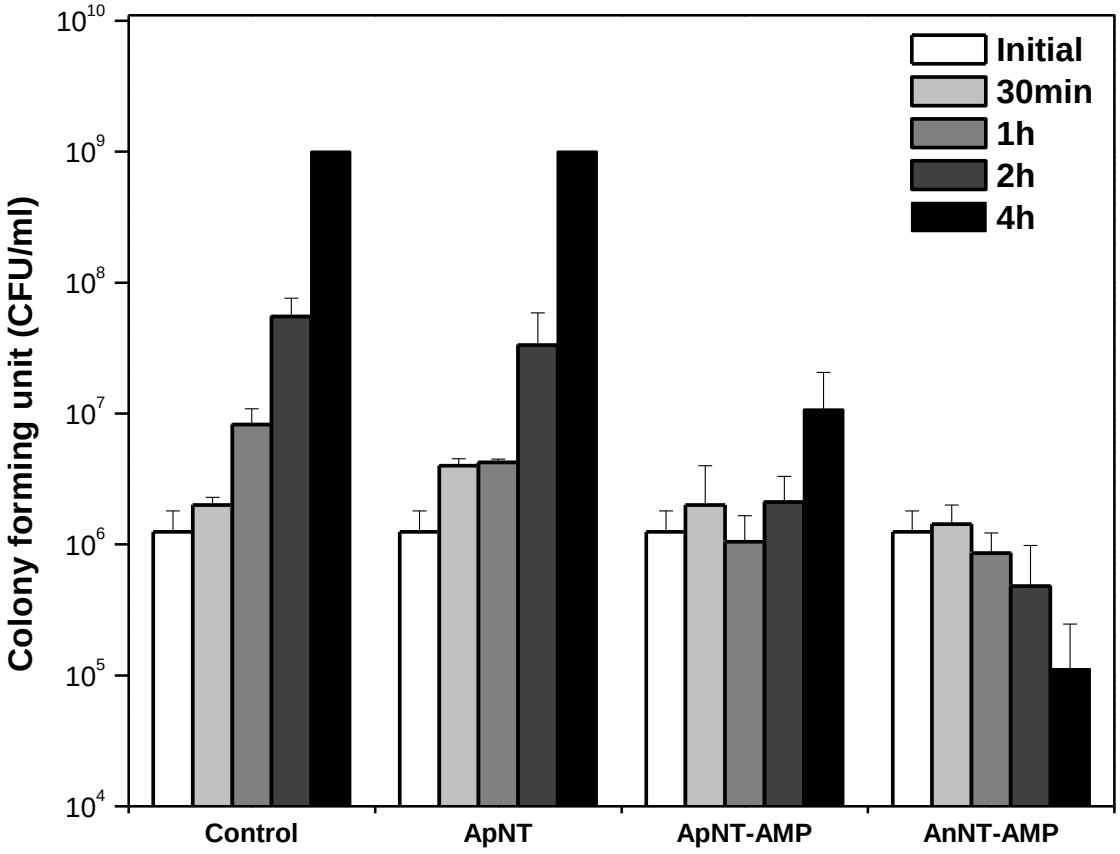

Figure 5. 18 Antimicrobial activity test 1 against *S.aureus.* Error bars indicate standard deviation (n=3).

5.3.2 Antimicrobial Test 2

Based on the positive results of antimicrobial test 1, we tried to improve the antimicrobial activities of the samples by changing our drug loading protocol (detailed information can be found in Chapter 4.2). It was found from the Test 1 that the annealed samples (crystalline) had better antimicrobial activity than the as-prepared samples (amorphous). To explain this interesting result, another positive control group of 400°C annealed TiO_2 nanotubes without peptide was included in this second test.

The results of antimicrobial activity against *S. aureus* from Test 2 are showed in Table 5.3 and Figure 5.19. One-way ANOVA tests (listed in Appendix A) were performed to calculate the P value of the five groups (Control, ApNT, ApNT-AMP, AnNT and AnNT-AMP) after 1 and 4 hours incubation. The result (P = 0.009 for 1hr and P= 0.000 for 4 hr) suggested statistical difference among the five groups. To identify which of the five groups are different from each other, Holm t- test was used for multiple comparisons (p values are listed in Table 5.4 and Table 5.5).

According to the P value of Holm t-test between every two groups, there is no significant difference between the control group, ApNT and AnNT groups, which indicates no antimicrobial activities of either as-prepared or annealed TiO_2 nanotubes. However, both ApNT-AMP and AnNT-AMP group demonstrated continuous bacteria killing, and approximately 99.9% of decrease in bacteria colony forming unit (CFU) after 4 hours of incubation. This result suggested that both as-prepared (amorphous) and annealed (crystalline) TiO_2 nanotubes loaded with AMP

can elute AMP gradually from the nanotubes and significantly inhibit the bacteria proliferation in the surrounding environment of the implant.

Table 5. 3 Antimicrobial activity test 2 against *S.aureus*

Mean±SD	***CFU/ml × 10 E06***				
Time (min)	**Control**	**ApNT**	**ApNT-AMP**	**AnNT**	**AnNT-AMP**
0	1.25±0.464	1.25±0.464	1.25±0.464	1.25±0.464	1.25±0.464
60	3.48±1.76	2.5±0.988	0.33±0.248	1.98±0.861	0.16±0.0874
240	106.67±26.58	126.67±30.77	0.0015±0.0023	93.3±23.38	0.00117±0.00204

Table 5. 4 P value of Holm t-test between every two groups for antimicrobial test 2 after 60 minutes incubation

1hr	**Control**	**ApNT**	**ApNT-AMP**	**AnNT**	**AnNT-AMP**
Control	-	0.98	0.003	0.093	0.002
ApNT		-	0.023	0.534	0.016
ApNT-AMP			-	0.068	0.837
AnNT				-	0.048

Table 5. 5 P value of Holm t-test between every two groups for antimicrobial test 2 after 240 minutes incubation

4hr	**Control**	**ApNT**	**ApNT-AMP**	**AnNT**	**AnNT-AMP**
Control	-	0.270	0.000	0.453	0.000
ApNT		-	0.000	0.080	0.005
ApNT-AMP			-	0.000	1.000
AnNT				-	0.000

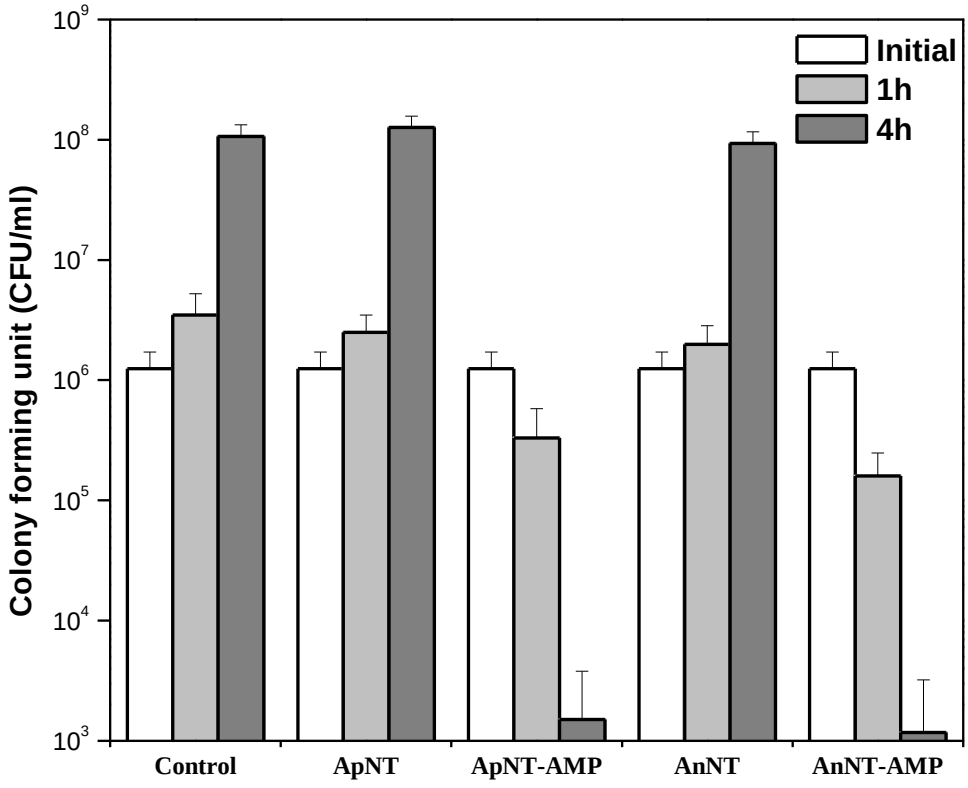

Figure 5. 19 Antimicrobial activity test 2 against *S.aureus.* Error bars indicate standard deviation (n=3).

5.3.3 Summary

Both antimicrobial tests against *S.aureus* confirmed promising bacteria killing ability of the AMP-loaded TiO_2 nanotube samples, which also indirectly indicated the successful loading of the peptides onto the nanotubes via the simple vacuum assisted physical adsorption method we used. Moreover, it suggests that the antimicrobial activities of the samples are highly dependent on the drug loading conditions. By changing AMP loading conditions (AMP solution concentration, vacuuming and shaking time), the bacteria killing rate increased approximately from 90% (Test 1) to 99.9% (Test 2) after 4 hour incubation.

5.4 Bacteria adhesion on sample surfaces

After surgery, the bacteria that can not attach quickly onto the implant surface will be killed by the immune system rapidly [13]. The adhesion of bacteria onto implanted biomaterial surfaces is a critical step for pathogenesis of implant-related infections. Therefore, in the current study, the bacteria adhesion on nanotubes was observed. The samples for antimicrobial Test 2, after 4 hours of bacteria culture, were fixed and then imaged using SEM.

The SEM images of *S.aureus* colonies on different sample surfaces are shown in Figure 5.20. The bacteria colonies on the different surfaces do not show significant differences, in terms of morphology. However, it is obvious that there are more bacteria colonies on the samples without peptide (ApNT & AnNT) than the peptide loaded samples (ApNT-AMP & AnNT-AMP). This result may be explained by the elution of AMP from the AMP-loaded samples that significantly reduced the *S.aureus* colony forming units on the surfaces. As discussed above, the bacteria attached onto the implant surface lead to infection. Thus, it is expected that using the AMP-loaded TiO_2 nanotube coatings for orthopaedic implants can effectively protect the surface from the colonization by microbes, which leads to lower possibility of peri-implant infections.

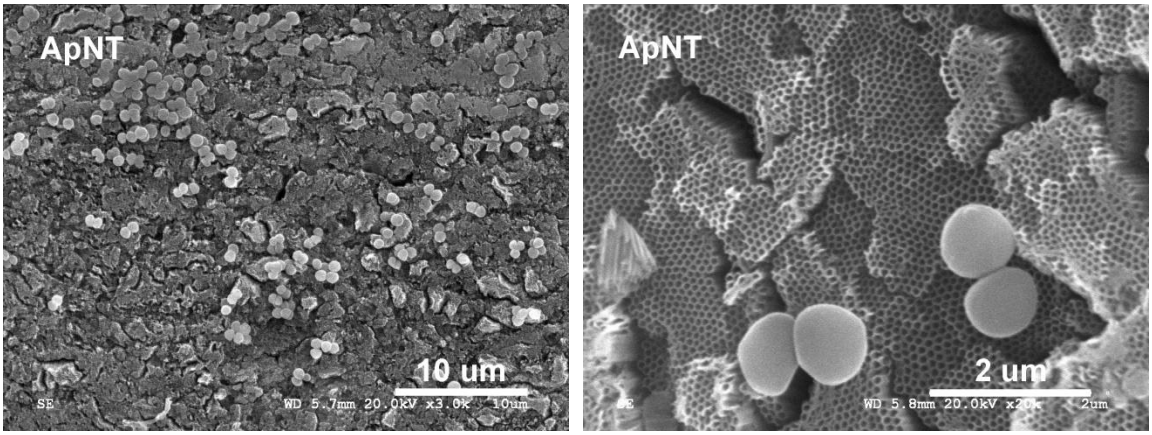

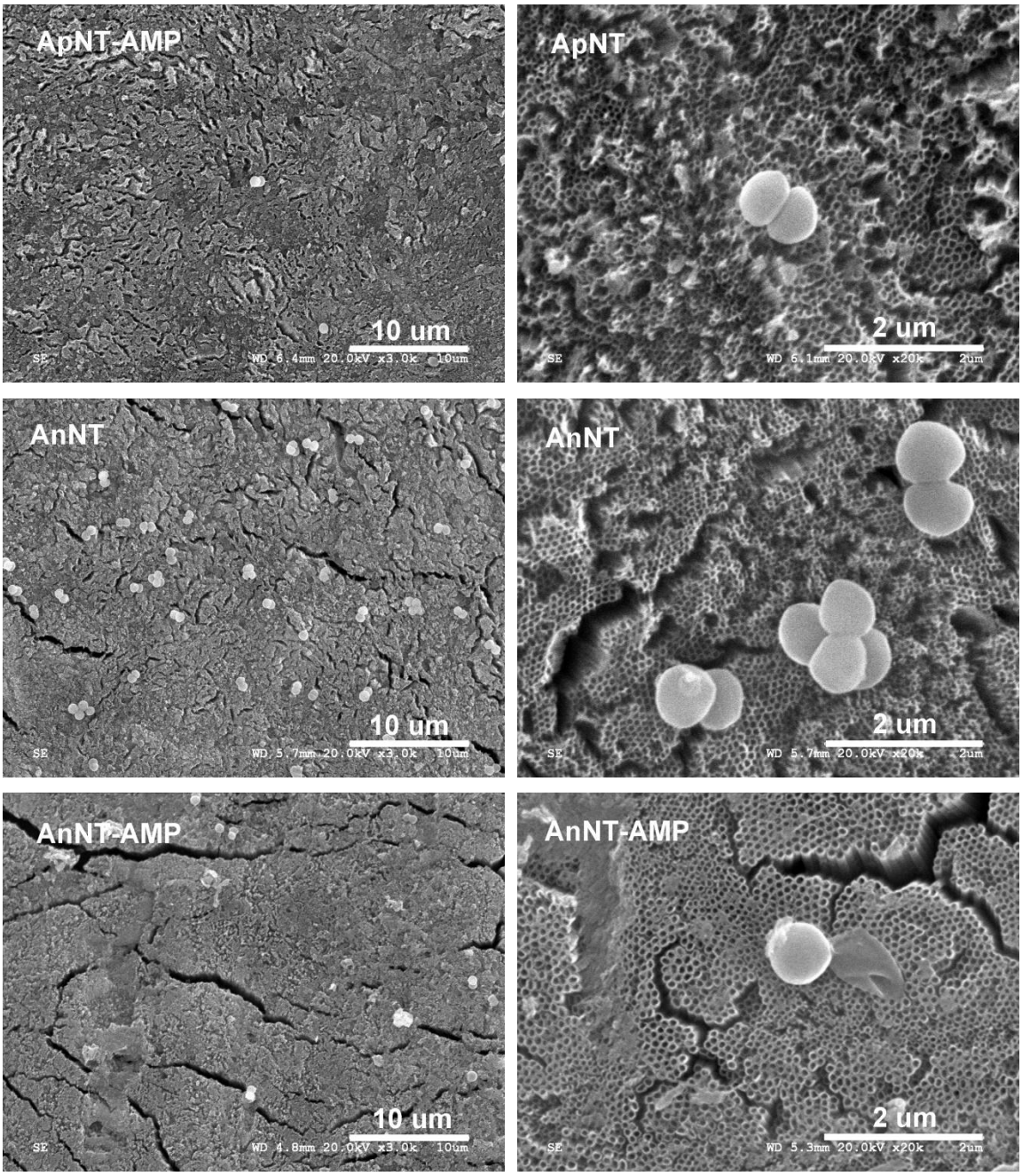

Figure 5. 20 SEM images of *S.aureus* colonies after 4 hour culture on: ApNT, ApNT-AMP, AnNT and AnNT-AMP respectively

5.5 *In vitro* release of AMP from TiO_2 nanotubes

The *in vitro* AMP release profile from TiO_2 nanotubes were tested by LC-MS up to 7 days. Unfortunately, we only managed to get the 1 hour release amount (shown in Figure 5.21). The as-prepared nanotube (ApNT-AMP) and 400 °C annealed nanotube (AnNT-AMP) groups showed an AMP release amount: 9.52±1.14 and 12.99±2.37 μg/cm^2 respectively. Higher amount of AMP were detected for the annealed samples, and this result was consistent with our antimicrobial activity test. After 7 days of release, the samples were examined with SEM; the nanotubes coatings were found to be intact on Ti surface.

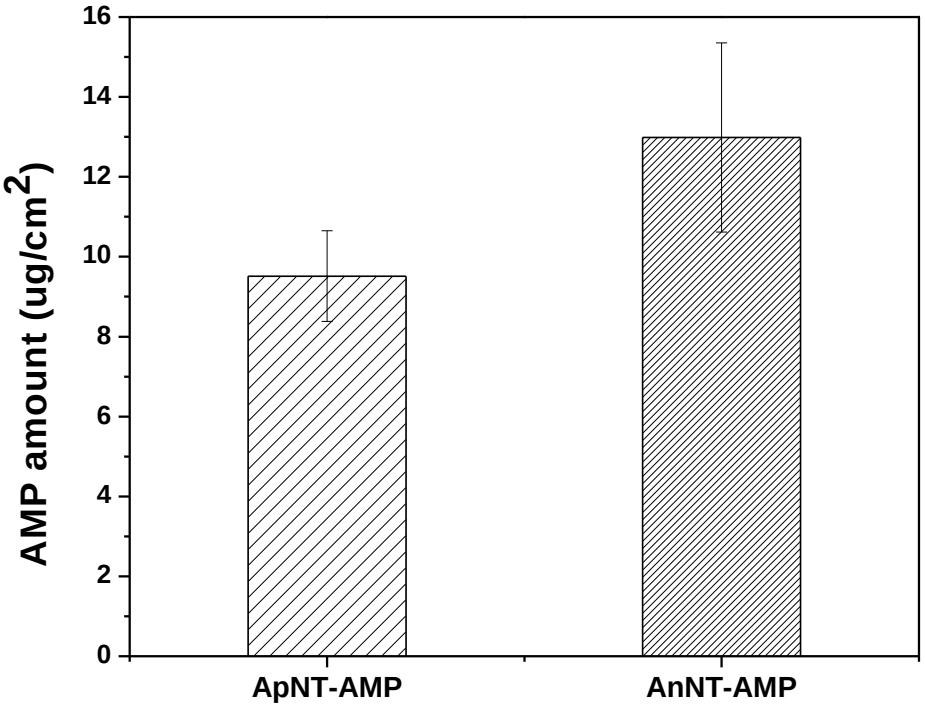

Figure 5. 21 The amount of peptide released from TiO_2 nanotubes in 1 hour. Error bars indicate standard deviation (n=3). The as-prepared nanotube and 400°C annealed nanotube groups showed an average AMP release amount of 9.52 and 12.99 μg/cm^2, respectively

5.6 Cell culture: adhesion of osteoblast-like cells on sample surfaces

The attachment of osteoblast onto implant surface is a critical step for the bone growth, leading to the success of the implantation. Since the aim for the current study is to develop an antimicrobial implant surface by applying AMP-loaded TiO_2 nanotubes as the coating for orthopaedic implants, study on osteoblast cells attachment on the sample surfaces is necessary. SEM images of the cells (MG-36) on TiO_2 nanotube surfaces after 30 hour culture are shown in Figure 5.22 SEM images of MG-36 cells after 30 hour culture on: ApNT, ApNT-AMP, AnNT and AnNT-AMP respectively. It shows that cells spread and attach onto the sample surfaces by filopodia for all four types of surfaces (ApNT, ApNT-AMP, AnNT, AnNT-AMP), which indicates all the surfaces are biocompatible. No big differences were found between the TiO_2 nanotubes with and without AMP, showing the AMP loaded on the nanotubes does not have any significant negative effect on the cell growth and attachment.

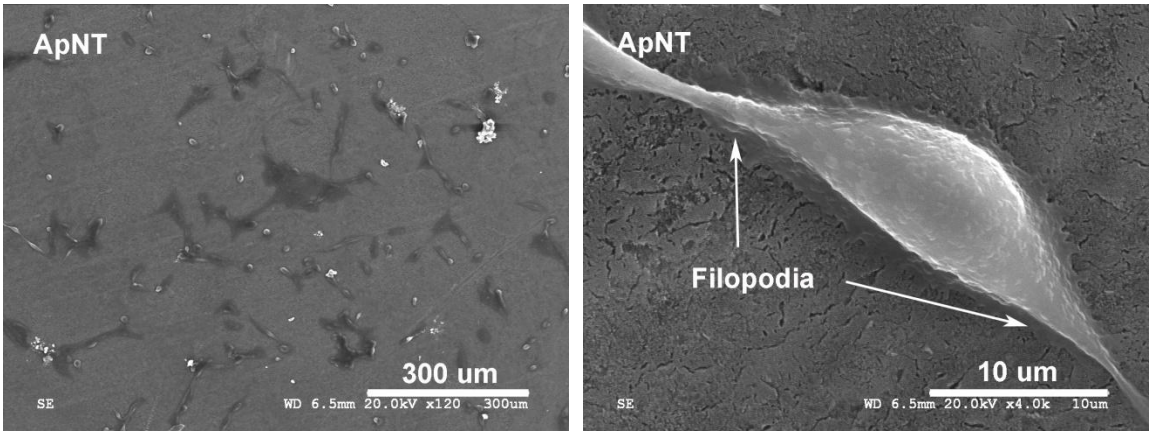

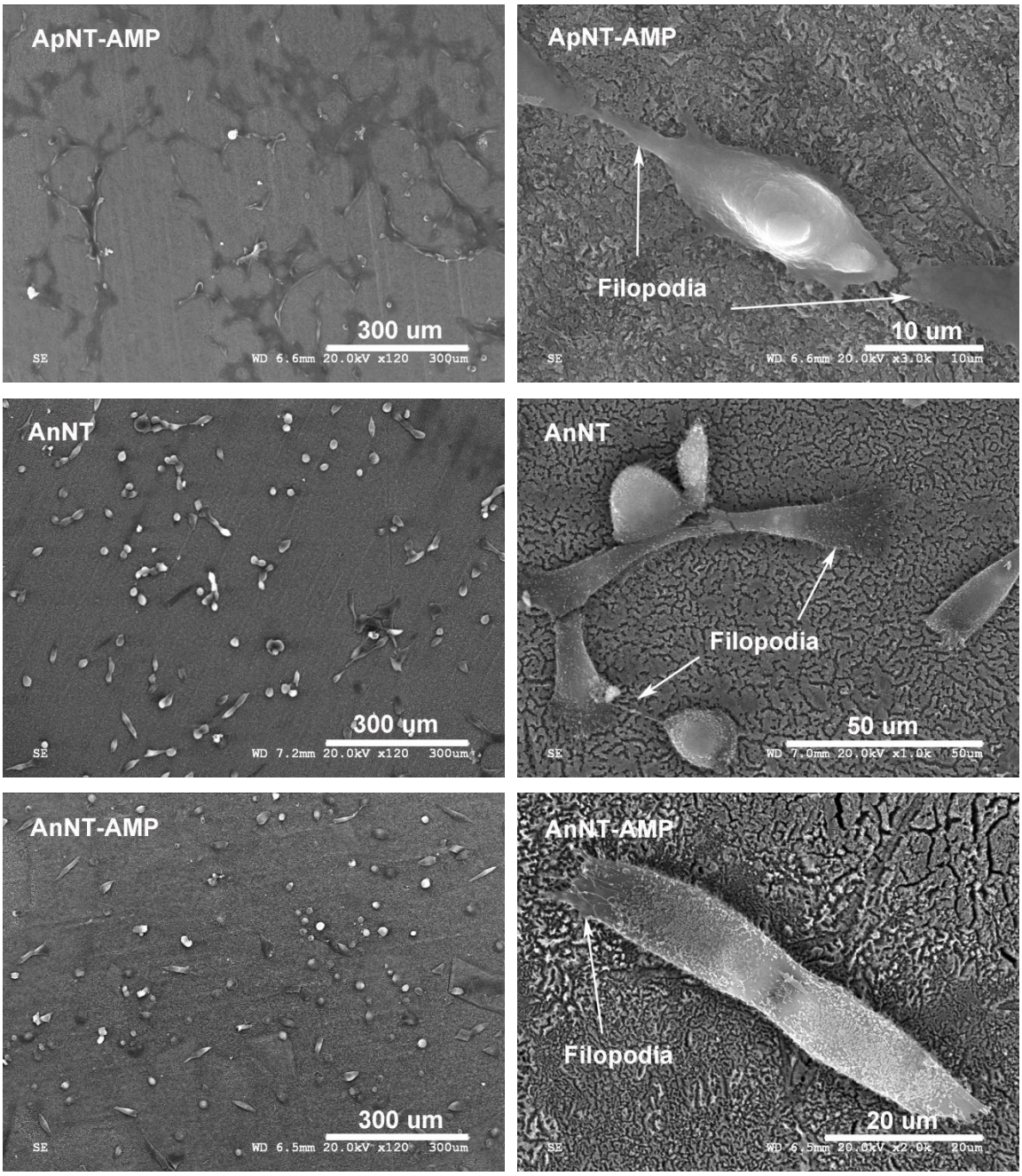

Figure 5. 22 SEM images of MG-36 cells after 30 hour culture on: ApNT, ApNT-AMP, AnNT and AnNT-AMP respectively

5.7 Cytotoxicity assay

5.7.1 MTT assay of AMPs

The result of MTT assay for HHC-36 solutions is shown in Figure 5.23. Holm t- test was used to identify if there is a statistical difference between the control and HHC-36 solutions. The results (Appendix B) indicates that there is no significant difference between the control group and HHC-36 until when the concentration is greater than 200µg/ml ($p=0.032<0.05$). In other words, HHC-36 does not show significant negative effect on cell proliferation, when the concentration is lower than 200µg/ml.

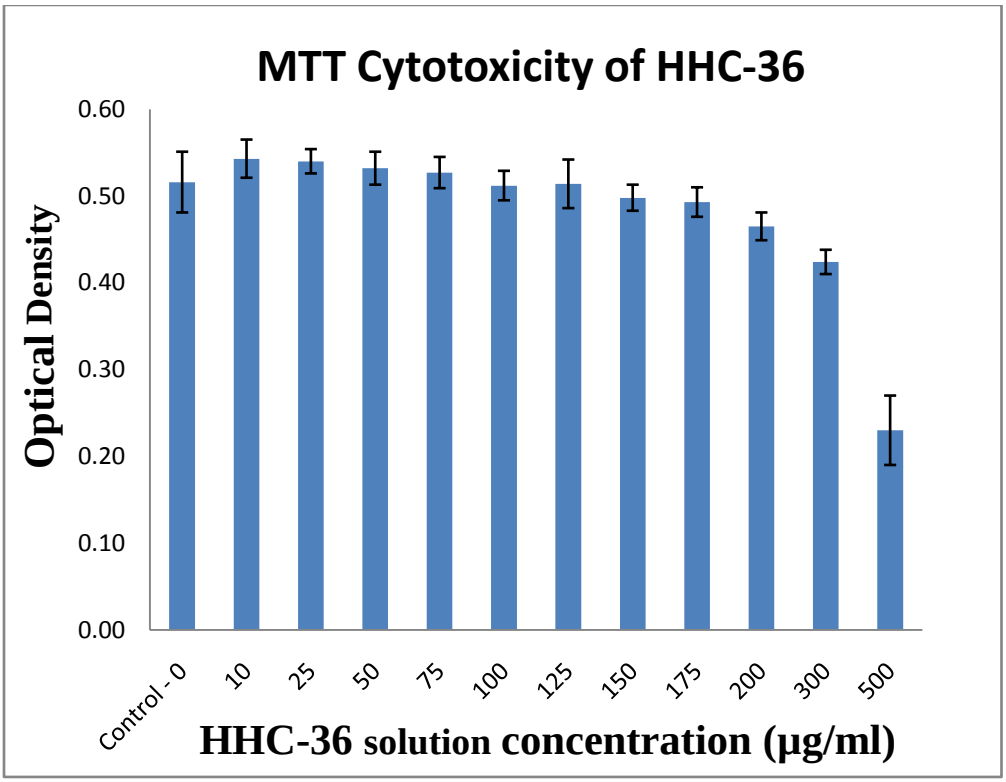

Figure 5. 23 MTT assay was performed to evaluate the cytotoxicity of HHC-36 with MG-63 osteoblast-like cell in the solution. Error bars indicate standard deviation (n=3). No statistical difference in cell activity between the control and HHC-36 solutions when the concentration is lower than 200µg/ml

5.7.2 MTT assay for TiO_2 nanotubes

The result of MTT assay for TiO_2 nanotube samples, with and without AMP, is shown in Figure 5.24. The cells on the all these surfaces showed consistent proliferation with time, indicating that all the surfaces are not cytotoxic for MG-36 osteoblast-like cells. However, high standard deviations were found for the nanotube samples (ApNT, ApNT-AMP, AnNT, AnNT-AMP). In other words, for the same group of samples, the cells proliferated well on some of the surfaces, but were perished on the others. The high standard deviations may be ascribed to the chemical contaminations on the samples, i.e. the residual electrolyte solution in the nanotubes. To address this result, further studies are needed.

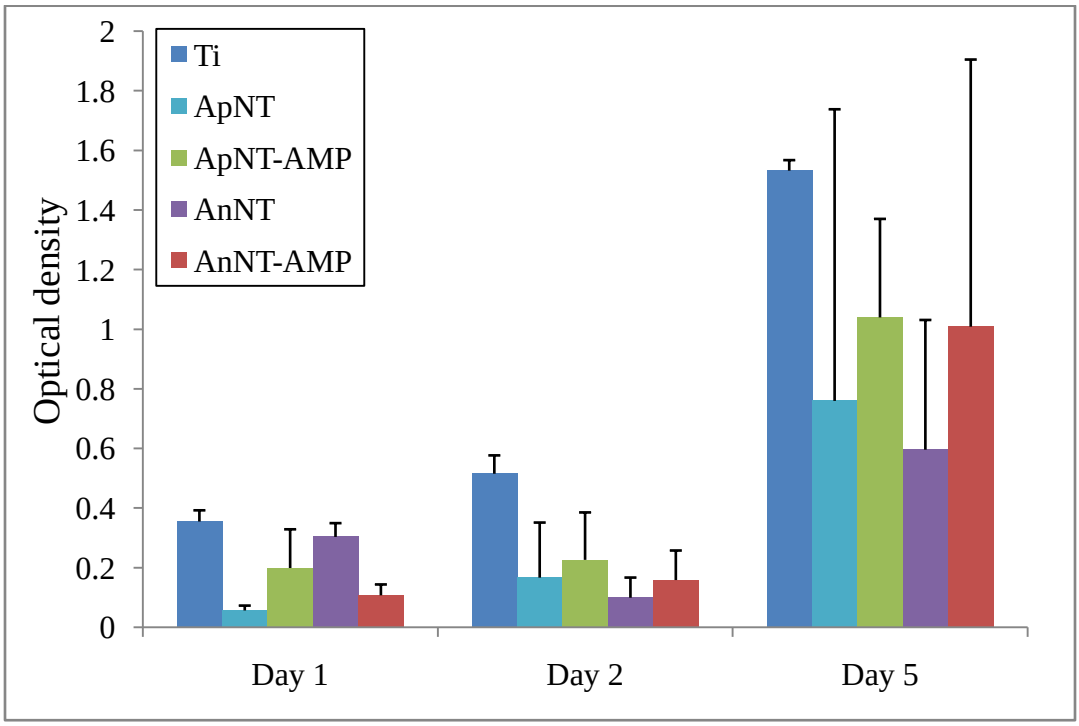

Figure 5. 24 MTT assay was performed to evaluate the cytotoxicity of TiO_2 nanotube samples with/without AMP. Error bars indicate standard deviation (n=3). High standard deviations were found for the nanotube samples

Chapter 6 Discussion

6.1 Selection of cationic antimicrobial peptides

As discussed in Chapter 2.1.3, the rising problem of infections caused by multi-antibiotic resistant bacteria, or so-called superbugs, makes traditional antibiotics less effective for peri-implant infections. Therefore, in the current study, cationic antimicrobial peptides were selected as alternatives to traditional antibiotics because of their rapid reaction on broad-spectrum bactericidal strains, low toxicity and immunogenicity, as well as the complex killing mechanism. The mechanism of the antimicrobial activity of AMPs is not very clear yet. Previous studies suggested that AMPs may interact with bacterial surfaces by either permeabilizing them or translocating across the cytoplasmic membrane to attack cytoplasmic targets [21]. More than one killing mechanism may be observed with a single peptide. As a result of the complex killing mechanisms, the possibility of developing a resistant mutant is significantly reduced.

HHC-36 (KRWWKWWRR) was selected as the test AMP in this study. It is one of the most potent peptides identified by the high-throughput peptide synthesis (peptide arrays on cellulose and rapid screening technologies) in combination with quantitative structure activity relationship (QSAR) modeling. *In vitro* tests demonstrated that this peptide has better antimicrobial activities against a broad array of multi-drug resistant “Superbugs”, such as methicillin-resistant *Staphylococcus aureus* (MRSA), than some of the highly used traditional antibiotics and the most advanced clinical candidate antimicrobial peptide (MX-226) [3]. Moreover, it showed very low toxicity in metabolically active cells and caused minimal red blood cell lysis for concentrations up to 251 mM [3].

6.2 HHC-36 loading onto TiO_2 nanotubes via physical adsorption method

Our previous studies suggested that the chemical immobilization of peptides onto a surface may limit the peptide mobility, which may compromise the antimicrobial activities of the peptide [70]. Therefore, in the current study, a simple vacuum assisted physical adsorption method was used for AMP loading. Reports have been made on the physical adsorption of various proteins on TiO_2 surface, such as human serum proteins [77-78], human plasma fibrinogen [79], lysine and/or arginine residues of MBP (maltose-binding protein) and Fe Cyt-c (horse heart cytochrome c) [80] and other biomolecules. The mechanism for physical adsorption on titanium dioxide surface is generally interpreted as a combination of electrostatic and van der Waals forces.

The iso-electric point (pI) of TiO_2 is about 4.5 [77,79], i.e. TiO_2 surface has a net negative charge at physiological pH (at pH ~7.4, which is also the pH value of the buffer solution used for drug loading). On the other hand, as we mentioned in chapter 2.2, most of the AMPs are cationic. The peptide used in the current study (HHC-36) has an isoelectric point of 12.7 (pI=12.7) with five positively charged residues (Arg and Lys), possesses a positive charge at physiological pH. Thus, a strong electrostatic interaction between TiO_2 nanotubes and HHC-36 molecules is expected, leading to a good drug loading effect. Furthermore, TiO_2 nanotube coating is super hydrophilic and highly polar surface, which make it attractive for water and water-soluble molecules in general [77].

6.3 Selection of nanotubes for AMPs delivery

In the current study, TiO_2 nanotubes were successfully prepared under several electrolyte systems: phosphoric acid based, ammonium sulphate based, glycerol based and ethylene glycol based electrolytes. For phosphoric acid based electrolytes, the thickness of the TiO_2 layer can only reach up to ~400-500nm, while using ammonium sulphate based and glycerol based electrolytes, the coating thickness can be increased up to 1.5-2μm. However, coatings thicker than 5μm were only achieved in the ethylene glycol based electrolytes. Depending on anodizing conditions, such as anodizing duration, the thickness changes from several microns to tens of microns. Moreover, by using water-free electrolytes (i.e. glycerol and ethylene glycol), nanotubes with extremely smooth walls and ultrahigh aspect ratio (length/diameter) can be obtained.

The thickness of the nanotube coatings (i.e. the length of the nanotubes) and diameter of the nanotubes were the two key factors considered for AMP carrier selection. The longer tubes means larger volumes available for drug loading and the smaller diameter may lead to slower drug release. Peng L et al [9] confirmed this idea: longer tubes performed better than the shorter ones, in terms of drug loading and elution. However, the thicker the oxide layer, the weaker the interface. When the nanotube layer is too thick, the weak interface between the coating and the Ti substrate makes it unsuitable for clinical applications. Therefore, in the current study, the TiO_2 nanotubes (thickness: ~7 μm and diameter: ~80nm) prepared in 98% ethylene glycol containing 0.27M NH_4F at 30V for 6 hour were chosen as the carrier for AMPs.

6.4 Effect of AMP loading conditions on drug loading efficiency

In the current study, a very simple vacuum assisted physical adsorption method was used for antimicrobial peptide loading onto TiO_2 nanotubes, and two antimicrobial tests (1&2), against *S.aureus*, confirmed promising results on the bacteria killing ability of this novel antimicrobial implant surface. In addition to the simplicity of this process, another very important advantage of this drug loading technology is its clinical feasibility. Both the implants and the drugs can be developed and packaged independently; thus, the drug loading process can be done in the operating room, which simplifies the regulation process and prolongs the shelf-time.

Comparing the results of the two antimicrobial tests, it can be concluded that the antimicrobial activities of the samples are highly dependent on the drug loading conditions. By changing the AMP loading conditions (such as AMP solution concentration, vacuuming time and shaking time), the bacteria killing rate after 4 hour incubation increased approximately from 90% (Test 1) to 99.9% (Test 2), at 100 times difference (shown in Figure 6.1). It is expected that the antimicrobial activities of AMP-loaded samples can be further improved by optimizing the drug loading protocol.

Moreover, in this study, in order to investigate the efficiency of TiO_2 nanotubes as a carrier for AMPs, the samples were rinsed with the buffer solution for 3 times, 30 seconds each, to remove the excess peptide on the surface (detailed information can be found in Chapter 4.2). However, in the clinical situations, this is not necessary. The excess peptide on the surface is

expected to be released quickly in the initial stage to kill the bacteria, which may lead to better bacteria killing effects of the AMP-loaded samples.

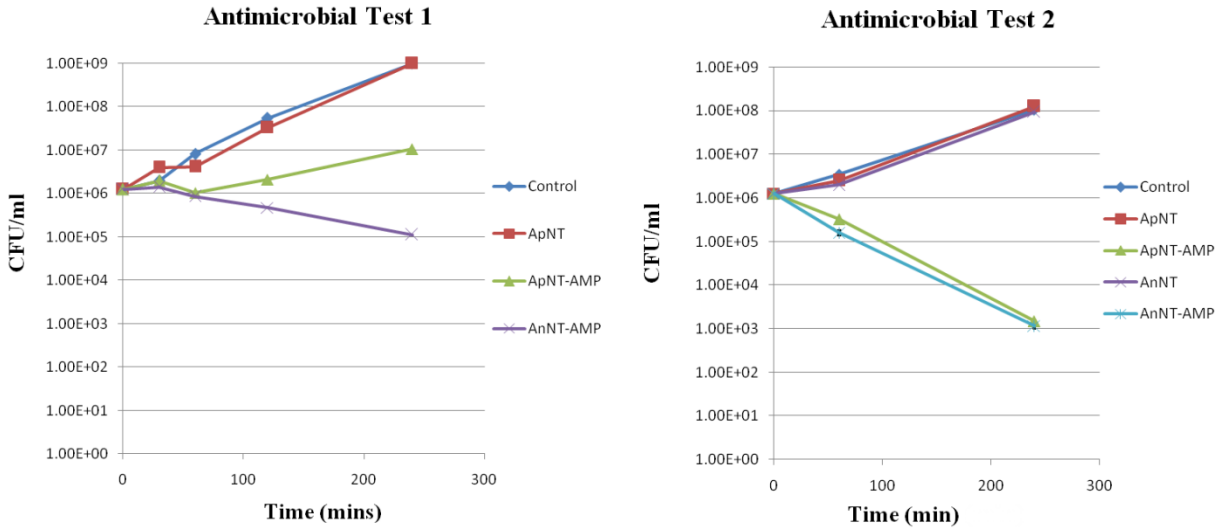

Figure 6. 1 Comparison of antimicrobial activities of samples loaded with different protocols

6.5 Effect of crystallinity on the AMP delivery

In order to investigate the effect of crystallinity on the drug loading efficacy, the antimicrobial activities of both as-prepared (amorphous) and 400°C annealed (anatase) TiO_2 nanotubes were test against *Staphylococcus aureus.*

For Test 1, although both as-prepared (amorphous) and annealed (crystalline) TiO_2 nanotubes with AMP showed positive bacterial inhibition after 60, 120 and 240 minutes incubation, better bacteria inhibition was observed in annealed nanotube samples (AnNT-AMP). At 240 minutes, the annealed samples showed approximately 100 times less bacteria colony unit

than that of the as-prepared samples. The difference may be explained by three possible reasons, or a combination of them:

1. The annealed TiO_2 nanotubes can kill the bacteria by themselves;
2. The annealed TiO_2 nanotubes have better AMP loading efficiency;
3. The annealed TiO_2 nanotubes have better AMP eluting profile.

To examine why the annealed samples has better antimicrobial activity than the as-prepared samples, another positive control group of annealed TiO_2 nanotubes without peptide (AnNT) was included in the second test.

The result of Test 2 showed that there was no significant difference between the control group, ApNT and AnNT groups, which indicated no antimicrobial activity of the annealed TiO_2 nanotubes. It is interesting to note that both as-prepared and annealed TiO_2 nanotubes loaded with AMP demonstrated continuous bacteria killing in Test 2 with approximately 99.9% decrease in bacteria colony forming unit (CFU) after 4 hour incubation. The reason for this is not clear yet. One possible explanation is that the annealed TiO_2 nanotubes have better AMP loading efficiency after soaking in the AMP solution for 1 hour. However, after 20 hours of soaking, both the as-prepared and annealed nanotubes were saturated with AMPs, which may result in no differences between these two groups, in terms of drug loading efficiency. To prove this hypothesis, further experiment is needed.

6.6 Amorphous vs. Anatase TiO_2 nanotubes

Although anatase TiO_2 nanotubes showed better antimicrobial activity than amorphous samples in the antimicrobial Test 1, there is no significant difference between these two groups (ApNT-AMP and AnNT-AMP), in terms of bacteria colony forming unit, in antimicrobial Test 2.

Previous studies suggested that the anatase phase TiO_2 is much more favorable for bone growth than the amorphous phase maybe because of the better lattice match with hydroxyapatite, the mineral component of natural bone tissue [31,34,81]. Recently, Yu and coworkers [82] also demonstrated that anatase phase TiO_2 nanotubes have better corrosion resistance, compared to the amorphous phase in naturally aerated Hank's solution. Furthermore, our preliminary study on the interface strength of TiO_2 nanotube coatings indicated that the annealed coatings were stronger than the as-prepared ones. It is hypothesized that residual stress in the coating is released when it is annealed. Therefore, although both amorphous and anatase phase TiO_2 nanotubes showed similar antimicrobial activities, anatase phase is expected to be a better candidate for the anti-infectious implant for clinical applications.

Chapter 7 Conclusions

This thesis studied the local delivery of one potent antimicrobial peptide (HHC-36) using TiO_2 nanotube arrays prepared by anodization method. The in *vitro* release of peptide from the nanotubes was tested by liquid chromatography-mass spectrometry, and the antimicrobial activities of the samples were evaluated against *S.aureus*, as well as the biocompatibility and cytotoxicity of the samples. Based on our experimental results, the following conclusions can be made:

1. Titanium dioxide nanotubes were successfully prepared by anodization method in both water based electrolytes (phosphoric acid based and ammonium sulphate based electrolytes) and organic based electrolytes (Glycerol based and Ethylene glycol based electrolytes). For water based electrolytes, the thickness of the nanotube layer was within the range of 0.5~1.5μm, while thicker coatings were obtained in glycerol based electrolyte (~2μm). However, coatings thicker than 5μm were only achieved in the ethylene glycol based electrolytes.

2. The morphology of the nanotubes (such as diameter, length, tube wall etc.) can be controlled by anodizing conditions. Our results showed that the diameter of nanotubes is proportional to the anodizing voltage; higher voltage can lead to larger diameters. For ethylene glycol based electrolytes, by prolonging the anodizing duration, the thickness of the coating increases from several microns to tens of micron. Furthermore, by using water free electrolytes (glycerol or ethylene glycol), TiO_2 nanotubes with extremely smooth wall (with few ripples) can be obtained.

3. Raman spectroscopy results indicated that the as-prepared nanotubes coating is amorphous. In order to obtain crystalline phase, post heat treatment is necessary. After 400℃ annealing, the amorphous phase of the nanotubes can be transformed into anatase phase.

4. Antimicrobial peptides were successfully loaded onto the nanotube samples via a simple vacuum assisted physical adsorption method, and the *in vitro* AMP release profile from TiO_2 nanotubes were tested by LC-MS. The as-prepared nanotube and 400 °C annealed nanotube groups showed an AMP release amount: 9.52±1.14 and 12.99±2.37μg/cm^2 respectively, in 1 hour.

5. Antimicrobial activity test against Gram-positive bacteria (*S. aureus*) demonstrated that this novel AMP-loaded nanotubular surface can significantly inhibit bacteria proliferation and effectively reduce bacterial adhesion on the surface. It also suggested that the antimicrobial activities of the samples are highly dependent on the drug loading conditions. By changing the loading conditions (such as AMP solution concentration, vacuuming time and shaking time), the bacteria killing rate can be increased dramatically from 90% (Test 1) to 99.9% (Test 2).

6. The cell adhesion and MTT assay studies showed that the peptide-loaded TiO_2 nanotubes surfaces are biocompatible and do not have significant side effect on osteoblast-like cells (MG-36).

Chapter 8 Recommendations for future work

Based on the results obtained so far, the following research is recommended for future studies:

1. Optimization of the anodizing process. Preparation of TiO_2 nanotube arrays with ideal hexagonal arrangement is useful, not only for drug loading purpose, but also for variety of other applications. To achieve that, a systemic study on the effects of anodizing conditions on the morphology is necessary.

2. Detection of the total amount of AMPs loaded onto the nanotubes as well as the *in vitro* release profile of the AMPs.

3. Investigating the effect of nanotube morphology (i.e. diameter and thickness) on the AMP loading and elution efficiency.

4. Improvement of the drug loading protocol. Our research results indicated that the antimicrobial activities of the peptide-loaded samples are highly dependent on the drug loading conditions. By optimizing this technology, it is expected to improve the bacteria killing results.

5. Selection of AMPs. HHC-36 was used as the test AMP in our research. It has been reported in the literature that some short peptides could selectively bind to solid surfaces. Identifying the specific AMPs that could effectively bind to TiO_2 nanotube surface may significantly improve the drug loading efficiency.

6. *In vivo* test. Although *in vitro* test showed positive results, the real situation in living body is unknown.

REFERENCES

1. Mookherjee N, Hancock REW. Cationic host defence peptides: Innate immune regulatory peptides as a novel approach for treating infections. Cell Mol Life Sci 2007;64:922-933.

2. Hilpert K, Elliott MR, Volkmer-Engert R, Henklein P, Donini O, Zhou Q, Winkler DFH, Hancock REW. Sequence requirements and an optimization strategy for short antimicrobial peptides. Chem Biol 2006;13:1101-1107.

3. Cherkasov A, Hilpert K, Jenssen H, Fjell CD, Waldbrook M, Mullaly SC, Volkmer R, Hancock REW. Use of Artificial Intelligence in the Design of Small Peptide Antibiotics Effective against a Broad Spectrum of Highly Antibiotic-Resistant Superbugs. ACS Chem Biol 2009;4:65-74.

4. Hilpert K, Volkmer-Engert R, Walter T, Hancock REW. High-throughput generation of small antibacterial peptides with improved activity. Nat Biotechnol 2005;23:1008-1012.

5. Zwilling V, Darque-Ceretti E, Boutry-Forveille A, David D, Perrin MY, Aucouturier M. Structure and physicochemistry of anodic oxide films on titanium and TA6V alloy. Surf Interface Anal 1999;27:629-637.

6. Macak JM, Tsuchiya H, Ghicov A, Yasuda K, Hahn R, Bauer S, Schmuki P. TiO2 nanotubes: Self-organized electrochemical formation, properties and applications. Current Opinion in Solid State and Materials Science 2007;11:3-18.

7. Losic D, Simovic S. Self-ordered nanopore and nanotube platforms for drug delivery applications. Expert Opin Drug Deliv 2009;6:1363-1381.

8. Balaur E, Macak JM, Taveira L, Schmuki P. Tailoring the wettability of TiO2 nanotube layers. Electrochem Commun 2005;7:1066-1070.

9. Peng L, Mendelsohn AD, LaTempa TJ, Yoriya S, Grimes CA, Desai TA. Long-Term Small Molecule and Protein Elution from TiO2 Nanotubes. Nano Lett 2009;9:1932-1936.

10. Popat KC, Eltgroth M, La Tempa TJ, Grimes CA, Desai TA. Titania nanotubes: A novel platform for drug-eluting coatings for medical implants? Small 2007;3:1878-1881.

11. Mariani BD, Tuan RS. Advances in the diagnosis of infection in prosthetic joint implants. Mol Med Today 1998;4:207-213.

12. Canadian Joint Replacement Registry. Hip and Knee Replacements in Canada 2008-2009 annual report.

13. Popat KC, Eltgroth M, LaTempa TJ, Grimes CA, Desai TA. Decreased Staphylococcus epidermis adhesion and increased osteoblast functionality on antibiotic-loaded titania nanotubes. Biomaterials 2007;28:4880-4888.

14. Campoccia D, Montanaro L, Arciola CR. The significance of infection related to orthopedic devices and issues of antibiotic resistance. Biomaterials 2006;27:2331-2339.

15. Bozic KJ, Kurtz SM, Lau E, Ong K, Vail TP, Berry DJ. The Epidemiology of Revision Total Hip Arthroplasty in the United States. J Bone Joint Surg -Am Vol 2009;91A:128-133.

16. Sculco TP. The Economic-Impact of Infected Joint Arthroplasty. Orthopedics 1995;18:871-873.

17. An YH, Friedman RJ. Concise review of mechanisms of bacterial adhesion to biomaterial surfaces. J Biomed Mater Res 1998;43:338-348.

18. Darouiche RO. Current concepts - Treatment of infections associated with surgical implants. N Engl J Med 2004;350:1422-1429.

19. Costerton JW, Stewart PS, Greenberg EP. Bacterial biofilms: A common cause of persistent infections. Science 1999;284:1318-1322.

20. Kazemzadeh-Narbat M, Kindrachuk J, Duan K, Jenssen H, Hancock REW, Wang R. Antimicrobial peptides on calcium phosphate-coated titanium for the prevention of implant-associated infections. Biomaterials 2010;31:9519-9526.

21. Hilpert K, Elliott M, Jenssen H, Kindrachuk J, Fjell CD, Koerner J, Winkler DFH, Weaver LL, Henklein P, Ulrich AS, Chiang SHY, Farmer SW, Pante N, Volkmer R, Hancock REW. Screening and Characterization of Surface-Tethered Cationic Peptides for Antimicrobial Activity. Chem Biol 2009;16:58-69.

22. Trebse R, Pisot V, Trampuz A. Treatment of infected retained implants. J Bone Joint Surg - Br Vol 2005;87B:249-256.

23. Moskowitz JS, Blaisse MR, Samuel RE, Hsu H, Harris MB, Martin SD, Lee JC, Spector M, Hammond PT. The effectiveness of the controlled release of gentamicin from polyelectrolyte multilayers in the treatment of Staphylococcus aureus infection in a rabbit bone model. Biomaterials 2010;31:6019-6030.

24. Zhao L, Chu PK, Zhang Y, Wu Z. Antibacterial Coatings on Titanium Implants. J Biomed Mater Res Part B 2009;91B:470-480.

25. Wu P, Grainger DW. Drug/device combinations for local drug therapies and infection prophylaxis. Biomaterials 2006;27:2450-2467.

26. Jenssen H, Hamill P, Hancock REW. Peptide antimicrobial agents. Clin Microbiol Rev 2006;19:491-.

27. Brown KL, Hancock REW. Cationic host defense (antimicrobial) peptides. Curr Opin Immunol 2006;18:24-30.

28. Fujishima A, Zhang X, Tryk DA. TiO2 photocatalysis and related surface phenomena. Surf Sci Rep 2008;63:515-582.

29. Matsuno H, Yokoyama A, Watari F, Uo M, Kawasaki T. Biocompatibility and osteogenesis of refractory metal implants, titanium, hafnium, niobium, tantalum and rhenium. Biomaterials 2001;22:1253-1262.

30. Leng YX, Huang N, Yang P, Chen JY, Sun H, Wang J, Wan GJ, Tian XB, Fu RKY, Wang LP, Chu PK. Structure and properties of biomedical TiO2 films synthesized by dual plasma deposition. Surface and Coatings Technology 2002;156:295-300.

31. Tsuchiya H, Macak JM, Muller L, Kunze J, Muller F, Greil P, Virtanen S, Schmuki P. Hydroxyapatite growth on anodic TiO2 nanotubes. J Biomed Mater Res Part A 2006;77A:534-541.

32.Regonini D. Anodised TiO2 Nanotubes: Synthesis, Growth Mechanism and Thermal Stability . 2008.

33. Brammer KS, Oh S, Cobb CJ, Bjursten LM, van der Heyde H, Jin S. Improved bone-forming functionality on diameter-controlled TiO2 nanotube surface. Acta Biomater 2009;5:3215-3223.

34. Oh S, Daraio C, Chen LH, Pisanic TR, Finones RR, Jin S. Significantly accelerated osteoblast cell growth on aligned TiO2 nanotubes. J Biomed Mater Res Part A 2006;78A:97-103.

35. Mor GK, Varghese OK, Paulose M, Shankar K, Grimes CA. A review on highly ordered, vertically oriented TiO2 nanotube arrays: Fabrication, material properties, and solar energy applications. Solar Energy Mater Solar Cells 2006;90:2011-2075.

36. Kim SE, Lim JH, Lee SC, Nam S, Kang H, Choi J. Anodically nanostructured titanium oxides for implant applications. Electrochim Acta 2008;53:4846-4851.

37. Prakasam HE, Shankar K, Paulose M, Varghese OK, Grimes CA. A new benchmark for TiO2 nanotube array growth by anodization. J Phys Chem C 2007;111:7235-7241.

38. Ghicov A, Schmuki P. Self-ordering electrochemistry: a review on growth and functionality of TiO2 nanotubes and other self-aligned MOx structures. Chem Commun 2009:2791-2808.

39. Sul YT, Johansson CB, Jeong Y, Albrektsson T. The electrochemical oxide growth behaviour on titanium in acid and alkaline electrolytes. Med Eng Phys 2001;23:329-346.

40. Li S, Zhang G, Guo D, Yu L, Zhang W. Anodization Fabrication of Highly Ordered TiO2 Nanotubes. J Phys Chem C 2009;113:12759-12765.

41. Crawford GA, Chawla N. Porous hierarchical TiO2 nanostructures: Processing and microstructure relationships. Acta Mater 2009;57:854-867.

42. Mor GK, Varghese OK, Paulose M, Shankar K, Grimes CA. A review on highly ordered, vertically oriented TiO2 nanotube arrays: Fabrication, material properties, and solar energy applications. Solar Energy Mater Solar Cells 2006;90:2011-2075.

43. Macak JM, Schmuki P. Anodic growth of self-organized anodic TiO2 nanotubes in viscous electrolytes. Electrochim Acta 2006;52:1258-1264.

44. Macak JM, Hildebrand H, Marten-Jahns U, Schmuki P. Mechanistic aspects and growth of large diameter self-organized TiO2 nanotubes. J Electroanal Chem 2008;621:254-266.

45. Taveira LV, Macak JM, Tsuchiya H, Dick LFP, Schmuki P. Initiation and growth of self-organized TiO2 nanotubes anodically formed in $NH_4F/(NH_4)_2SO_4$ electrolytes. J Electrochem Soc 2005;152:B405-B410.

46. Macak JM, Tsuchiya H, Schmuki P. High-aspect-ratio TiO2 nanotubes by anodization of titanium. Angew Chem -Int Edit 2005;44:2100-2102.

47. Albu SP, Ghicov A, Macak JM, Hahn R, Schmuki P. Self-organized, free-standing TiO2 nanotube membrane for flow-through photocatalytic applications. Nano Lett 2007;7:1286-1289.

48. Tsuchiya H, Macak JM, Ghicov A, Schmuki P. Self-organization of anodic nanotubes on two size scales. Small 2006;2:888-891.

49. Albu SP, Ghicov A, Aldabergenova S, Drechsel P, LeClere D, Thompson GE, Macak JM, Schmuki P. Formation of Double-Walled TiO2 Nanotubes and Robust Anatase Membranes. Adv Mater 2008;20:4135-.

50. Macak JM, Albu S, Kim DH, Paramasivam I, Aldabergerova S, Schmuki P. Multilayer TiO2-nanotube formation by two-step anodization. Electrochem Solid State Lett 2007;10:K28-K31.

51. Macak JM, Tsuchiya H, Ghicov A, Yasuda K, Hahn R, Bauer S, Schmuki P. TiO2 nanotubes: Self-organized electrochemical formation, properties and applications. Current Opinion in Solid State and Materials Science 2007;11:3-18.

52. Regonini D, Jaroenworaluck A, Stevens R, Bowen CR. Effect of heat treatment on the properties and structure of TiO2 nanotubes: phase composition and chemical composition. Surf Interface Anal 2010;42:139-144.

53. Bjursten LM, Rasmusson L, Oh S, Smith GC, Brammer KS, Jin S. Titanium dioxide nanotubes enhance bone bonding in vivo. J Biomed Mater Res Part A 2010;92A:1218-1224.

54. Oh S, Brammer KS, Li YSJ, Teng D, Engler AJ, Chien S, Jin S. Stem cell fate dictated solely by altered nanotube dimension. Proc Natl Acad Sci U S A 2009;106:2130-2135.

55. Brammer KS, Oh S, Gallagher JO, Jin S. Enhanced cellular mobility guided by TiO2 nanotube surfaces. Nano Lett 2008;8:786-793.

56. Burns K, Yao C, Webster TJ. Increased chondrocyte adhesion on nanotubular anodized titanium. J Biomed Mater Res Part A 2009;88A:561-568.

57. von Wilmowsky C, Bauer S, Lutz R, Meisel M, Neukam FW, Toyoshima T, Schmuki P, Nkenke E, Schlegel KA. In Vivo Evaluation of Anodic TiO2 Nanotubes: An Experimental Study in the Pig. J Biomed Mater Res Part B 2009;89B:165-171.

58. Song Y, Schmidt-Stein F, Bauer S, Schmuki P. Amphiphilic TiO2 Nanotube Arrays: An Actively Controllable Drug Delivery System. J Am Chem Soc 2009;131:4230-.

59. Lai Y, Lin C, Wang H, Huang H, Zhuang H, Sun L. Superhydrophilic-superhydrophobic micropattern on TiO2 nanotube films by photocatalytic lithography. Electrochem Commun 2008;10:387-391.

60. Vasilev K, Poh Z, Kant K, Chan J, Michelmore A, Losic D. Tailoring the surface functionalities of titania nanotube arrays. Biomaterials 2010;31:532-540.

61. Wang D, Liu Y, Liu X, Zhou F, Liu W, Xue Q. Towards a tunable and switchable water adhesion on a TiO2 nanotube film with patterned wettability. Chem Commun 2009:7018-7020.

62. Kalbacova M, Macak JM, Schmidt-Stein F, Mierke CT, Schmuki P. TiO2 nanotubes: photocatalyst for cancer cell killing. Phys Status Solidi-Rapid Res Lett 2008;2:194-196.

63. Oh SH, Finones RR, Daraio C, Chen LH, Jin SH. Growth of nano-scale hydroxyapatite using chemically treated titanium oxide nanotubes. Biomaterials 2005;26:4938-4943.

64. Puleo DA, Nanci A. Understanding and controlling the bone-implant interface. Biomaterials 1999;20:2311-2321.

65. Lind M, Overgaard S, Glerup H, Soballe K, Bunger C. Transforming growth factor-beta 1 adsorbed to tricalciumphosphate coated implants increases peri-implant bone remodeling. Biomaterials 2001;22:189-193.

66. Lind M, Overgaard S, Ongipattanakul B, Nguyen T, Bunger C, Soballe K. Transforming growth factor-beta 1 stimulates bone ongrowth to weight-loaded tricalcium phosphate coated implants - An experimental study in dogs. J Bone Joint Surg -Br Vol 1996;78B:377-382.

67. Nanci A, Wuest JD, Peru L, Brunet P, Sharma V, Zalzal S, McKee MD. Chemical modification of titanium surfaces for covalent attachment of biological molecules. J Biomed Mater Res 1998;40:324-335.

68. Silverman BM, Wieghaus KA, Schwartz J. Comparative properties of siloxane vs phosphonate monolayers on a key titanium alloy. Langmuir 2005;21:225-228.

69. Verron E, Khairoun I, Guicheux J, Bouler J. Calcium phosphate biomaterials as bone drug delivery systems: a review. Drug Discov Today 2010;15:547-552.

70. Shanshan Lu. Immobilization of antimicrobial peptides onto titanium surfaces. Master thesis UBC 2009.

71. Bauer S, Kleber S, Schmuki P. TiO2 nanotubes: Tailoring the geometry in H3PO4/HF electrolytes. Electrochem Commun 2006;8:1321-1325.

72. Macak JM, Tsuchiya H, Taveira L, Aldabergerova S, Schmuki P. Smooth anodic TiO2 nanotubes. Angew Chem -Int Edit 2005;44:7463-7465.

73. Cheng N. Formula for the viscosity of a glycerol-water mixture. Ind Eng Chem Res 2008;47:3285-3288.

74. Xiao X, Liu R, Tian T. Preparation of bioactive titania nanotube arrays in HF/Na2HPO4 electrolyte. J Alloys Compounds 2008;466:356-362.

75. Wang J, Lin Z. Anodic Formation of Ordered TiO2 Nanotube Arrays: Effects of Electrolyte Temperature and Anodization Potential. J Phys Chem C 2009;113:4026-4030.

76. Luo B, Yang H, Liu S, Fu W, Sun P, Yuan M, Zhang Y, Liu Z. Fabrication and characterization of self-organized mixed oxide nanotube arrays by electrochemical anodization of Ti-6Al-4V alloy. Mater Lett 2008;62:4512-4515.

77. Ellingsen JE. A Study on the Mechanism of Protein Adsorption to Tio2. Biomaterials 1991;12:593-596.

78. Sousa SR, Moradas-Ferreira P, Saramago B, Melo LV, Barbosa MA. Human serum albumin adsorption on TiO2 from single protein solutions and from plasma. Langmuir 2004;20:9745-9754.

79. Cacciafesta P, Humphris ADL, Jandt KD, Miles MJ. Human plasma fibrinogen adsorption on ultraflat titanium oxide surfaces studied with atomic force microscopy. Langmuir 2000;16:8167-8175.

80. Topoglidis E, Cass AEG, Gilardi G, Sadeghi S, Beaumont N, Durrant JR. Protein adsorption on nanocrystalline TiO2 films: An immobilization strategy for bioanalytical devices. Anal Chem 1998;70:5111-5113.

81. Uchida M, Kim HM, Kokubo T, Fujibayashi S, Nakamura T. Structural dependence of apatite formation on titania gels in a simulated body fluid. J Biomed Mater Res Part A 2003;64A:164-170.

82. Yu W, Qiu J, Xu L, Zhang F. Corrosion behaviors of TiO2 nanotube layers on titanium in Hank's solution. Biomed Mater 2009;4:065012.

APPENDICES

Appendix A: ANOVA for antimicrobial test 2

Table 1 ANOVA tables for antimicrobial test 2 after 60 minutes incubation

Source of Variation	Sum of squares	DF	Mean square	F	P
Between Groups	24.4	4	6.101	6.25	0.009
Within Groups	9.768	10	0.9768		
Total	34.17	14			

Table 2 ANOVA tables for antimicrobial test 2 after 240 minutes incubation

Source of Variation	Sum of squares	DF	Mean square	F	P
Between Groups	4.437e+04	4	1.109e+04	25.21	0.000
Within Groups	4400	10	440		
Total	4.877e+04	14			

Appendix B: MTT assay for AMPs

Table 3 P value of Holm t-test on the results of MTT assay for HHC-36

HHC36 concentration (μg/ml)	10	25	50	75	100	125	150	175	200	300	500
Control	0.437	0.361	0.647	0.703	0.842	0.928	0.356	0.260	0.032	0.001	0.000